DOT/FAA/AR-98/53

Residual Strength Test on Stiffened Panels With Multiple-Site Damage

February 1999

Final Report

19990406 079

U.S. Department of Transportation
Federal Aviation Administration

DTIC QUALITY INSPECTED 2

NOTICE

This document is disseminated under the sponsorship of the U.S. Department of Transportation in the interest of information exchange. The United States Government assumes no liability for the contents or use thereof. The United States Government does not endorse products or manufacturers. Trade or manufacturer's names appear herein solely because they are considered essential to the objective of this report.

This report is available at the Federal Aviation Administration William J. Hughes Technical Center's Full-Text Technical Reports page: www.tc.faa.gov/its/act141/reportpage.html in Adobe Acrobat portable document format (PDF).

1. Report No. DOT/FAA/AR-98/53	2. Government Accession No.	3. Recipient's Catalog No.	
4. Title and Subtitle RESIDUAL STRENGTH TEST ON STIFFENED PANELS WITH MULTIPLE-SITE DAMAGE		5. Report Date February 1999	
		6. Performing Organization Code	
7. Author(s) H.J. ten Hoeve, L. Schra, A.L.P.J. Michielsen, and H. Vlieger		8. Performing Organization Report No. NLR CR 96792 L	
9. Performing Organization Name and Address Nationaal Lucht-En Ruimtevaartlaboratorium National Aerospace Laboratory NLR The Netherlands		10. Work Unit No. (TRAIS)	
		11. Contract or Grant No.	
12. Sponsoring Agency Name and Address U.S. Department of Transportation Federal Aviation Administration Office of Aviation Research Washington, DC 20591		13. Type of Report and Period Covered Final Report	
		14. Sponsoring Agency Code AAR-431	

15. Supplementary Notes
The Federal Aviation Administration William J. Hughes Technical Center COTR is Dr. Paul Tan

16. Abstract

In Federal Aviation Administration and the Netherlands Department of Civil Aviation (FAA/RLD) collaboration, residual strength tests were carried out on stiffened panels with multiple-site damage (MSD). The main purpose of this test program was to generate experimental data to verify tools to predict the residual strength of such panels. In this report these tests are described and the results are presented in such a way that they can be used to verify new and existing models.

17. Key Words Buckling, Crack opening displacement, R-curve, Rivets, Stress, Strain	18. Distribution Statement Document is available to the public through the National Technical Information Service (NTIS), Springfield, Virginia 22161.		
19. Security Classif. (of this report) Unclassified	20. Security Classif. (of this page) Unclassified	21. No. of Pages 77	22. Price

Form DOT F1700.7 (8-72)   Reproduction of completed page authorized

TABLE OF CONTENTS

LIST OF FIGURES

LIST OF TABLES

EXECUTIVE SUMMARY

In Federal Aviation Administration and the Netherlands Department of Civil Aviation (FAA/RLD) collaboration, residual strength tests were carried out on stiffened panels with multiple-site damage (MSD). The main purpose of this test program was to generate experimental data to verify tools to predict the residual strength of such panels. In this report these tests are described and the results are presented in such a way that they can be used to verify new and existing models.

1. INTRODUCTION.

After the Aloha Airline accident in 1988, the significance of multiple-site damage (MSD) was generally recognized. Several working groups were formed in different countries to investigate crack initiation, crack growth, and residual strength of panels with multiple cracks. The aim of these groups was not only to improve the knowledge on these topics, but also to provide tools to predict crack initiation and crack growth life in the presence of MSD. These tools can serve as a basis for the preparation of guidelines for maintenance of aging aircraft.

At the National Aerospace Laboratory (NLR), work is ongoing on MSD in the framework of Federal Aviation Administration/Netherlands Department of Civil Aviation (FAA/RLD) collaboration agreement. In previous years, the research was mainly focused on crack initiation and growth in lap joints. An extensive test program was performed on large, flat lap joint specimens which were loaded biaxially [1–6]. A lap joint is a very complex joint; it usually consists of two or three rivet rows. Not all rows carry a proportional part of the load. The load is transferred via the rivets and via friction between the sheets. In addition, since the two sheets are not in the same plane, secondary bending is introduced, and it is known from the literature that the rivet force (or squeezing force) has a considerable influence on the fatigue life of a lap joint.

Since 1995, attention has been paid to the residual strength problem. A software tool was developed for the prediction of the residual strength in flat stiffened panels with multiple cracks. The computer program was based on the Strip Yield model and ARREST, a computer program developed at NLR for the prediction of the residual strength in stiffened panels with one crack [7]. The Strip Yield model was used for the calculation of the J-integral at each tip, which was used to predict the static growth. The influence of the stiffeners was taken into account as it was in ARREST.

On fuselages, MSD may occur in riveted longitudinal lap joints. In the computer program under development, this lap joint was not modeled, but the influence of the stiffener and multiple cracks was taken into account. Secondary bending is usually taken into account via the stress-intensity factor. The load in a lap joint is partially transferred via the rivets and partially via friction between the sheets. The ratio of the loads transferred in these two ways is usually assessed on the basis of engineering judgement. The influence of the rivet force is usually not taken into account. The finite element method can be used to predict this phenomenon, although it is usually very time consuming and expensive. The influence of the rivet force on the stress distribution after riveting has been calculated by R. Müller [8], but to the authors' knowledge, it has never been incorporated into a crack growth calculation. The latter is not very simple if the influence of the crack on the stress distribution is taken into account. Secondary bending, the complex load transfer, and the influence of the rivet force are neglected in the software tool.

From the open literature only limited information is available to verify a computer program as described above. It was decided to do a series of experiments on stiffened panels designed according to the capabilities of the computer program. This implies flat panels with riveted stiffeners but without a lap joint. In this report these tests are reported to serve as verification data for computer programs as described above.

These tests have limited significance for real aircraft structures. On the other hand, they are indispensable for the verification of simple computer programs like the one just described. Simple tests, like the tests given in this report, are also useful to verify complex computer programs. They provide the information to verify certain options, in this case the influence of riveted stiffeners on multiple cracks.

In the next section, the panel configurations are described. Section 3 gives a description of the tests, the test program, the manufacturing of the panels, and the test results. In addition to the tests on the stiffened panels, experiments were carried out to obtain other relevant properties, such as Young's modulus, the residual strength curve for the sheet material, and the flexibility of the stiffener-skin connection. These tests and the results are given in section 4.

2. PANEL CONFIGURATIONS USED IN TESTING.

The configurations and dimensions of the tested panels were chosen such that the test results would be applicable to the behavior of cracks in a longitudinal fuselage lap joint of an actual aircraft. However, owing to geometrical limitations dictated by the testing machine used, the ultimate panel configurations were a compromise of a number of requirements. The frames are represented by stiffeners in the test specimens.
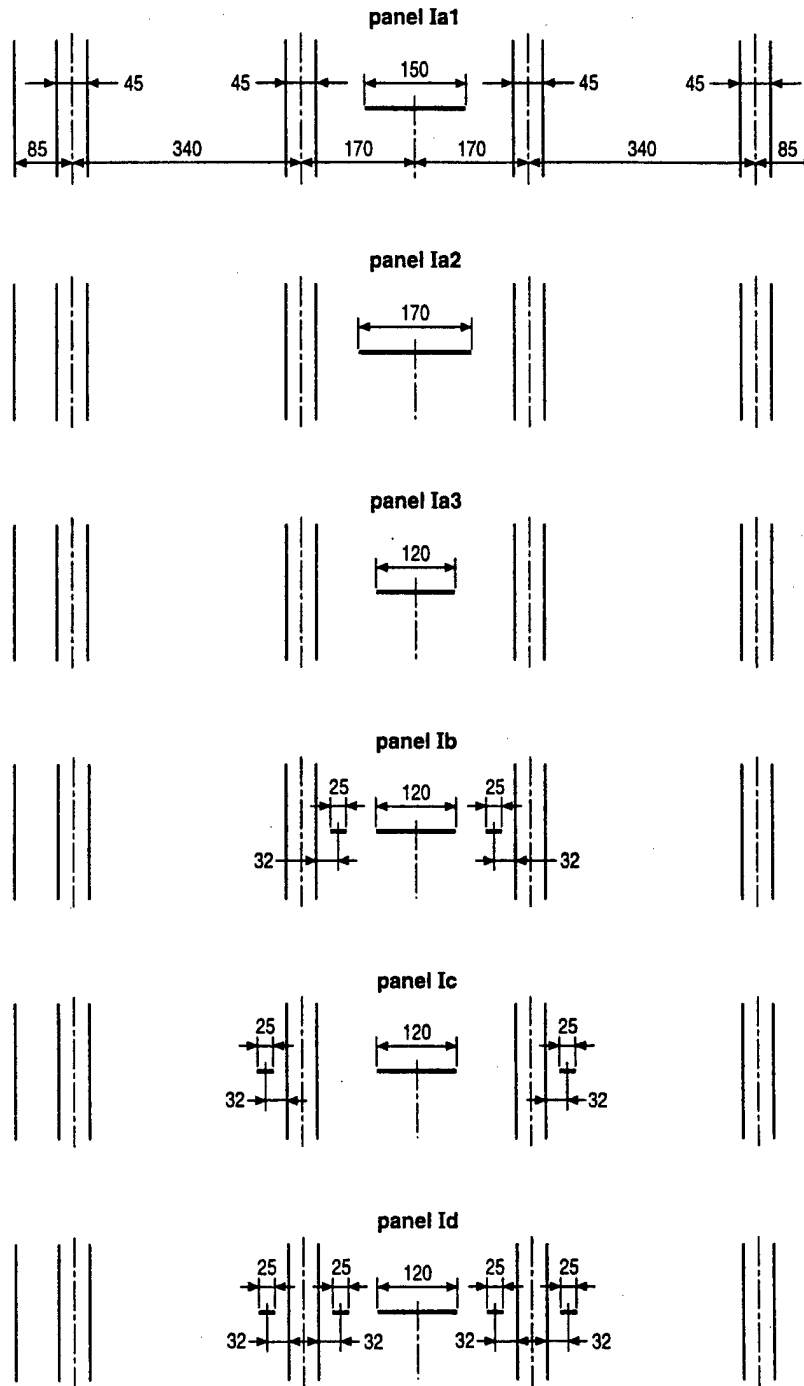
The panel configurations were chosen such that for panels containing a skin (lead) crack with a certain panel width and stiffener spacing there are three cracked skin-stiffener combinations that could be tested, namely

(a)   a skin crack extending between two stiffeners (Configuration I)
(b)   a skin crack extending under an intact stiffener (Configuration II)
(c)   a skin crack extending under a broken stiffener (Configuration III)

The width of the panels was limited to the nominal available width of 1200 mm. To allow a configuration of a lead crack with a number of MSD cracks in the same stiffener bay, a stiffener spacing of 340 mm was chosen. Four stiffeners were used for Configuration I panels (figures 1a and 1b) and 3 stiffeners were used for Configuration II and III panels (figures 1a and 1c). To avoid load eccentricities in the clamping areas, a stiffener strip was located at each stiffener on both sides of the skin. A nominal skin thickness of 1.27 mm (0.05 in) was chosen. The strip stiffener dimensions were taken such that the stiffening ratio was about the same as that found in the fuselage cross section of an actual aircraft (see figure 2). The stiffeners were cut from nominal 2.04-mm (0.08-in) -thick sheet material and had a width of 45 mm (resulting in a stiffening ratio of 0.7, approximately equal to the 0.65 shown in figure 2). The skin material used was 2024-T3, and the stiffener material used was 7075-T6 (see figures 1b and 1c). The mechanical properties of the materials used are given in section 4.1.

The stiffeners were connected to the skin by 4.0-mm DD-rivets (protruding head type), and a continuous rivet pattern was used. Each stiffener was connected to the skin by two rows of rivets in the longitudinal direction 20 mm apart and with an edge distance of 12.5 mm. A rivet spacing of 20 mm was used over a length of 100 mm at either side of the cracked section; a rivet spacing of 25 mm was used outside these regions (see figures 1b and 1c). To guarantee a constant stiffener spacing in all panels and to facilitate the connection of the stiffeners to the

Configuration I, 4 stiffeners, all intact

panel Ia1

85 — 45 | 45 — 150 — 45 | 45 — 85
340 | 170 — 170 | 340

panel Ia2

170

panel Ia3

120

panel Ib

25 — 120 — 25
32 — 32

panel Ic

25 — 120 — 25
32 — 32

panel Id

25 — 25 — 120 — 25 — 25
32 — 32 — 32 — 32

all units in mm

FIGURE 1a. OVERVIEW OF CRACK CONFIGURATIONS IN PANELS

FIGURE 1a. OVERVIEW OF CRACK CONFIGURATIONS IN PANELS (CONTINUED)

4

FIGURE 1b. DESIGN OF PANEL CONFIGURATION I

5
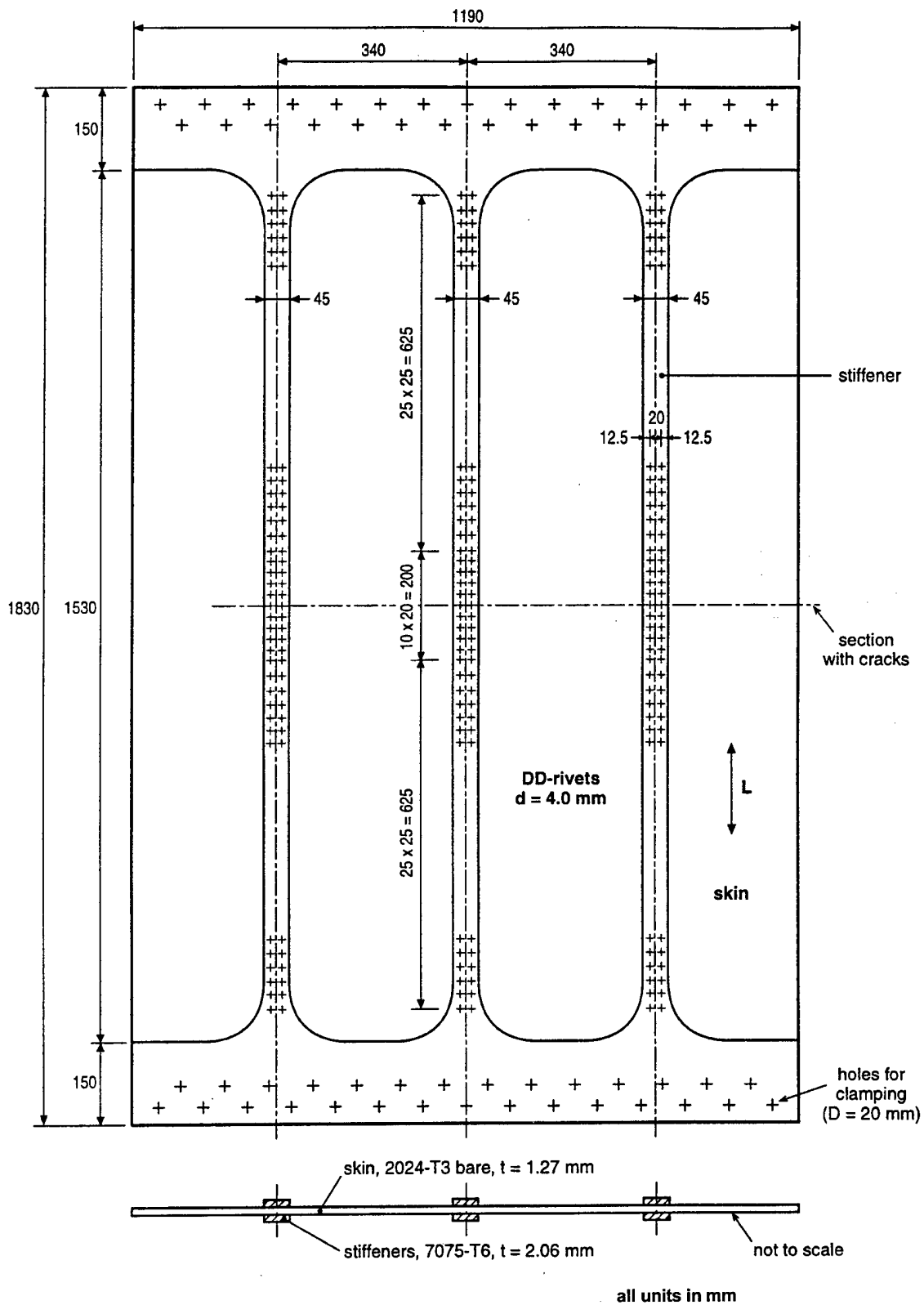
FIGURE 1c. DESIGN OF PANEL CONFIGURATIONS II AND III

R = 1650 mm
L = 500 mm

frames
longerons

cross section A-A

20.0

0.8

skin (1.0 mm)

castellation
(A = 55.36 mm^2)

30.0

0.8

2.0

50.0

8.0

2.0

60.0

material:
skin   : 2024-T3
castellation : 2024-T3
ring stiffener: 7075-T73

ring-stiffener
(A = 217.6 mm^2)

1.6

2.0   2.0

8.0

26.0

stiffening ratio: $\dfrac{A_{skin}}{A_{skin} + A_{stiff}}$ = 0.65
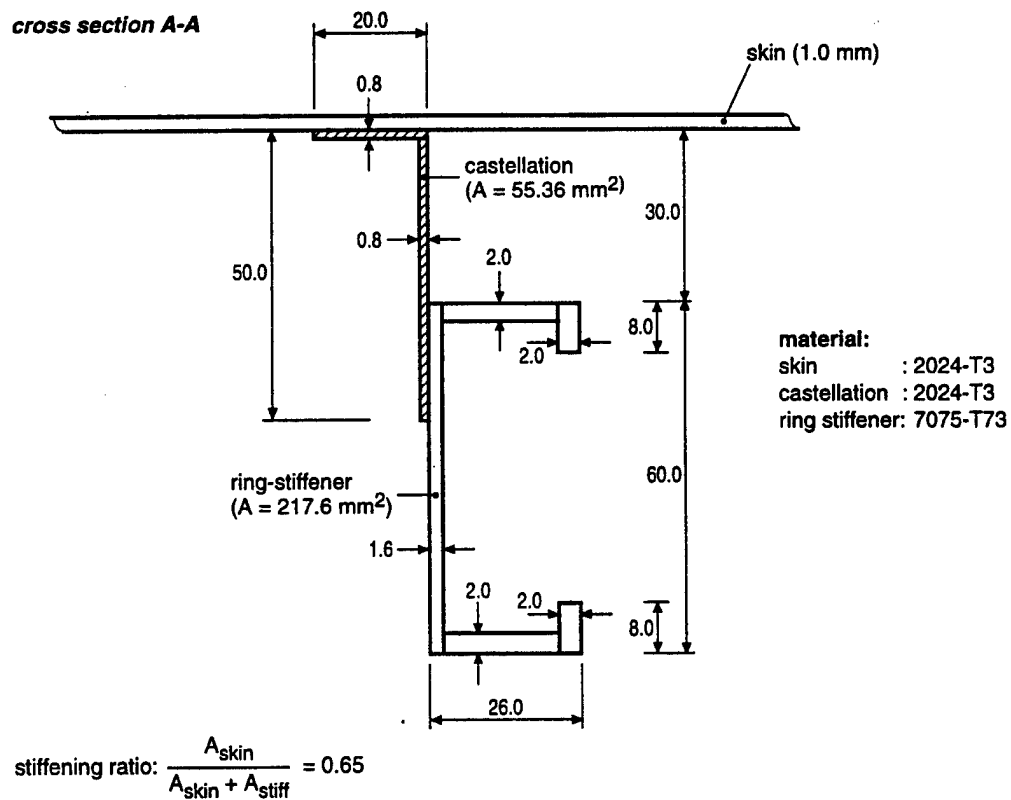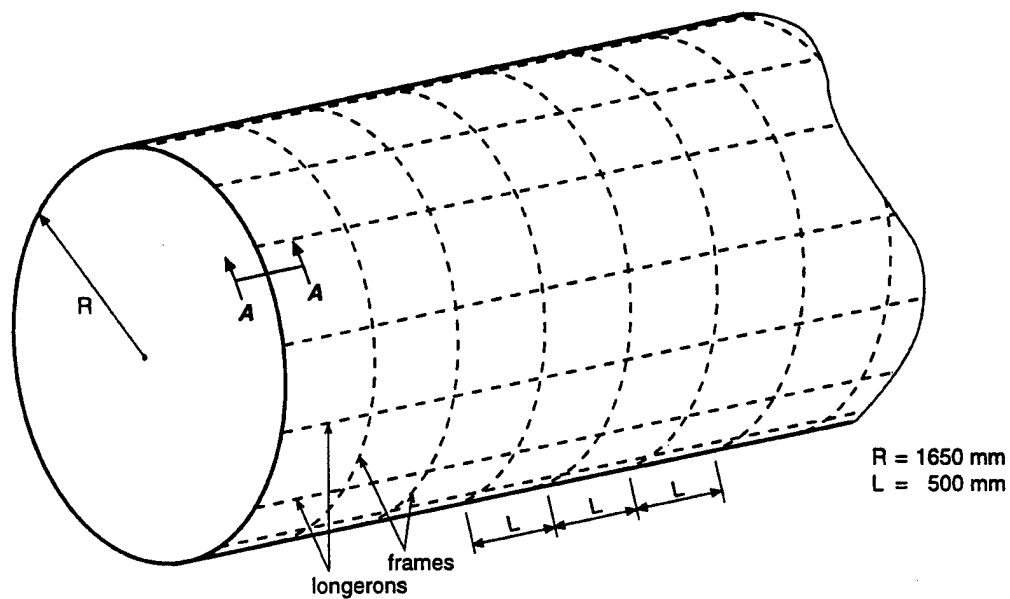
all units in mm

FIGURE 2. FOKKER 100 FUSELAGE DESIGN DETAILS (TYPICAL)

7

(relatively thin) skin during the riveting process, the stiffeners were made out of 1200-mm-wide sheets by milling away the material between the stiffeners in the central part of these sheets and leaving the material at the ends (see figures 1b and 1c). In this way, a uniform load distribution was introduced at the stiffened panel ends.

3. TESTING OF STIFFENED PANELS.

3.1 TEST PROGRAM.

Panels with only a central lead crack and panels with a combination of a lead crack and secondary cracks were tested. An overview of the crack configurations used in the different types of panels is given in figure 1a. For Configurations I and III, panels with central cracks of different lengths were tested first. This allowed the selection of the most useful length of the central lead crack for use with the secondary cracks. All secondary cracks were 25 mm long.

The main objective of testing panel Configuration I was to investigate the residual strength with a central lead crack and secondary cracks inside the inner stiffeners, outside the inner stiffeners, and both inside and outside the inner stiffeners. The main objective of testing panel Configuration III was to investigate the effect of linkup on the residual strength of the central lead crack and two or four secondary cracks, all inside the outer stiffeners.

Panel IIa had intact central stiffeners crossing a central crack with the same length as in panel IIIa1. Testing these panels will show the effect of a broken central stiffener on the residual strength. Testing the panels in Configuration II with secondary cracks was not considered useful.

For all panels a load (stress) -crack length relationship was determined until failure of the panel. In addition, panel Ia1 was instrumented with strain gauges to measure the strain distribution in the panel. Further, the strain in the central stiffeners of panel IIa was measured during growth of the central crack. Also, the opening angle during growth of the central crack in panel Ia2 was measured. During testing, rather severe buckling of the panels occurred. The buckling pattern was determined, and the extent of the buckling was measured in most of the panels.

3.2 MANUFACTURE OF PANELS.

The central lead crack and the secondary cracks in the skin of the panels were precracked in fatigue before the residual strength test. The skins of the panels were fatigue precracked before the stiffeners were riveted to the skin.

The following procedure was used to fatigue precrack and rivet of the panels.

- Saw cut 23-mm-long slits in the skin at the locations of the secondary cracks.

- Fatigue the skin until 1-mm crack growth was obtained at both ends of the saw cut slits, resulting in a 25-mm-long secondary crack.

- Saw cut a slit for the central lead crack 2 mm smaller than the length of that crack.

- Fatigue the skin until 1 mm of crack growth is obtained at both ends of the slit and the desired length of the lead crack was reached.

- Rivet the stiffeners to the skin.

- Drill and bore 20-mm-diameter holes for mounting the panel in the clamping plates of the testing machine.

Fatigue precracking was done at a stress ratio of R = 0.1. The test frequency was about 1 Hz. The fatigue loads were selected such that $K_{f,max}$ was about 20 MPa$\sqrt{}$ m. It took between 2500 and 3000 cycles to grow the saw cut slit 1 mm at both ends of the slit. The fatigue loads were much lower for the lead crack than for the secondary cracks. Therefore, fatigue loading of the lead crack did not result in significant growth of the secondary cracks, which were already present.

To properly position the rivets, one of the stiffeners for each panel contained 2-mm-diameter pilot holes. The stiffeners and the skin were positioned and clamped together. Four-mm-diameter pilot holes were drilled and, after deburring, the stiffeners were hand riveted to the skin following the Fokker specifications (D = 1.25d-1.65d). Riveting was done in turn from both sides of the panel to prevent curvature of the panel. First, the 15 most central rivets were driven from the front side of the panel, then the next 12 rivets toward each end were driven from the rear side of the panel, and the final 11 rivets were driven from the front side of the panel. A total of 488 rivets were used for the panels with Configuration I, and a total of 366 rivets were used for the panels with Configurations II and III.

3.3 EXPERIMENTAL DETAILS.

3.3.1 General.

The tests were done in a biaxial fatigue testing frame. Hydraulic actuators can be mounted to load in horizontal and vertical directions. For the present investigation, only a vertical actuator was used with a maximum load capacity of 1000 kN. A double-bridge load cell was mounted at the rod end of the actuator. The applied loads were controlled by a closed-loop servo system. Figure 3a shows a panel of Configuration I mounted in the testing frame. Tensile rods were used to prevent horizontal deflection of the frame during loading.

Load control was used to fatigue precrack the panel skins. The residual strength tests were done under displacement control to statically grow the crack beyond the point of maximum load. During the residual strength test, the displacement was gradually increased until failure of the panel. The displacement increase was periodically interrupted for visual reading of the crack length using a travelling microscope combined with a crack monitoring device (Sony Magnescale EA-210, see figure 3a). This enabled the crack length to be read to 0.01 mm.

A clip gauge for displacement measurement was seated in the central hole of the skin. The beams of the clip gauge were provided with conical hard steel inserts to obtain point contacts with the center of the panel. During the residual strength test, records were made of load versus displacement in the central hole.
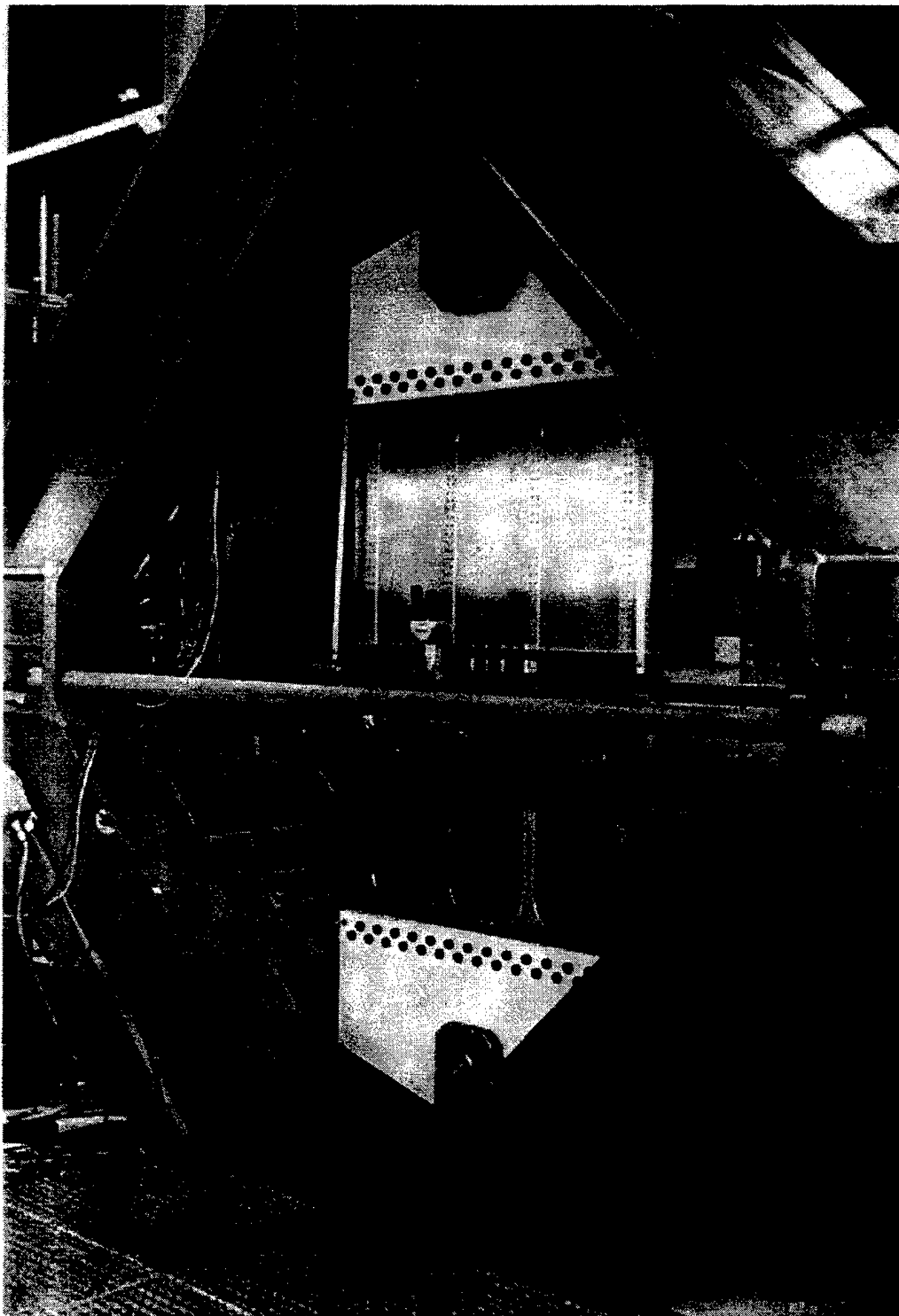
FIGURE 3a. TEST SETUP WITH PANEL OF CONFIGURATION I MOUNTED
IN THE TEST FRAME

Half-section I-beams 10 cm high were used to restrain buckling of the panel. A 70-cm-long and 4-cm-wide cutout was made in the web of the d-beam at the front side of the panel to read the crack length. Initially, a limited number of aluminum blocks were used between the half-section I-beams and the skin to support the skin. The blocks were provided with low friction foil to prevent load transfer to the antibuckling guide. During the first panel test, the panel buckled. A more efficient support of the skin was devised by using blocks along the entire width, as shown in figure 3b. Fifteen-mm-wide blocks were used in the skin area with the fatigue cracks. These blocks could be shifted to read the crack length. Despite this improvement, the panel still buckled. The buckling of the panels will be discussed in more detail in section 3.4.5.
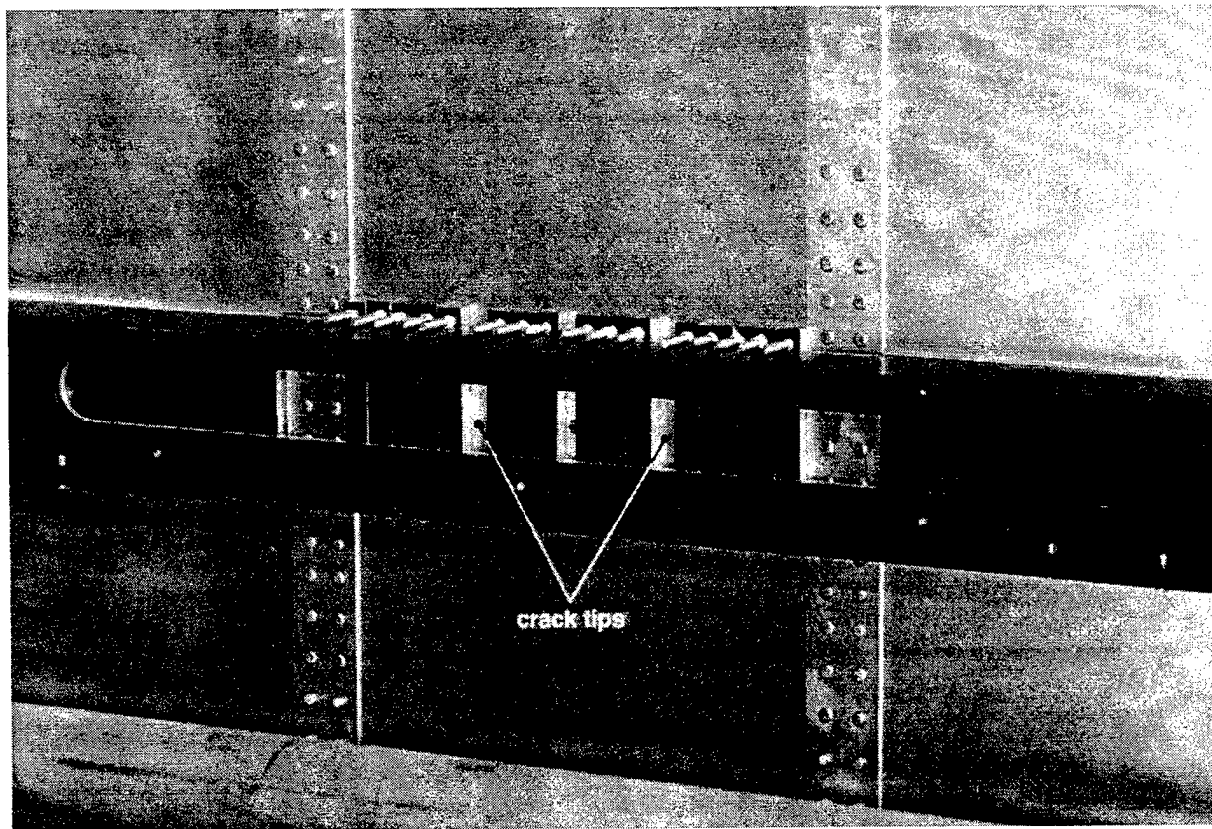
FIGURE 3b. DETAIL OF ANTIBUCKLING GUIDE WITH MOVABLE BLOCKS TO SUPPORT THE SKIN AND ENABLING CRACK LENGTH READING

3.3.2 Strain Distribution.

Before residual strength testing, the strain distribution was measured in the first panel (panel Ia1). Twelve strain gauges (six on the front side and six on the rear side, opposite to those at the front side) were bonded on the skin of the panel at the locations shown in figure 4. A set of six strain gauges was positioned in the centerline of the panel, and a similar set was positioned 400 mm above it. All strain gauges were positioned on the centerline of the skin between the stiffeners. The strains were measured in 10 load steps of 8 kN up to a maximum load of 80 kN. The measurements were done in triplicate for the uncracked panel and after the introduction of a central crack 150 mm long.
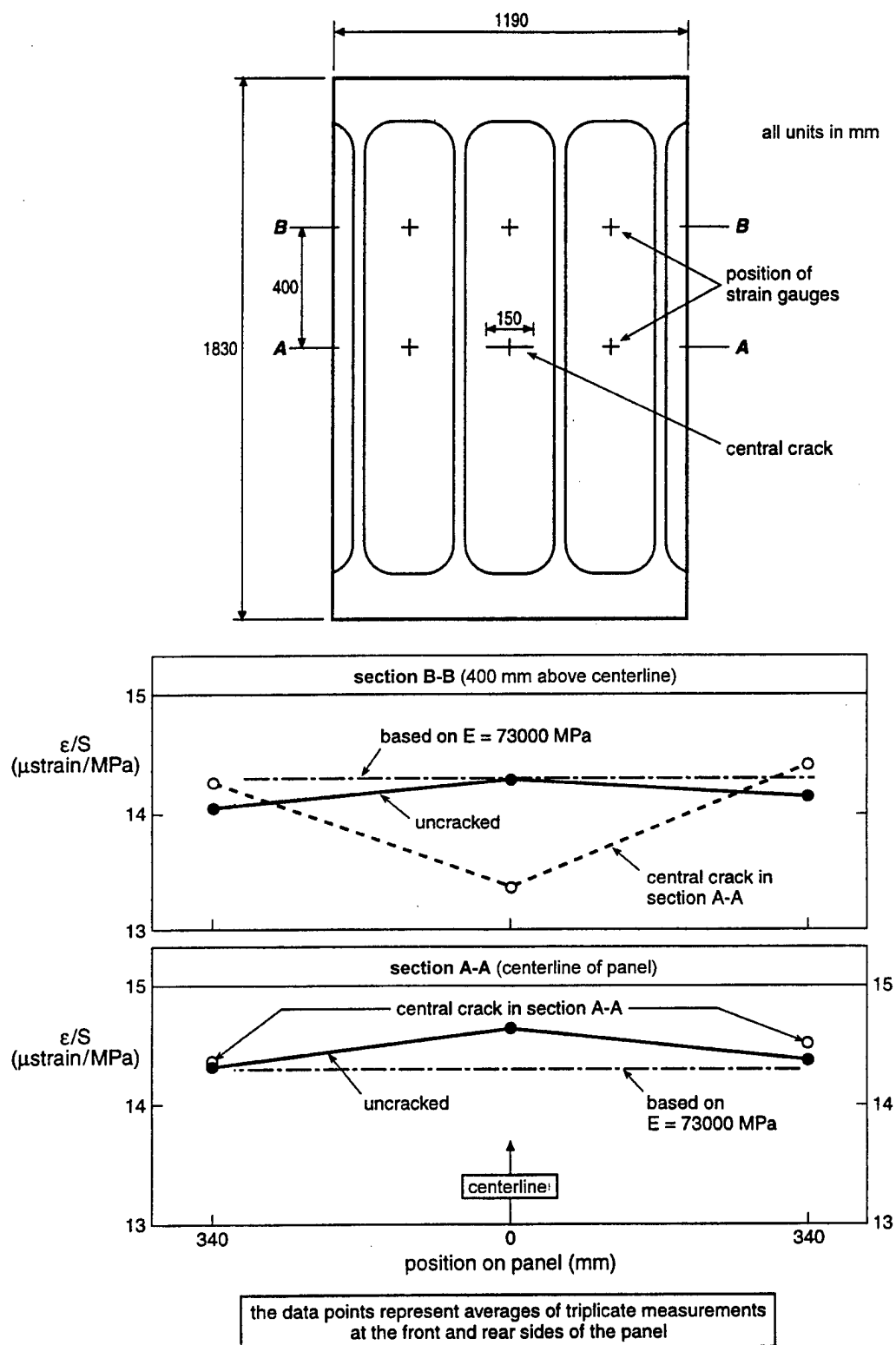
FIGURE 4. STRAIN DISTRIBUTIONS IN PANEL Ia1 WITH AND WITHOUT A
CENTRAL CRACK

There were only small differences between the strains measured on the front and rear sides of the skin in the centerline of the panel. The mean difference between opposite strain gauges was 2.4 percent of the average strain (maximum difference 4.2 percent) at 8 kN load. The differences between opposite strain gauges were larger in the section 400 mm above the centerline. In this section the mean difference between opposite strain gauges was 6.4 percent of the average strain (maximum difference 8.4 percent). The differences are probably due to the fact that the riveting process introduces more plastic deformations at the formed-head side.

Average strains, ε, were calculated from the measurements at the front and rear sides of the panel. Linear regression was then applied to every set of load-strain pairs to determine ε/S (average strain/stress). The stress S was calculated by dividing the applied load by the gross section of the panel. There were only negligible differences between the results of the triplicate measurements.

Mean values of ε/S at different locations on the panel, with and without a central crack, are shown in figure 4. An ε/S value based on an elastic modulus E = 73,000 MPa is also shown. The following trends were observed.

- The strain in the skin between the inner stiffeners is slightly higher than the strain in the skins between the outer and inner stiffeners (a difference of 1.3 and 2.0 percent for centerline and 400 mm above centerline, respectively).

- The mean strain in the centerline of the panel is slightly higher and the mean strain in the section 400 mm above the centerline is slightly lower than the strain based on an elastic modulus of 73,000 MPa. This indicates that there is some load transfer from the stiffeners to the skin along the panel length from 400 mm above the centerline to the centerline.

- A 150-mm-long crack in the center results in only a minor increase (0.7 percent) in the strain in the outer skin fields. This indicates that most of the load is transferred through the inner stiffeners.

- The effect of a 150-mm-long crack in the center of the skin on the strain in the section at 400 mm above that centerline is a substantial decrease in the strain in the central skin field (6.2 percent) and a small increase of the strain in the outer skin field (1.7 percent).

Generally, it can be concluded that there is an almost uniform strain distribution in the central section of the skin containing the fatigue cracks.

Figure 5 shows the strain at different positions in the skin with increasing nominal stress during the residual strength test of the panel. Only negligible differences between the strains in comparable outer skin fields can be observed. Again, this indicates a symmetric load introduction in the panel. A linear relationship between nominal stress and measured strains exists up to a stress of 150 MPa. At higher nominal stresses, there is a larger increase of the strains in the outer skin fields and a leveling off of the strain measured in the central skin field above the central crack. This is due to growth of the central crack during residual strength testing (see figure 6).
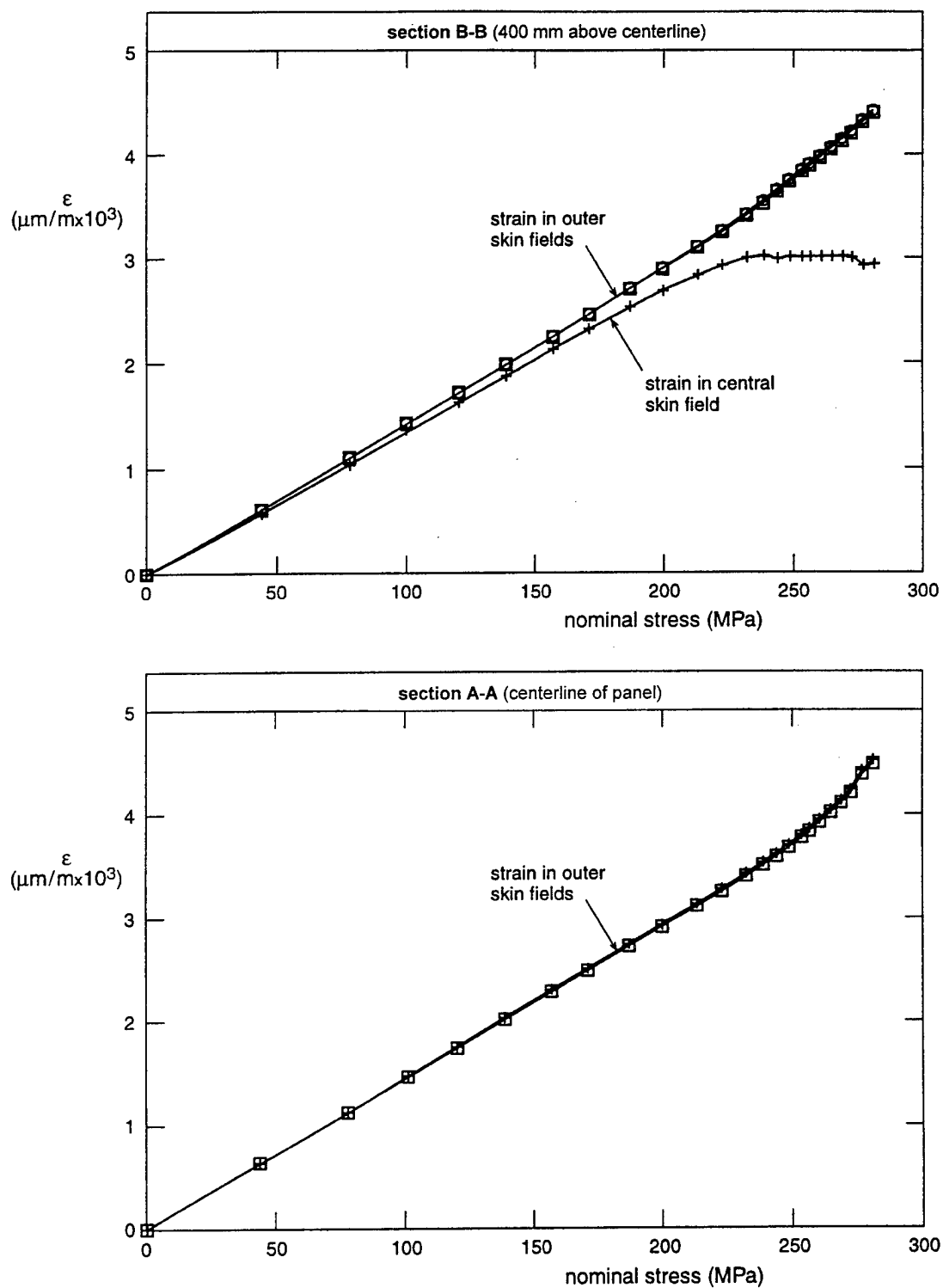
FIGURE 5. STRAIN AT DIFFERENT POSITIONS IN THE SKIN WITH
INCREASING NOMINAL STRESS IN THE PANEL
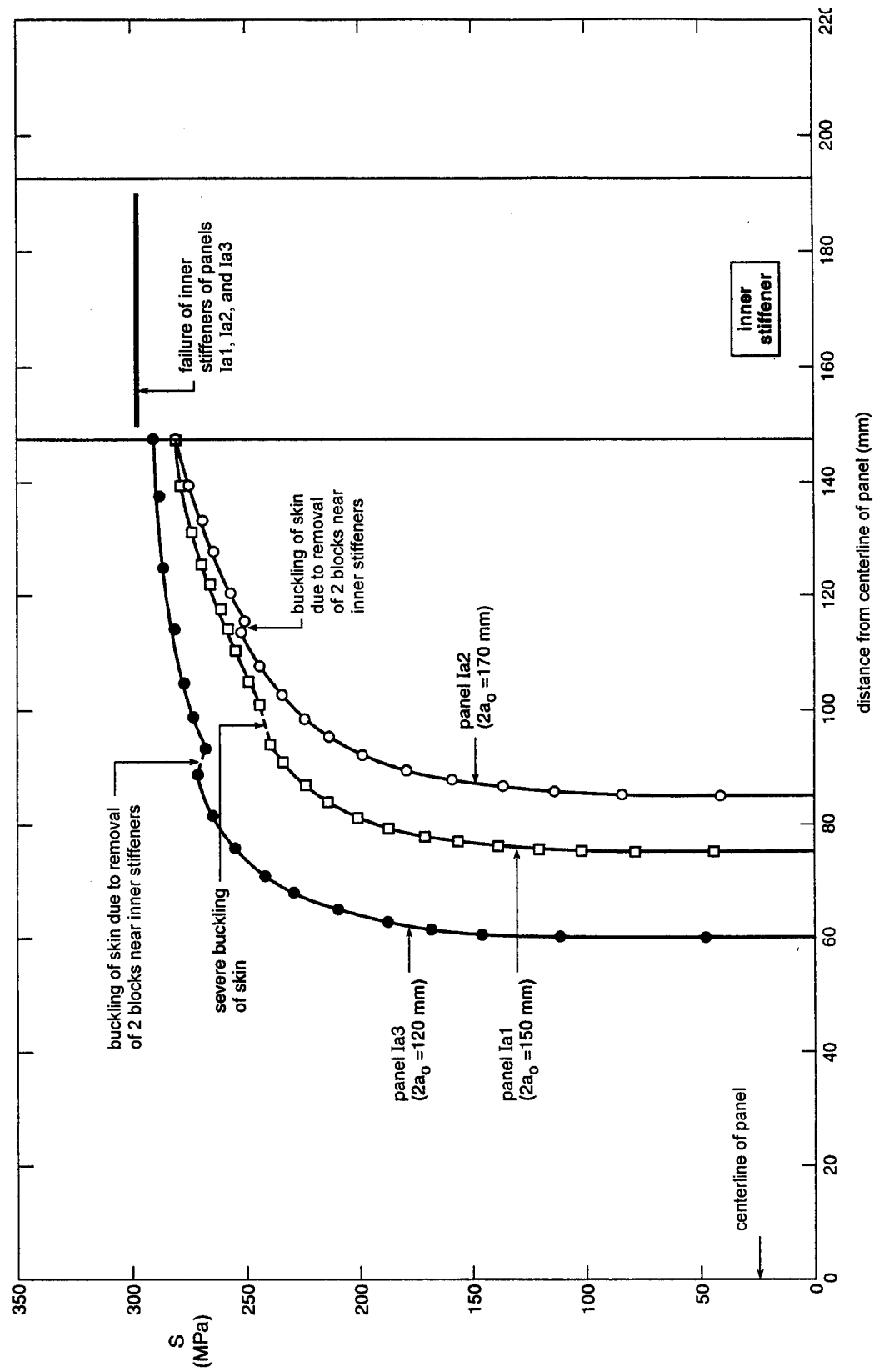(See figure 4 for positions of strain gauges.)

14

FIGURE 6. CRACK GROWTH CURVES FOR THREE PANELS OF CONFIGURATION I WITH DIFFERENT
LENGTHS, a_o, OF THE CENTRAL CRACK

3.4 RESULTS.

3.4.1 Crack Growth Data.

During the residual strength tests, static crack growth occurred in all panels. Crack lengths were measured as a function of the applied load. Stresses were calculated from the applied loads by dividing them by the actual gross section (based on actual thickness of skin plus stiffeners) of the panel. The nominal gross sections for Configuration I were: (1190 x 1.27 mm) + (8 x 45 x 2.06 mm) = 2253 mm^2 and for Configurations II and III: (1190 x 1.27 mm) + (6 x 45 x 2.06 mm) = 2068 mm^2.

In this section, stress-crack length relationships will be given for the different panel configurations. Crack growth was very symmetric for all panels. Therefore, only mean values are reported for crack growth at the left and right sides of the center of the panel.

3.4.1.1 Panel Configuration I.

Crack growth data for Configuration I (four stiffeners) panels are given in tabular form in tables 1 through 3 and in graphical form in figures 6 through 9. Figure 6 shows crack growth curves for three panels with different lengths a_0 of the central crack (no secondary cracks were present in these panels). Discontinuities can be observed in the curves for all three panels. This is due to buckling of the panels. Panel Ia1 was tested first. Support of the skin of this panel was not optimal (see section 3.3). At a half crack length of 94 mm, severe buckling occurred. For panels Ia2 and Ia3 the support of the skin was improved but the skin buckled when the small blocks closest to the inner stiffeners were removed from the front of the panel. This was done to read the crack length. The buckling caused the crack to grow at a lower stress.

For all three panels the crack reached the inner stiffeners before the stiffeners failed. The failure stresses for the inner stiffeners were almost equal for the three panels. For panel Ia3 with a central crack of 120 mm, the stress, when the crack grew to the inner stiffeners, was closest to the failure stress of the stiffeners. This was considered to be a favorable situation for investigation of the influence of added secondary cracks on the residual strength behavior of the panel. Therefore, a length of 120 mm was selected for the central lead crack of panels Ib, Ic, and Id, all with secondary cracks.

Figure 7 shows crack growth curves for panel Ib with a central lead crack and secondary cracks inside the inner stiffeners. The crack growth curve for panel Ia3 with only a central crack of the same length is added for comparison. The effect of the secondary crack on the growth of the central crack becomes apparent at a stress of about 125 MPa. Linkup of the central crack and the secondary cracks occurred far below the failure stress of the inner stiffeners (stress at linkup is 70 percent of failure stress). After linkup further static crack growth took place and the crack reached the inner stiffeners at a substantially lower stress than that for panel Ia3 with a central crack only. But, failure of the inner stiffeners occurred at an almost equal stress for both panels.

16

TABLE 1. CRACK GROWTH DATA FOR PANELS Ia1, Ia2, AND Ia3

Panel Ia1		Panel Ia2		Panel Ia3	
S, MPa	a_1, mm	S, MPa	a_1, mm	S, MPa	a_1, mm
44.3	75.00	40.9	84.98	44.5	60.06
77.8	75.00	84.5	84.98	111.6	60.12
102.0	75.22	114.3	85.48	145.7	60.70
120.9	75.60	136.8	86.51	168.6	61.79
139.5	76.12	159.6	87.76	187.6	62.84
157.4	76.95	179.3	89.26	209.5	64.68
171.5	78.14	199.0	92.03	228.5	67.62
187.4	79.40	213.4	95.05	241.7	70.88
200.4	81.24	224.3	98.29	255.2	75.37
213.8	84.08	234.7	102.39	265.0	81.40
223.6	87.02	244.2	107.75	270.8	87.60
239.6	91.20	252.4	113.44	267.7	93.21
244.7	93.98	250.6	115.57	273.6	98.71
249.3	100.99	257.3	120.56	277.0	104.46
254.2	104.92	264.7	127.83	280.9	114.01
257.2	110.05	269.4	133.32	285.7	124.81
261.1	113.99	275.3	139.24	287.7	137.28
265.5	117.50	281.6	147.50	290.5	147.50
269.5	121.88	297.4	failure of inner stiffeners	296.5	failure of inner stiffener
273.6	125.47				
278.6	131.12				
281.7	139.42				
296.6	147.00 failure of inner stiffeners				

position of inner stiffener

Figure 8 shows crack growth curves for panel Ic with a central lead crack and secondary cracks outside the inner stiffeners. Again, the crack growth curve for the panel with only a central crack is also shown. It can be seen that the growth of the central crack was hardly influenced by the secondary cracks. However, failure of the inner stiffeners occurred at a 7 percent lower stress than that for the panel with a central crack only.
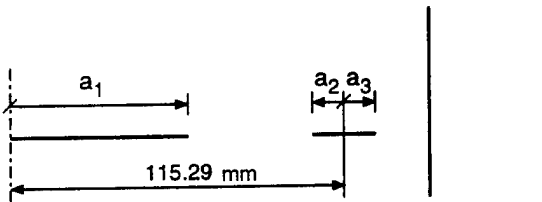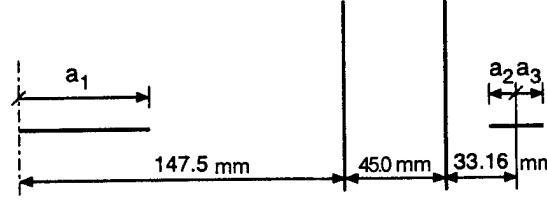
TABLE 2. CRACK GROWTH DATA FOR PANELS Ib AND Ic

Panel Ib				Panel Ic			
S MPa	Crack length, mm			S MPa	Crack length, mm		
	a_1	a_2	a_3		a_1	a_2	a_3
45.1	60.03	12.49	12.49	45.6	60.51	12.57	12.57
90.6	60.12	12.49	12.49	111.8	60.60	12.57	12.57
115.7	60.39	12.49	12.49	135.6	61.07	12.57	12.57
139.0	61.02	12.49	12.49	160.9	61.81	12.57	12.57
161.1	61.93	12.62	12.83	183.2	63.11	12.57	12.57
177.3	63.18	12.73	13.14	204.2	64.73	12.57	12.57
192.8	66.01	13.19	14.54	223.4	67.27	12.86	12.68
201.7	68.30	14.02	15.37	239.0	71.12	13.06	13.06
207.2	linkup	linkup		254.1	76.10	13.31	13.35
203.7			20.90	262.3	82.07	13.60	13.64
212.9			22.20	267.5	92.04	14.50	14.33
221.7			25.07	270.1	101.77	15.35	14.68
230.2			27.83	272.4	108.30	15.99	15.73
237.6			30.31				
243.9			32.70				
294.8	failure of inner stiffeners			275.9	failure of inner stiffeners		

Figure 9 shows crack growth curves for panel Id with a central lead crack and secondary cracks inside and outside the inner stiffeners. The crack growth curves for the panels with only a central crack and with a central crack plus secondary cracks inside the inner stiffeners are shown for comparison. It can be seen that the secondary cracks outside the inner stiffeners only have a small influence on the growth of the central crack and on that of the secondary cracks inside the inner stiffeners. Linkup of the central crack and the secondary cracks inside the stiffeners occurred at a 1.2 percent lower stress than that for panel Ib which did not have secondary cracks outside the inner stiffeners. After the first linkup, the large central crack grew under the stiffeners and linked up with the secondary cracks outside the stiffeners. The second linkup

18

TABLE 3. CRACK GROWTH DATA FOR PANEL Id

S MPa	Crack length, mm				
	a_1	a_2	a_3	a_4	a_5
44.9	60.02	12.62	12.62	12.45	12.45
91.8	60.21	12.62	12.62	12.45	12.45
122.3	60.61	12.62	12.62	12.45	12.45
142.3	61.15	12.72	12.62	12.45	12.45
159.4	61.89	12.91	12.75	12.45	12.45
172.8	62.63	13.10	13.01	12.49	12.45
186.7	64.42	13.69	13.16	12.56	12.50
195.0	66.53	14.67	13.43	12.58	12.52
202.3	69.86	16.42	14.53	12.60	12.53
204.3	72.48	18.39	15.61	12.77	12.65
204.8	linkup	linkup			
200.4			21.33	13.07	12.83
210.9			23.30	13.28	13.03
219.2			26.06	13.68	13.37
225.2			28.70	14.07	13.80
231.2			31.88	14.62	14.39
235.6			crack	15.76	15.20
238.7			under	16.24	15.77
247.6			stiffener	18.95	17.88
253.6				21.49	20.28
256.6			linkup	linkup	
238.9					44.15
245.6					51.32
245.8	failure of inner stiffeners				

stress was 13 percent lower than the stress at failure of the inner stiffeners of panel Ib. After some further crack growth, the inner stiffeners failed at a lower stress than the second linkup stress. It must be noted that the inner stiffeners would have failed at the second linkup stress if the test had been done under load control.
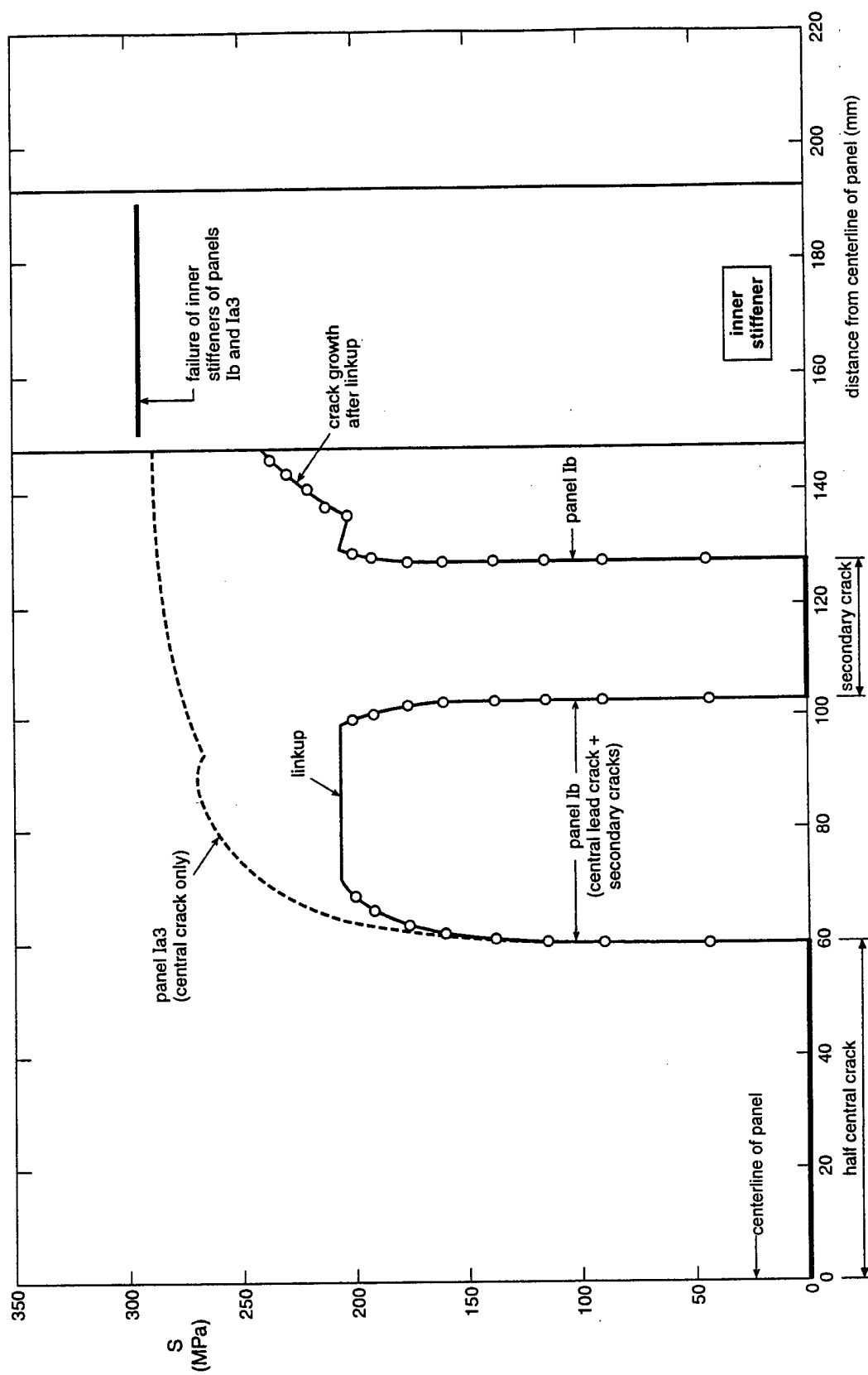
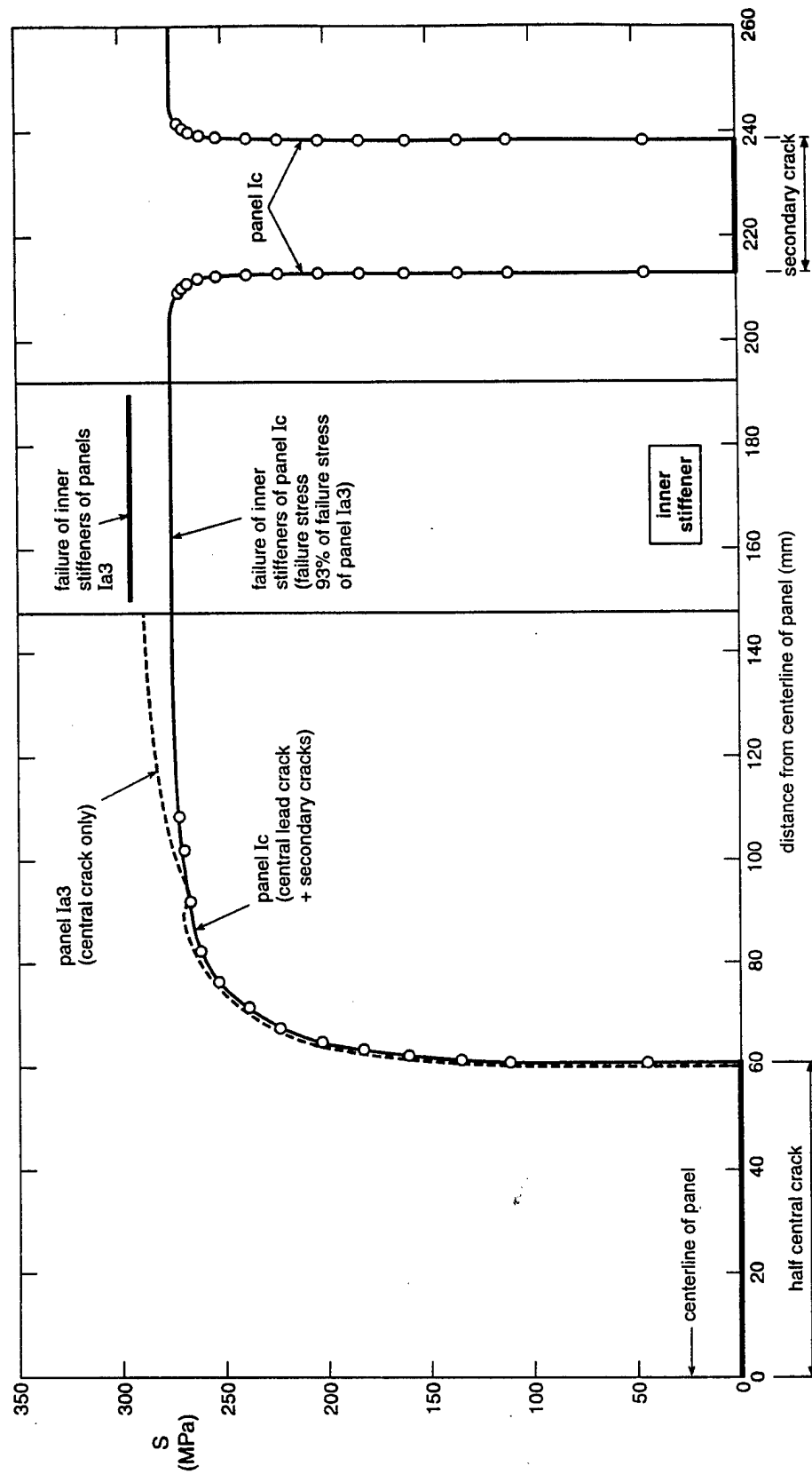FIGURE 7. CRACK GROWTH CURVE OF PANEL Ib COMPARED WITH THAT OF PANEL Ia3

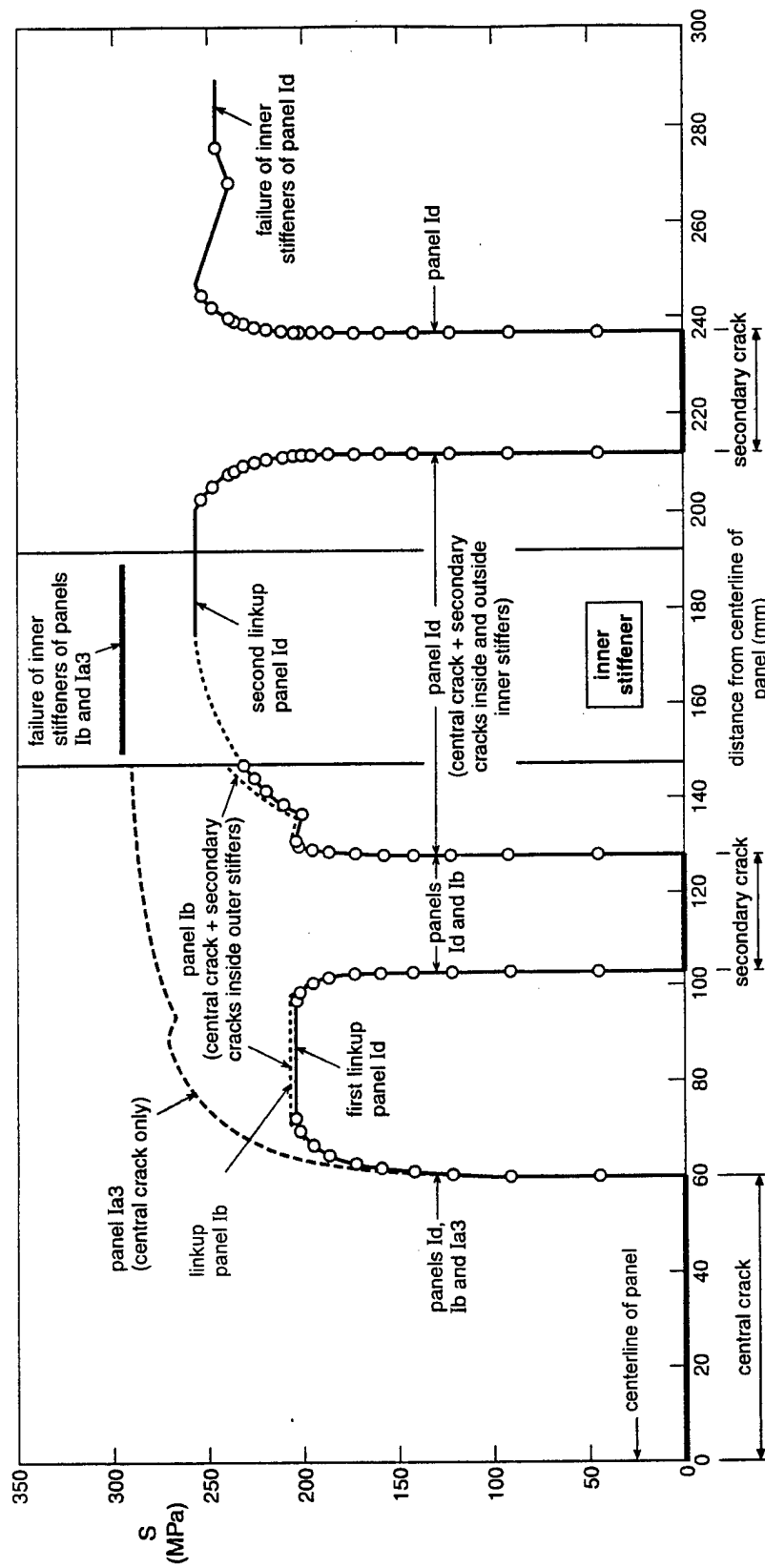FIGURE 8. CRACK GROWTH CURVE OF PANEL Ic COMPARED WITH THAT OF PANEL Ia3

21

FIGURE 9. CRACK GROWTH CURVE OF PANEL Id COMPARED WITH THOSE OF PANELS Ia3 AND Ib

3.4.1.2 Panel Configuration III.

Crack growth data for the panels with Configuration III (three stiffeners, central stiffener cut) are given in tables 4 through 6 and are shown in figures 10 through 12. Figure 10 shows crack growth curves for two panels with different lengths of the central crack. For panel IIIa1, with an initial crack length of 300 mm, the stress first peaked at a half crack length of 215 mm. The stress then decreased with further crack growth and then increased again until the crack reached the stiffeners. The panel failed after a 6 percent increase of the stress.

A maximum stress in panel IIIa2 occurred at a half crack length of 145 mm. The stress significantly decreased with further crack growth and slightly increased before the crack reached the stiffeners and the panel failed. The failure stress was slightly higher than that for panel IIIa1, which had a longer initial crack. It was decided to use a length of 160 mm for the central crack in panels IIIb and IIIc, both with secondary cracks. A relatively small initial length of the central crack was selected so that a large crack range was available for the investigation on the effect of the linkup of the secondary cracks.
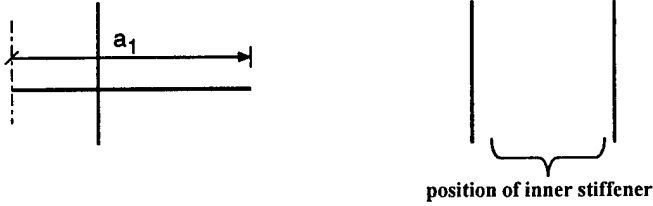
The residual strength behavior would have been different if the residual strength tests had been done under load control instead of displacement control. For panel IIIa1, unstable crack extension would have occurred at a half crack length of 215 mm when the first peak in the stress was reached. The crack growth would have stopped before the stiffeners were reached and the panel would have failed at the same stress as in the present test. For panel IIIa2 also, the crack extension would have become unstable at the maximum stress at a half crack length of 145 mm. But in this case, the unstable crack extension would have resulted in failure of the panel because this maximum stress was higher than the failure stress of the panel.

Figure 11 shows crack growth curves for panel IIIb with a central lead crack and two secondary cracks, each of them located between the central stiffener and one of the outer stiffeners. The crack growth curve for panel IIIa2 with only a central crack is shown for comparison. The growth of the central crack in panel IIIb was only influenced by the secondary cracks at stresses above 140 MPa. Linkup of the central crack and the secondary cracks occurred at a stress level that was 8% lower than the maximum stress for panel IIIa2 without secondary cracks. After linkup, crack growth continued until the crack reached the stiffener. Failure occurred at a stress that was 2.5% lower than that for the panel without secondary cracks. In the case of load control unstable crack extension would have occurred after linkup and the crack would probably have arrested at the stiffeners.

Figure 12 shows the crack growth curves for panel IIIc with a central lead crack and four secondary cracks, i.e., with two secondary cracks between the central stiffener and one of the outer stiffeners. Again, the growth of the central crack was only slightly influenced by the secondary cracks. The first linkup stress is 11 percent below the maximum stress for the panel without secondary cracks. So linkup occurred at a slightly smaller stress for panel IIIc than for panel IIIb with only two secondary cracks. After the first linkup a second linkup occurred at a lower stress and the tips of the resulting large crack were close to the stiffeners. Failure occurred after a load increase at a stress level nearly identical to the failure stress of panel IIIb. In case of load control the central crack would have jumped to the stiffeners at the first linkup stress.

23

TABLE 4. CRACK GROWTH DATA FOR PANELS IIa, IIIa1, AND IIIa2

Panel IIa		Panel IIIa1		Panel IIIa2	
S, MPa	a_1, mm	S, MPa	a_1, mm	S, MPa	a_1, mm
49.7	150.1	40.6	150.1	48.7	80.3
74.2	150.1	64.7	150.3	74.7	80.6
97.8	150.2	82.5	151.3	94.5	81.1
120.5	150.8	99.2	153.0	113.3	82.3
141.4	151.4	113.7	155.7	130.5	84.4
158.9	152.1	128.8	160.5	143.8	86.5
175.1	153.2	139.7	167.7	155.1	89.2
192.0	154.7	147.3	175.7	163.9	93.5
203.7	156.0	153.9	190.3	174.6	99.0
211.5	157.9	154.8	198.3	178.9	103.5
219.7	160.1	157.0	208.5	185.4	120.3
226.1	162.6	156.1	228.1	189.2	131.9
231.9	165.6	155.7	248.1	190.3	141.9
235.8	167.8	157.3	265.9	187.8	169.2
239.2	171.5	159.0	277.8	186.3	188.0
242.1	176.0	161.4	286.8	181.5	218.0
245.5	184.3	165.4	301.9	178.6	241.7
246.5	193.6	178.6	panel	178.4	265.9
245.5	207.3		failure	178.5	279.9
245.0	220.5			180.2	300.8
	failure			181.3	312.0
	of central			183.3	panel
	stiffener				failure
192.0	262.7				
199.3	306.0				
194.5	panel				
	failure				

position of inner stiffener

TABLE 5. CRACK GROWTH DATA FOR PANEL IIIb

Panel IIIb			
S MPa	Crack length, mm		
	a_1	a_2	a_3
48.8	80.27	12.59	12.59
73.2	80.74	12.59	12.59
92.7	81.11	12.59	12.59
112.6	82.61	12.59	12.59
129.7	84.24	12.59	12.59
147.4	87.34	12.73	12.59
157.8	90.64	12.91	12.68
166.8	96.14	13.19	12.91
171.8	101.09	13.62	13.20
173.0	106.47	14.90	13.66
173.7	113.62	16.38	14.63
174.2	linkup	linkup	
150.4			37.42
154.6			44.86
155.1			55.71
157.1			66.17
162.7			87.04
166.3			97.96
170.8			110.76
178.7	panel failure		
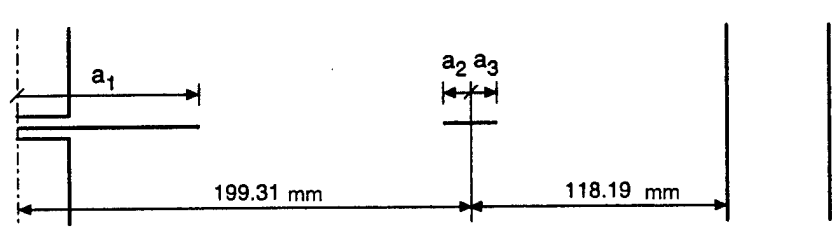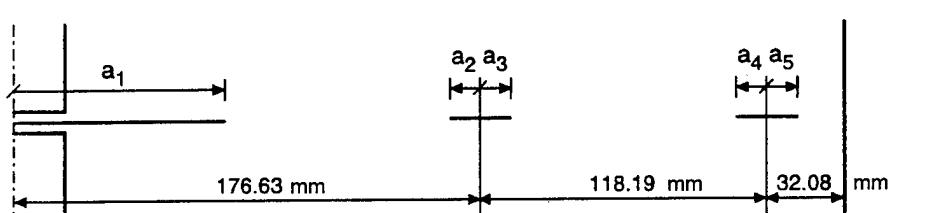
TABLE 6. CRACK GROWTH DATA FOR PANEL IIIc

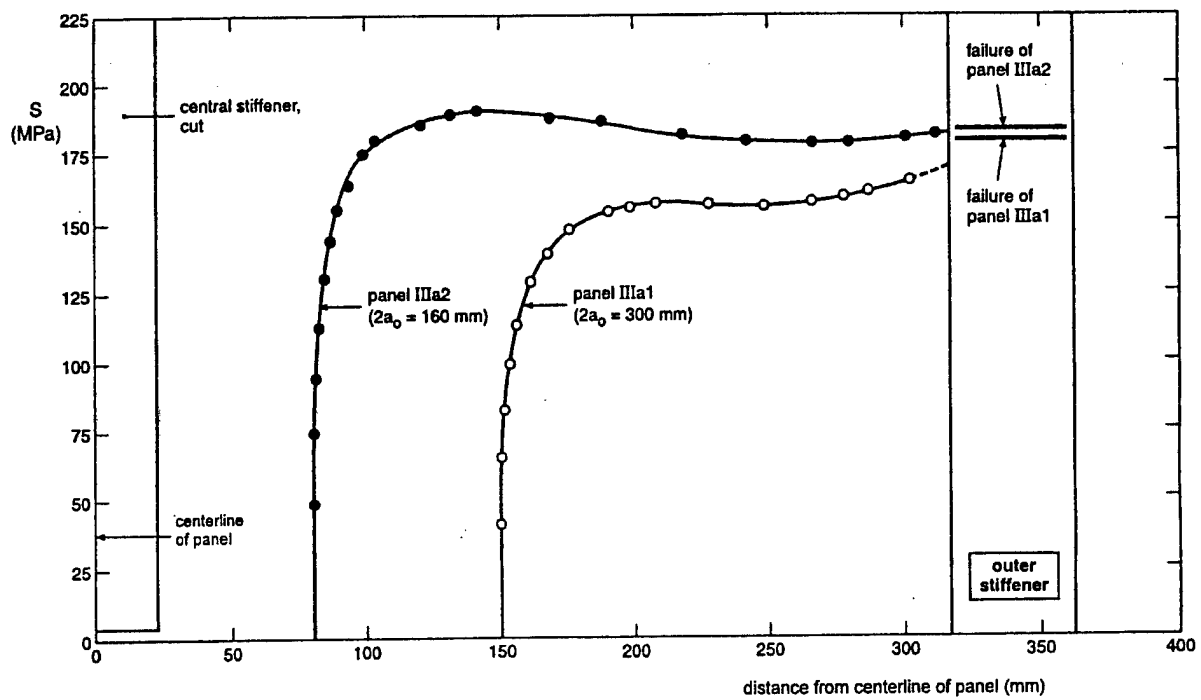| Panel IIIc					
S MPa	Crack length, mm				
	a_1	a_2	a_3	a_4	a_5
50.8	80.01	12.57	12.57	12.57	12.57
76.3	80.26	12.57	12.57	12.57	12.57
97.6	80.84	12.57	12.57	12.57	12.57
116.8	82.28	12.61	12.57	12.57	12.57
136.2	84.84	12.70	12.57	12.57	12.57
147.6	86.75	12.88	12.57	12.63	12.57
157.7	90.31	13.23	12.77	12.73	12.57
163.7	93.91	13.90	13.20	12.84	12.57
166.4	98.14	14.63	12.70	12.88	12.63
168.1	102.52	16.09	14.39	12.92	12.74
168.6	linkup	linkup			
144.0			76.85	20.86	17.54
146.5			linkup	linkup	
133.7					27.86
136.1					29.15
177.1	panel failure				

FIGURE 10. CRACK GROWTH CURVES FOR TWO PANELS OF CONFIGURATION III
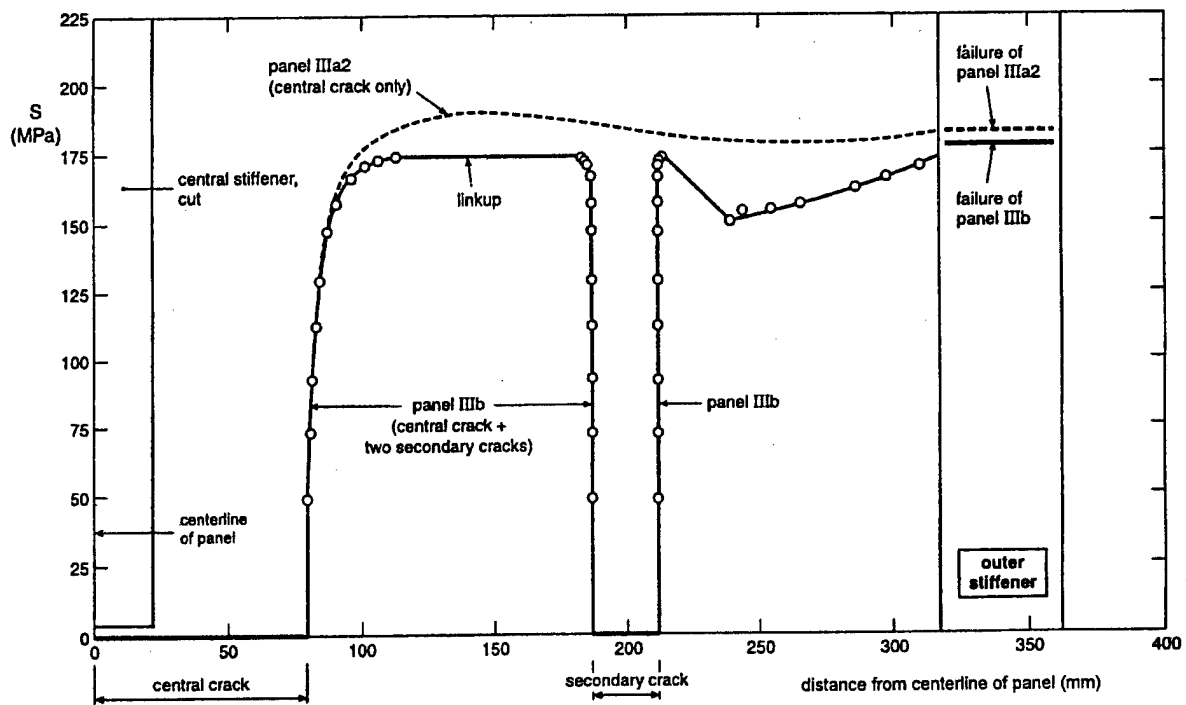WITH DIFFERENT LENGTHS, a_o, OF THE CENTRAL CRACK

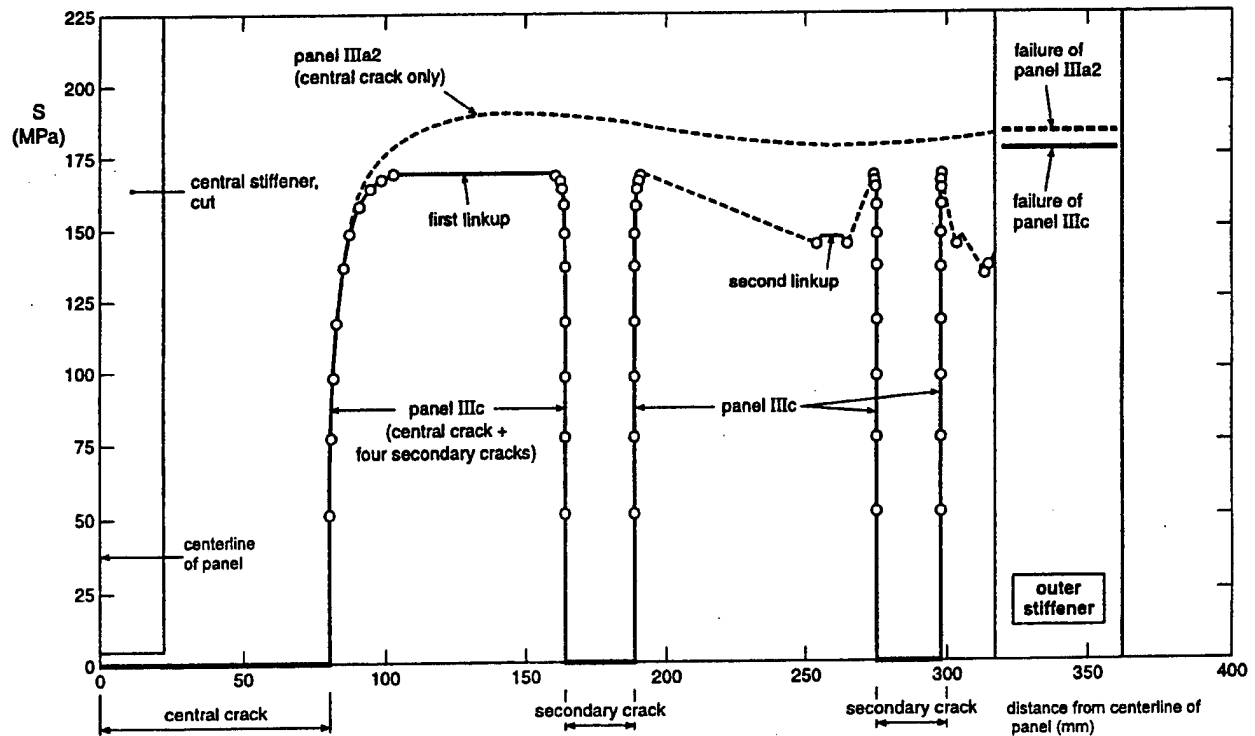FIGURE 11. CRACK GROWTH CURVE OF PANEL IIIb COMPARED WITH
THAT OF PANEL IIIa2

27

FIGURE 12. CRACK GROWTH CURVE OF PANEL IIIc COMPARED WITH
THAT OF PANEL IIIa2

3.4.1.3 Panel Configuration II.

Crack growth data for panel IIa (3 stiffeners, all intact) are given in table 4 and are shown in figure 13. The crack growth curve for panel IIIa1, with the same initial crack length but with a cut central stiffener, is added for comparison. It can be seen that a much higher maximum stress is reached with an intact central stiffener. The central stiffener failed at a half crack length of 225 mm. The crack arrested and after further crack growth at a much lower stress the panel failed. If load control had been applied, the failure of the central stiffener would have resulted in failure of the panel. In this case the failure stress of the panel with an intact central stiffener would have been 37 percent higher than that of the panel with a broken central stiffener.
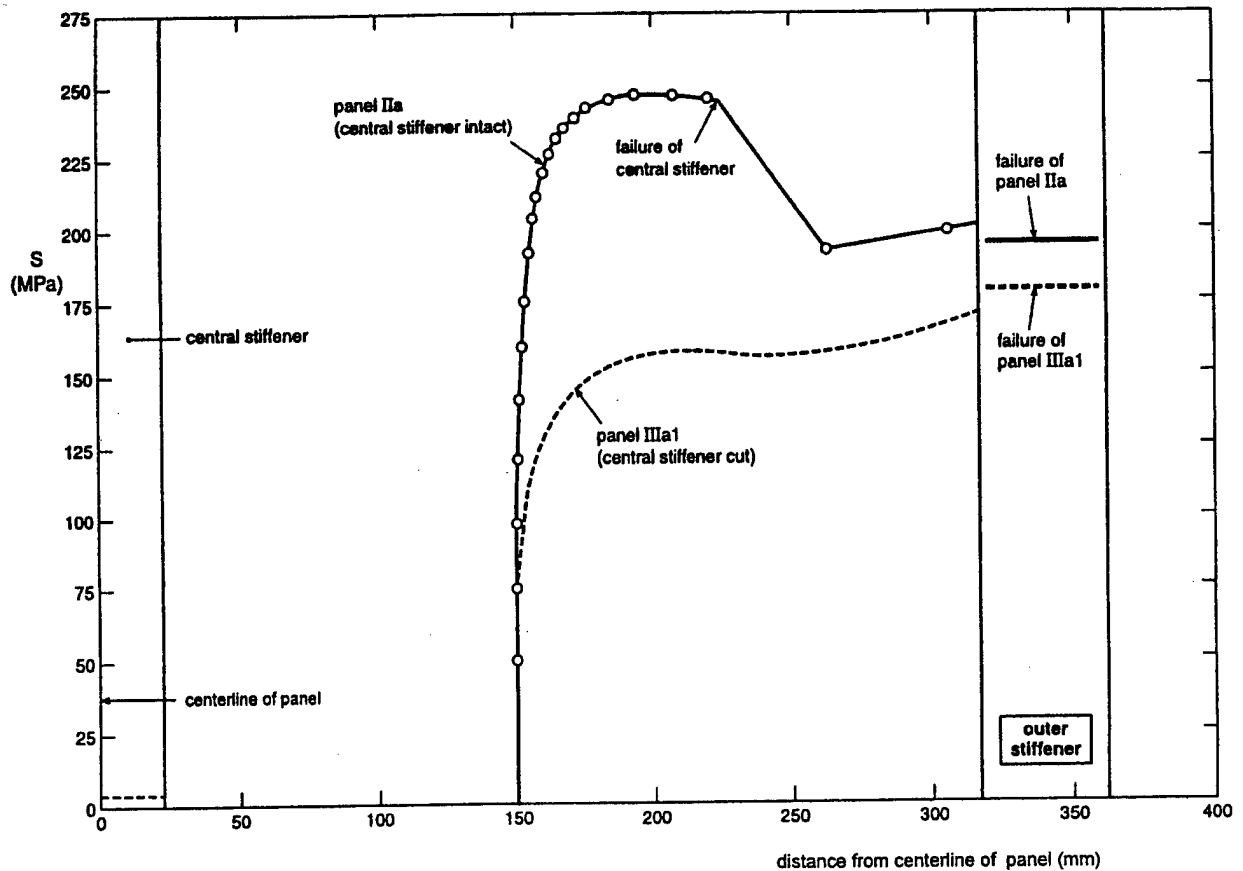
FIGURE 13. CRACK GROWTH CURVE OF PANEL IIa COMPARED WITH
THAT OF PANEL IIIa1

3.4.2 Stress-COD Curves.

During the residual strength tests, records were made of load versus crack opening displacement (COD). The COD was generally measured in the center of the central crack in the panels (the location of COD measurement was different for panel IIa). Stress-COD curves were derived from the load-COD curves and are presented in appendix A for all tested panels. In figure 14 the curves for panels Ia3 and Id are shown as an example. The effect of the secondary cracks in panel Id can clearly be observed. The stress-COD curves can be used as a reference for analytical COD determinations.
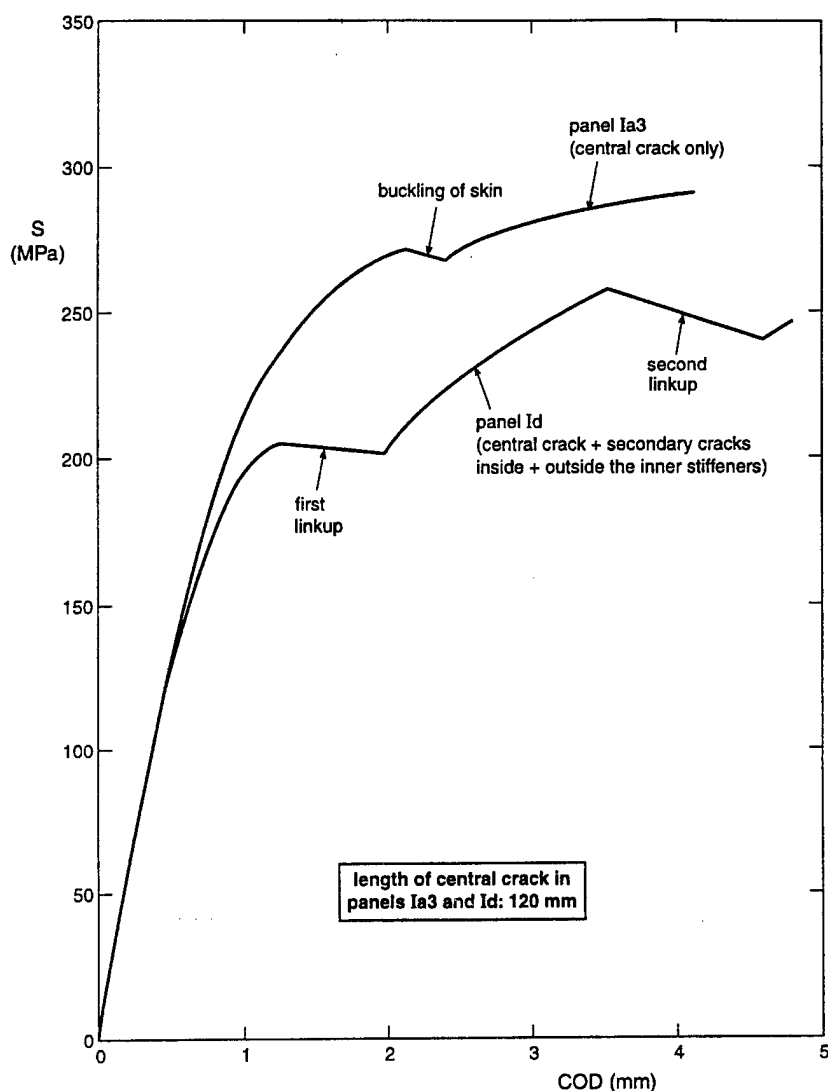
FIGURE 14. STRESS-COD CURVES FOR TWO CONFIGURATION I PANELS

3.4.3 Strains in Central Stiffeners of Panel IIa.

During residual strength testing of panel IIa, strains were measured in the central stiffeners that crossed the central crack. Fourteen strain gauges were bonded to the stiffeners, 7 on the stiffener on the front side and 7 on the stiffener on the back side of the panel; the strain gauges on the back were placed opposite to the strain gauges on the front side of the panel. The positions of the strain gauges are indicated in figure 15.

Substantial differences were found between the strains measured with the strain gauges on the front and back, e.g., the strain differences were 3.8 to 18.1 percent (mean 9.2 percent) of the average strain at a nominal stress of 200 MPa. The strains were consistently higher in the stiffener on the front side of the panel. Figure 15 shows the average strains of opposite strain gauges as a function of the nominal stress (load divided by gross section of skin plus stiffeners).

30

The strains at comparable positions above and below the central crack are combined in one figure. The average strains at these positions are identical. Unfortunately, there was premature failure of strain gauge number 8 at a stress of about 210 MPa.
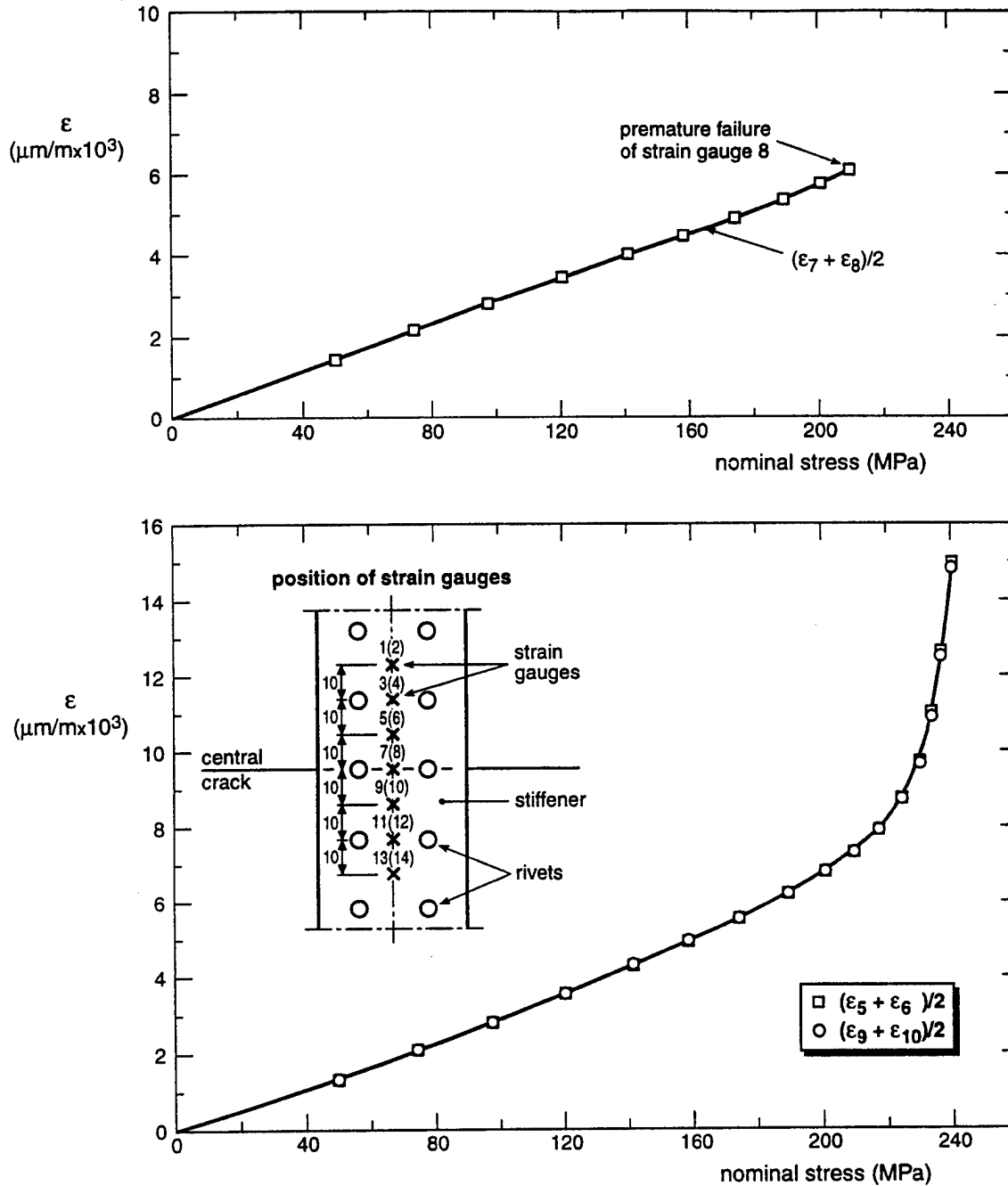

FIGURE 15. STRAINS AT DIFFERENT POSITIONS ON CENTRAL STIFFENER OF PANEL IIa AS A FUNCTION OF NOMINAL STRESS
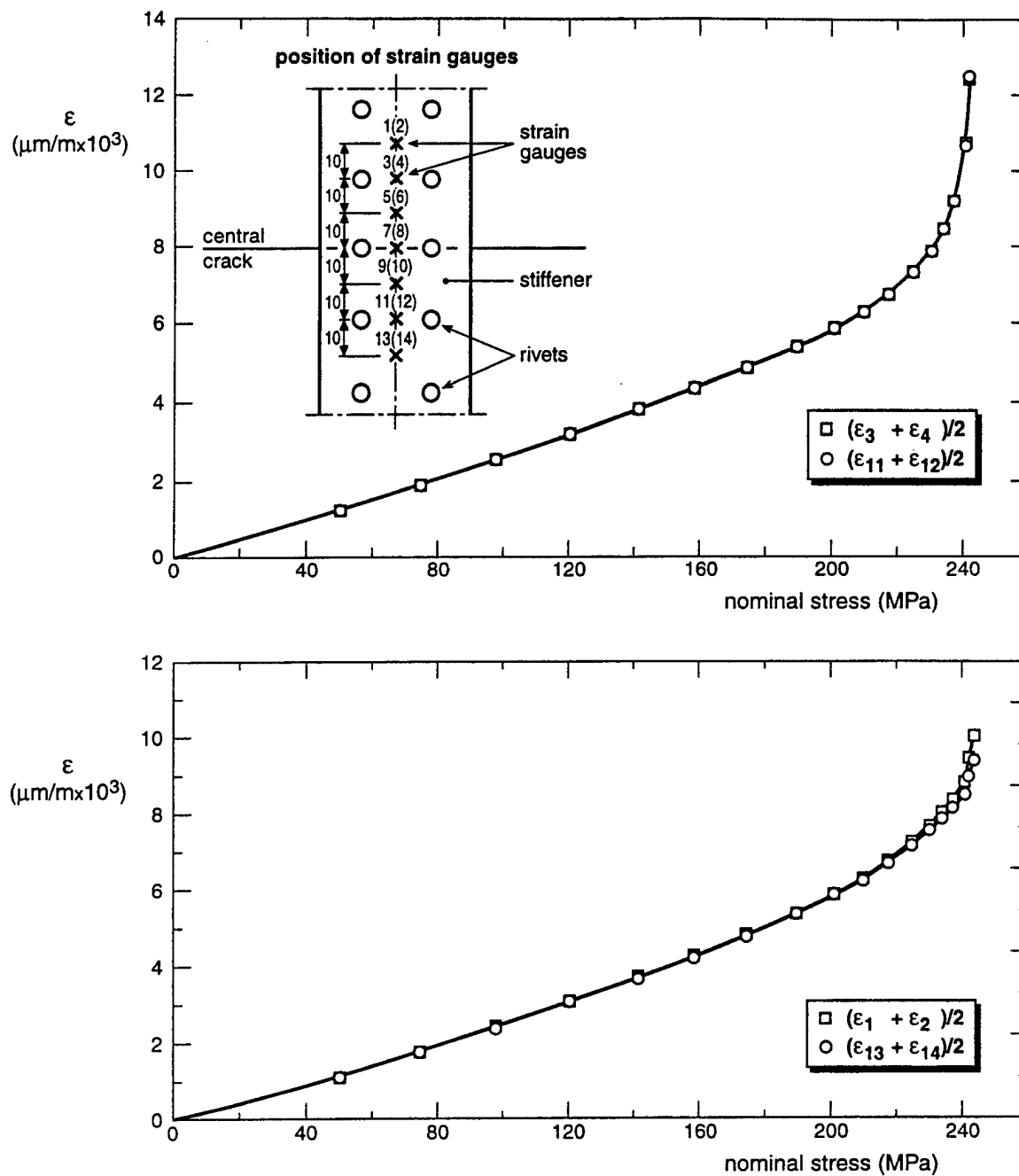
FIGURE 15. STRAINS AT DIFFERENT POSITIONS ON CENTRAL STIFFENER OF
PANEL IIa AS A FUNCTION OF NOMINAL STRESS (Continued)

Figure 16 compares the avenge strains for different positions on the central stiffeners. The strain data for comparable positions above and below the central crack were combined. Generally, there are only small differences between the strains at different positions, although the strains at a distance of 10 mm above the central crack are slightly higher than those at other positions. However, there is a difference in behavior between the strains in the stiffeners directly above the central crack (strain gauges 7 and 8) and the strains in the stiffeners at positions remote from the central crack. The stress-strain curves for positions remote from the central crack show an increasing rate of strain increase with increasing nominal stress, especially for large nominal stresses which result in the growth of the central crack (see figure 13). The strain increase at these large stresses is faster for positions nearer to the central crack. Contrary to this behavior an almost linear relation can be observed between the strains in the stiffeners directly above the central crack for nominal stress up to 210 MPa. Unfortunately, there is no strain data available for larger stresses.
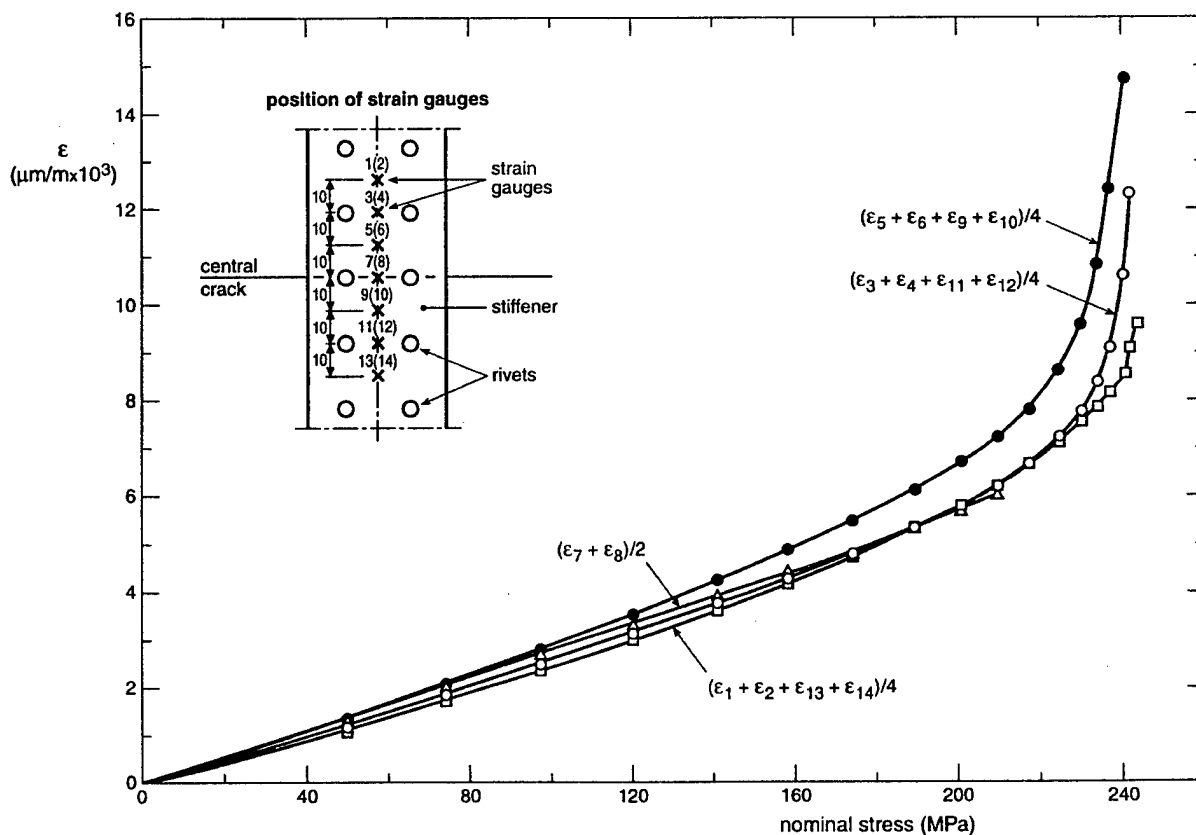

FIGURE 16. COMPARISON OF STRAINS AT DIFFERENT POSITIONS ON CENTRAL
STIFFENER OF PANEL IIa

3.4.4 Crack Opening Angle.

The crack opening angle (COA) was determined for different crack lengths in panel Ia2. During the residual strength test of this panel, photographs were taken of both crack tips while the

33

displacement controlled loading was stopped for a crack length measurement. The crack was fully open at the moment that the photographs were taken. Figure 17 shows, as an example, a photograph taken at a crack length of 127.8 mm.
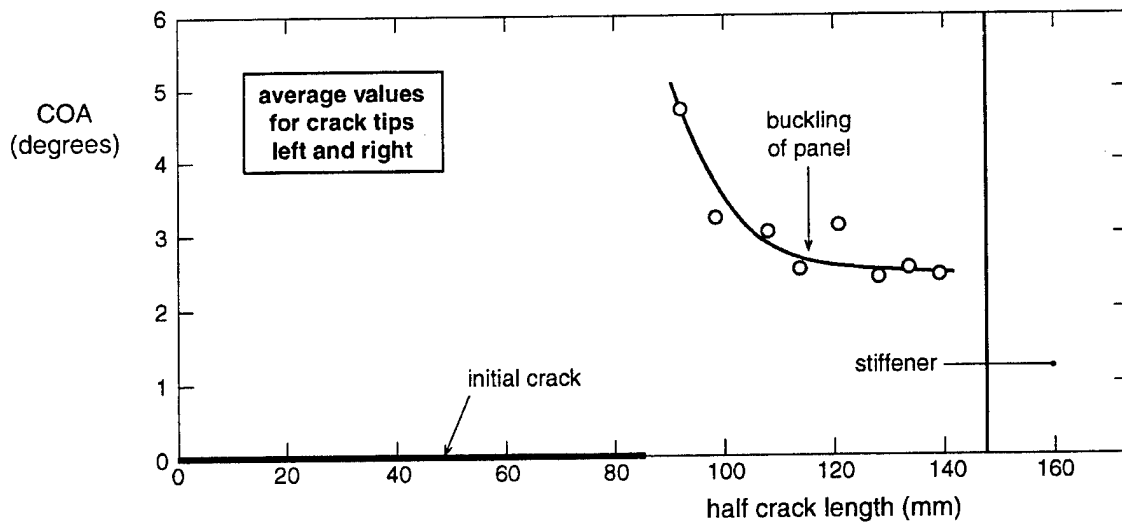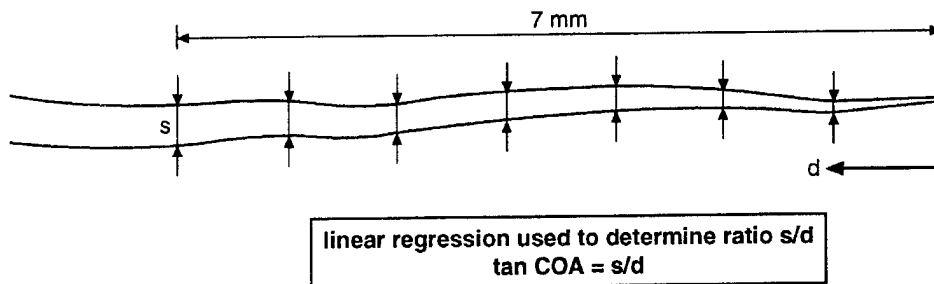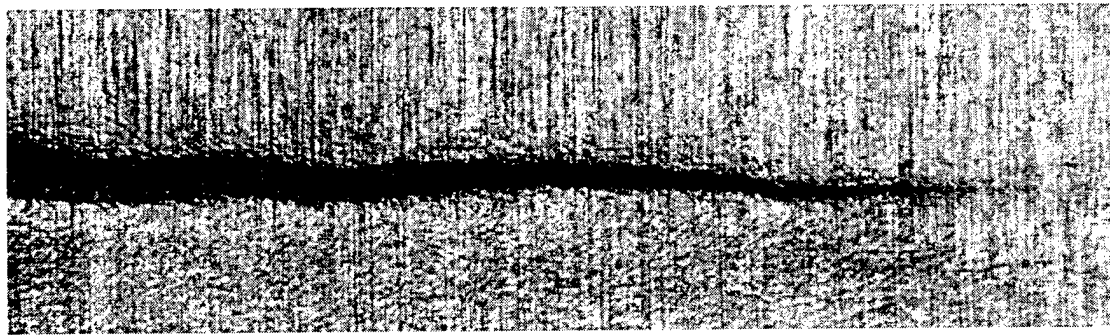

FIGURE 17. CRACK OPENING ANGLE AS A FUNCTION OF CRACK LENGTH FOR PANEL Ia2

34

The distances, s, between the crack faces were measured from the photograph at regularly increasing distances, d, from the crack tip, as indicated in figure 17. Linear regression was used to determine the ratio s/d. The crack opening angle was calculated from tan (COA) = s/d. Generally, the last 7 mm of crack length nearest the crack tip and intervals of 15 mm on the photograph were used to determine the s/d ratio.

The results of the COA determinations are also given in figure 17. The data points represent average values for left- and right-hand crack tips. An initially decreasing COA with increasing crack length can be observed, until a more or less constant value of 2.5° is reached at a half crack length of about 120 mm. The relatively large COA at a half crack length of 120.6 mm may be due to buckling of the panel shortly before photographing the crack tips.

3.4.5 Buckling.

During testing of the first panel (Ia1) severe buckling occurred. A more efficient support of the skin was then used (see section 3.3.1) but substantial buckling still occurred in the next panel (Ia2) tested. All further panels were supported in the same way as was done for panel Ia2. During the residual strength tests on these panels, the out-of-plane deformations were measured at a number of crack lengths to obtain an impression of the pattern and magnitude of the deformations. The results of the measurements are presented in appendix B.

Figure 18 shows, as an example, the buckling pattern at the rear side of panel IIIb, from just before linkup of the central crack with the secondary cracks until failure of the panel. The stresses for each are indicated on the photographs. The measured crack lengths at these stresses can be found in table 5 and figure 11.

It can be seen that linkup increased the magnitude of the out-of-plane deformations but did not change the buckling pattern. Increasing the stress resulted in increased buckling. The buckling pattern remained rather symmetric until the crack approached the stiffeners and grew beneath them. Then more severe buckling occurred on one side of the panel (see photographs of stresses at 170.8 and 172.1 MPa in figure 18).

Figure 19 shows the front side of panel IIIb. The panel broke in two on one side of the panel. For the Configuration I panels failure of the inner stiffeners did not result in total failure of the panel, but the crack arrested in the skin between the inner and outer stiffeners. An example of a Configuration I panel after failure of the inner stiffeners is shown in figure 20.

35

S = 173.7 MPa (before linkup)
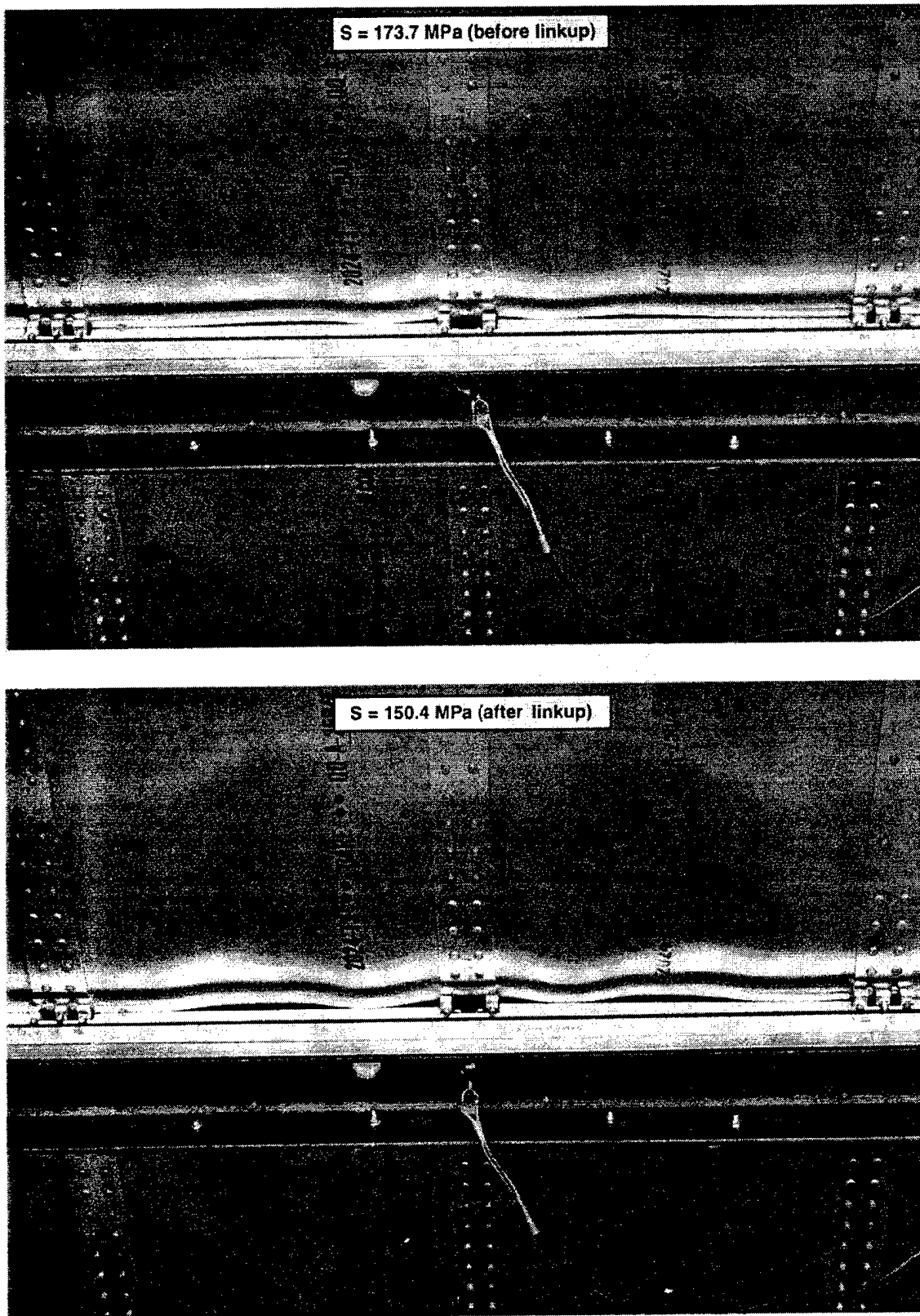
S = 150.4 MPa (after linkup)

FIGURE 18. BUCKLING OF PANEL IIIb IN DIFFERENT PHASES OF THE RESIDUAL
STRENGTH TEST (VIEW AT REAR SIDE OF PANEL)

FIGURE 18. BUCKLING OF PANEL IIIb IN DIFFERENT PHASES OF THE RESIDUAL
STRENGTH TEST (VIEW AT REAR SIDE OF PANEL) (Continued)

S = 166.3 MPa

S = 170.8 MPa
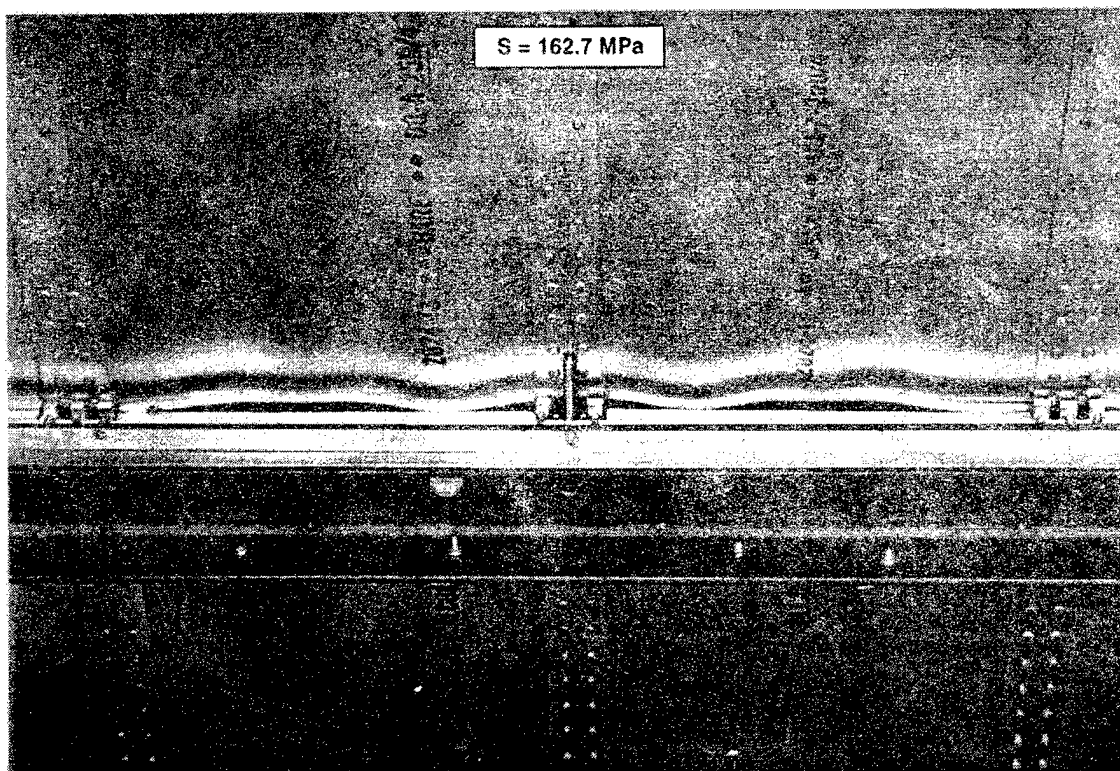
FIGURE 18. BUCKLING OF PANEL IIIb IN DIFFERENT PHASES OF THE RESIDUAL
STRENGTH TEST (VIEW AT REAR SIDE OF PANEL) (Continued)
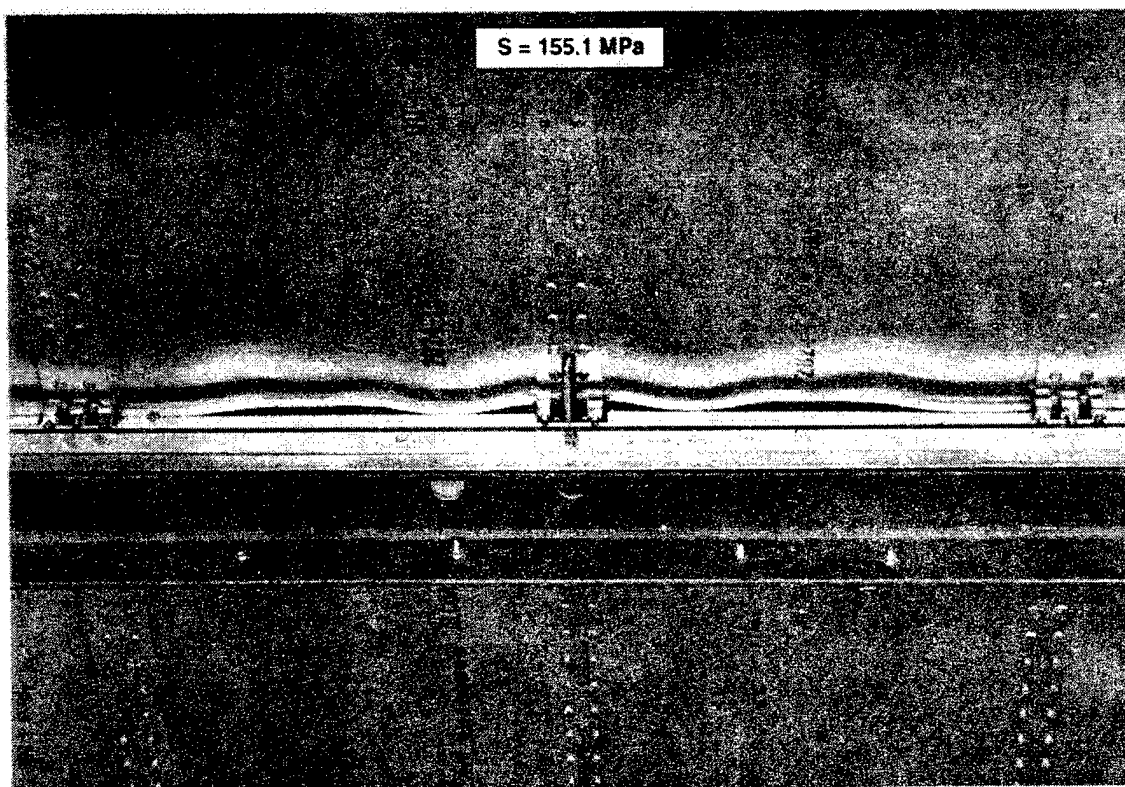
S = 172.1 MPa (crack under stiffeners)

after failure of panel

FIGURE 18. BUCKLING OF PANEL IIIb IN DIFFERENT PHASES OF THE RESIDUAL
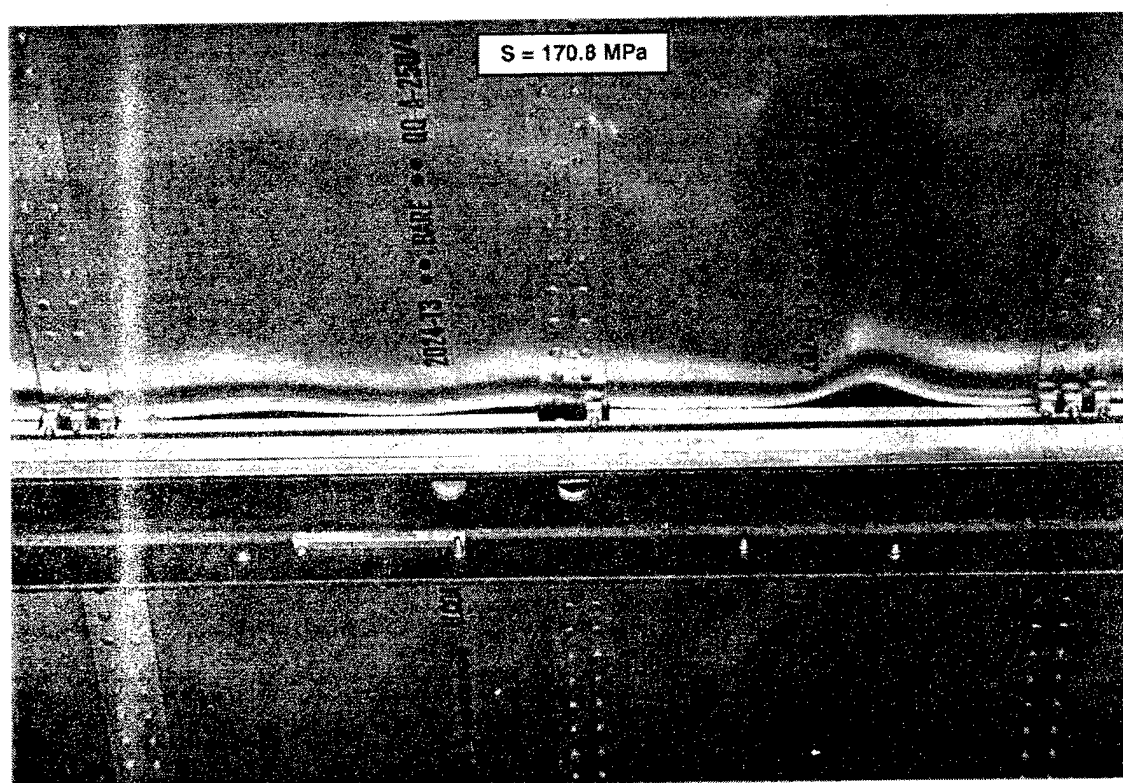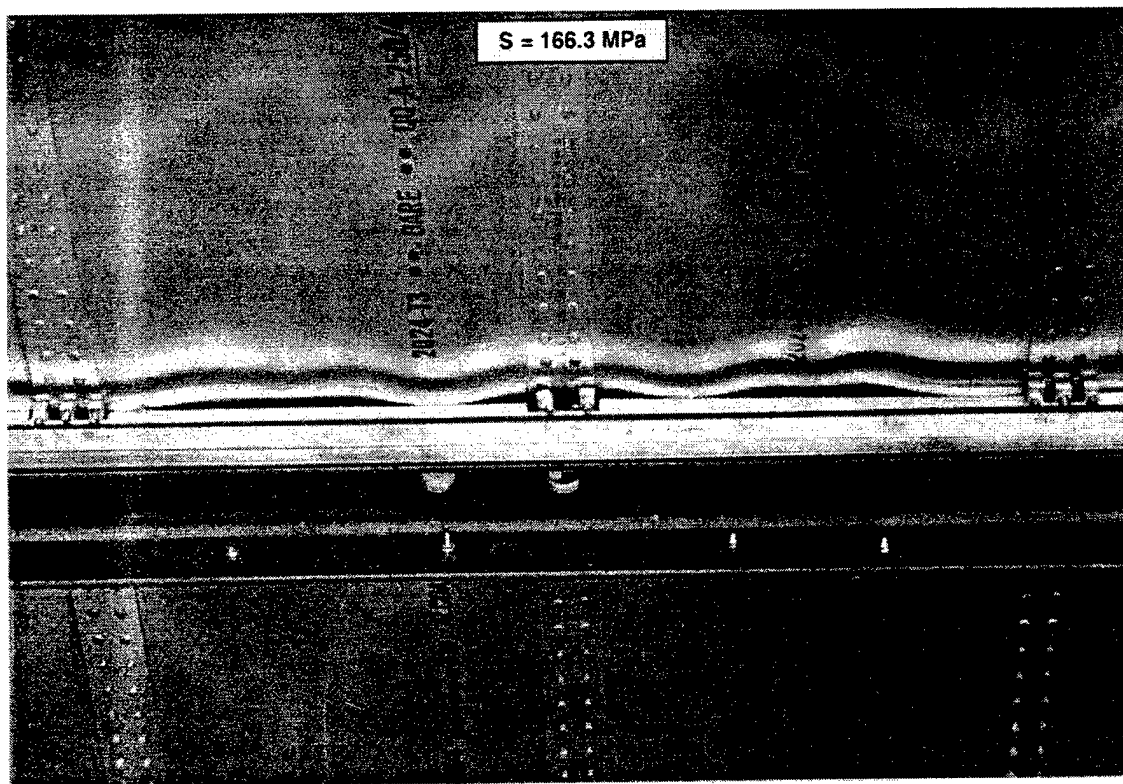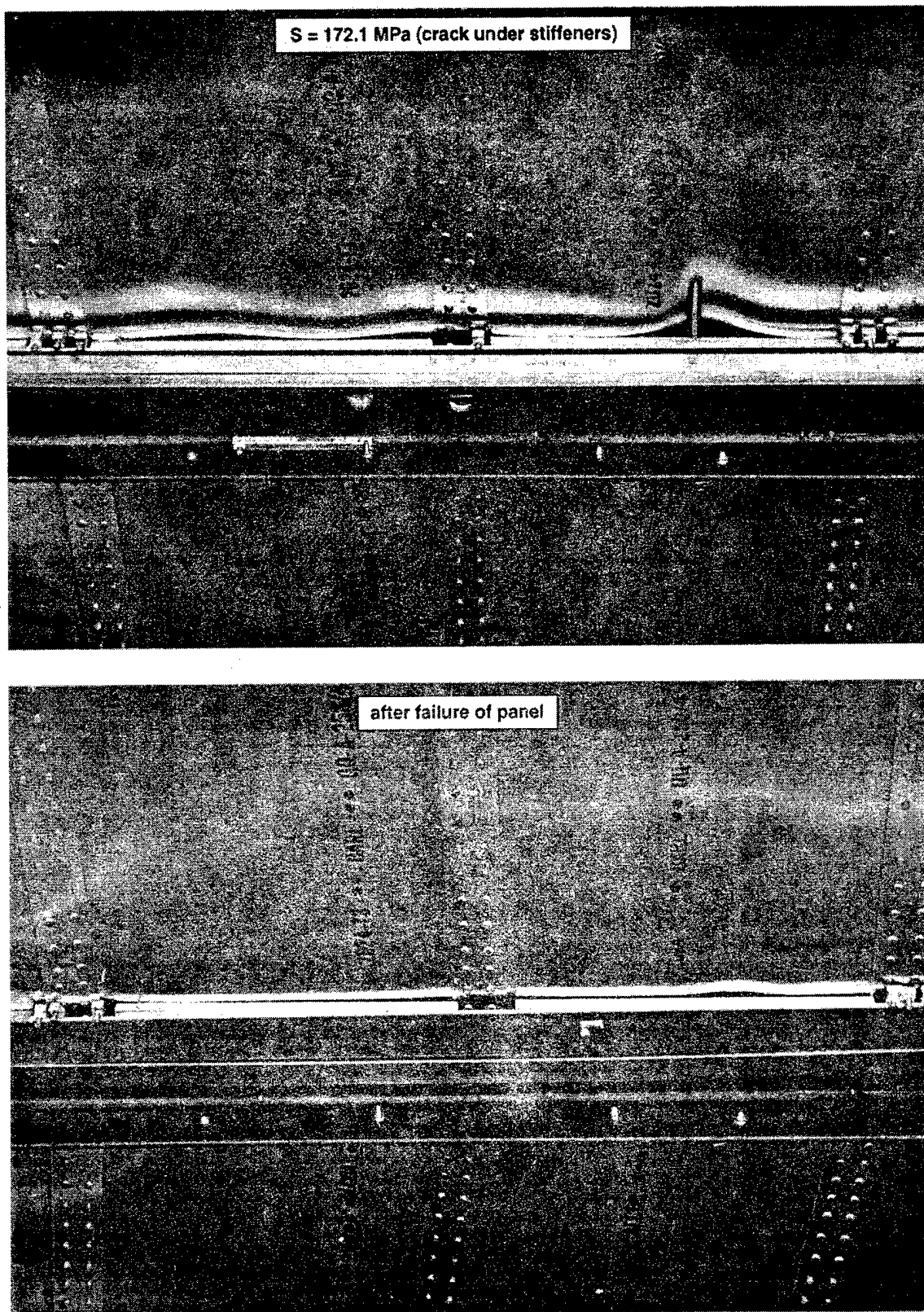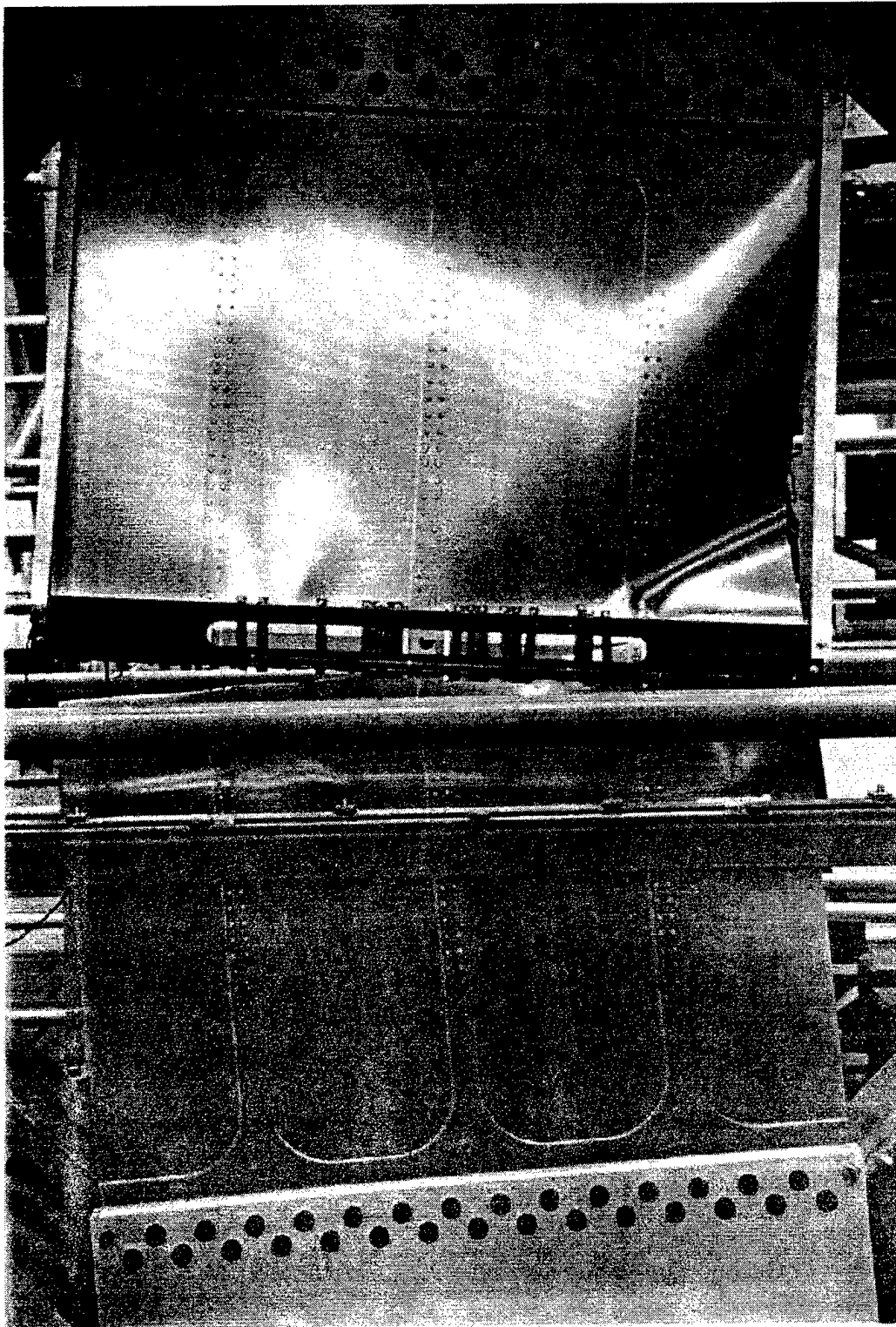STRENGTH TEST (VIEW AT REAR SIDE OF PANEL) (Continued)

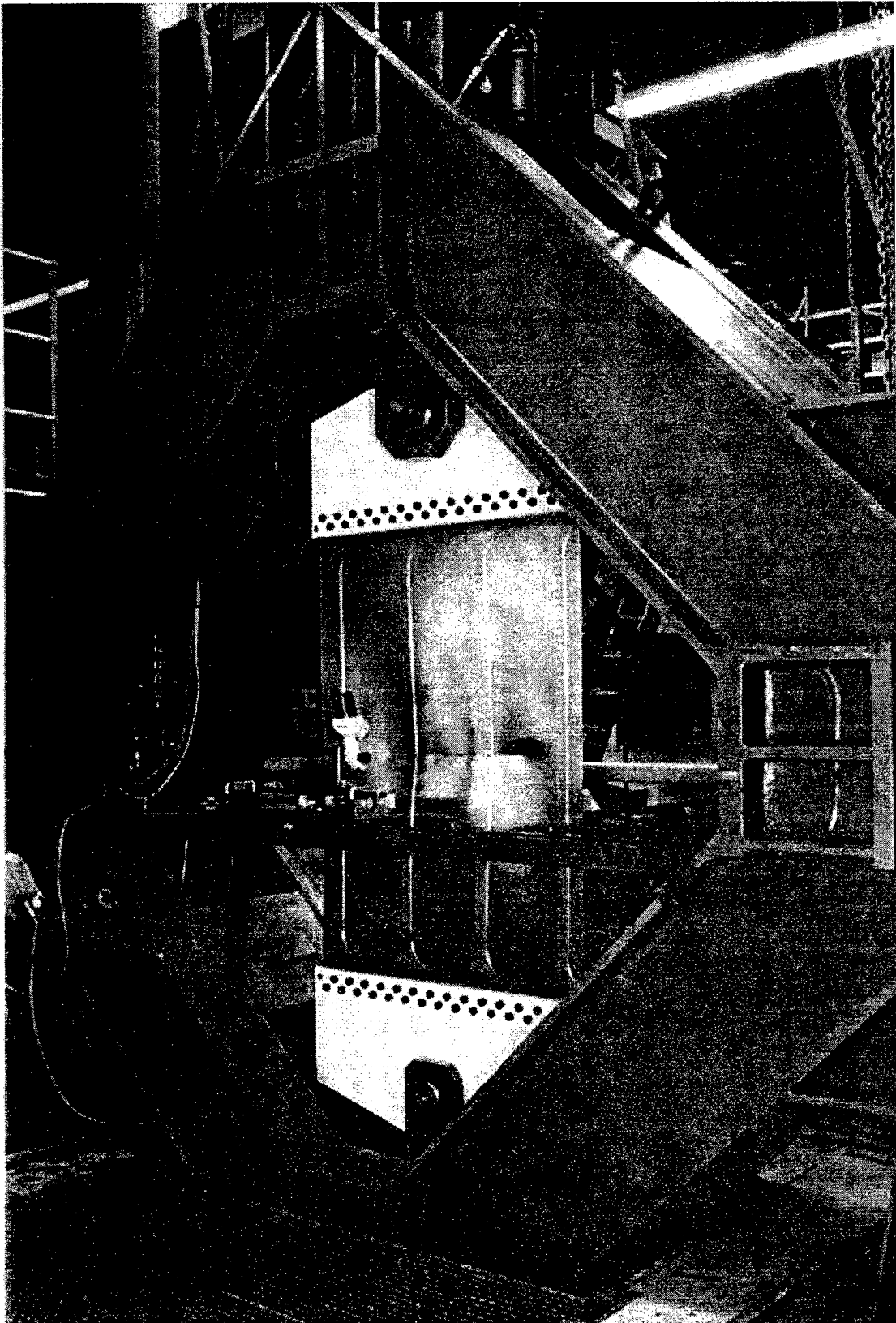FIGURE 19. FRONT SIDE OF PANEL IIIb AFTER FAILURE

40

FIGURE 20. VIEW OF A CONFIGURATION I PANEL AFTER FAILURE

4. MATERIAL AND STIFFNESS PROPERTIES OF STIFFENED PANEL COMPONENTS.

In addition to the tests on the stiffened panels, a number of tests were performed to obtain data that can be used as an input for the analytical work to predict the residual strength of stiffened panels. The additional tests determined:

- Mechanical properties of the skin and stiffener material.
- Residual strength properties of unstiffened skin material (A-curve).
- Mechanical properties of the riveted stiffener flange.
- Stiffness properties of stiffener to skin rivet connection.

### 4.1 MECHANICAL PROPERTIES OF THE SKIN AND STIFFENER MATERIAL.

Tensile tests were done according to ASTM specification E8M-89b to determine the longitudinal mechanical properties of the skin and stiffener materials. The tests were done on flat specimens of 12.5 mm wide and a thickness equal to the sheet thickness. The tests were carried out in a Schenck Trebelservo-mechanical testing machine with a 250-kN load capacity and equipped with a 60-kN load cell. An extensometer was used for displacement measurement. The load-displacement signals were processed to load-strain curves using a personal computer. The 0.2 percent yield stress, the ultimate tensile stress, and the elastic modulus were derived from the load-strain records using the original cross section of the specimen. The elongation was measured after failure along a gauge length of 50 mm.

All tests were done in triplicate. There were only negligible differences between the results of similar tests. Average results for both materials are given in figure 21. The yield stress, the ultimate tensile stress, and the elongation amply meet the minimum requirements as given in reference 9. The elastic moduli are rather low. Typical handbook values are 73,000 MPa for 2024-T3 and 72,000 MPa for 7075-T6 [9]. It is not unusual to find rather low values for the elastic modulus when they are determined from the initial straight part of the load-strain record in a tensile test.

For the 7075-T6 material, load-strain behavior was recorded until failure of the specimen. A representative record is shown in figure 21. This information can be used to describe the plastic behavior of the stiffeners in the panels.

4.2 RESIDUAL STRENGTH PROPERTIES OF UNSTIFFENED SKIN MATERIAL.

To obtain the residual strength properties of unstiffened skin material, two residual strength tests were carried out on the 1.28-mm-thick skin material. Fracture toughness properties as well as an R-curve were determined. A description of the test details and the results of the tests are given in appendix C and the resulting R-curve is presented in figure 22. The R-curve is given in the form of the crack growth resistance, K_R, versus the increase of the effective crack length, Δa_e. The curve is valid up to $\Delta a_e = 75$ mm. For larger crack lengths the net section stress exceeds the yield stress, indicating extensive yielding. The stress-intensity factor approach is not applicable in this situation.

load-strain record for 7075-T6

cross section: 25.81 mm^2

load (kN) — strain (%)
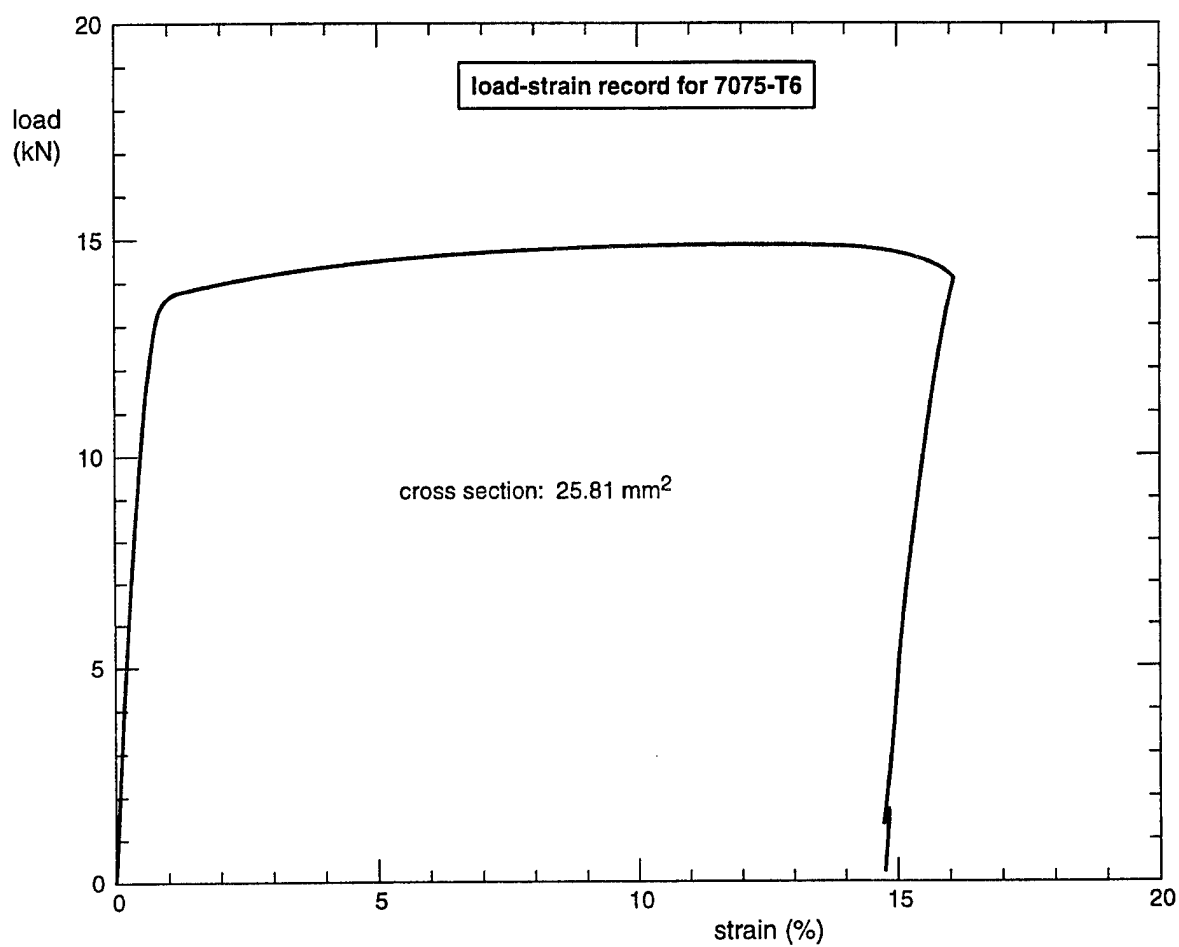
longitudinal mechanical properties					
material	thickness (mm)	$\sigma_{0.2}$ MPa	σ_{ult} MPa	δ_{50} %	E* MPa
2024-T3	1.27	366	482	17.3	71,100
7075-T6	2.06	525	579	16.0	67,000

* The elastic modulus was determined from the initial straight part of the load-strain records

FIGURE 21. THE MECHANICAL PROPERTIES OF THE 2024-T3 SKIN MATERIAL AND THE 7075-T6 STIFFENER MATERIAL
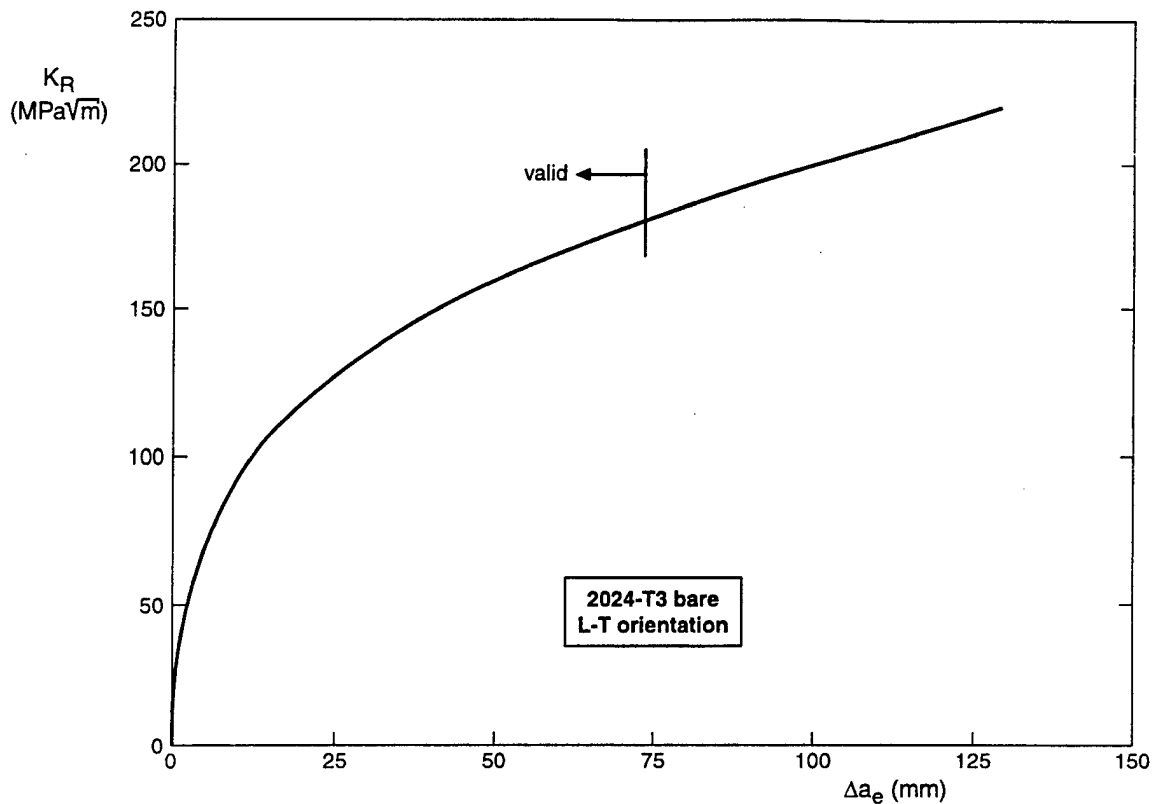
FIGURE 22. R-CURVE FOR THE SKIN MATERIAL OF THE STIFFENED PANELS

The data presented in appendix C enable the construction of other curves, for example, crack growth resistance versus the increase of the physical crack length.

4.3 MECHANICAL PROPERTIES OF A STIFFENER STRIP WITH RIVET HOLES.

In modeling stiffeners in analytical work, the upper part (web and top) and skin flange have to be considered separately. This is necessary because the skin flange contains rivet holes and it is obvious that the behavior of the flange with rivet holes under an increasing tensile load will differ from that of the remaining part. In this research program strip stiffeners were used, so only the stiffener skin flange with rivet holes had to be modeled and the stiffness properties of such a flange with holes and load transfer had to be obtained.

The elastic-plastic properties of the stiffener skin flange can be found from a force-strain diagram as presented in figure 24. Such diagrams were determined from tensile tests using specimens as depicted in figures 23a and 23b. The specimens consisted of a central strip Al 2024-T3 connected to two continuous 2.0-mm-thick Al 7075-T6 outer strips by means of four or six rivets (D = 4.0 mm, type DO). Such a specimen design was chosen to fill the rivet holes and to transfer load from the central strip to the flange. The symmetry of the specimens prevents bending during load application. The outer strips simulate the riveted stiffener skin flange under remote tensile loading. In the central part of the specimen, the outer strips will have to carry

additional load due to the load transfer from the central strip via the rivets. By varying the thickness of the central strip (indicated by t in figures 23a and b), different ratios of the load transfer via the rivets can be considered, e.g., the central strip thickness over the sum of outer strip thicknesses. To consider the case where the load transfer is 0 percent, a specimen with an intact central strip was tested. The specimens with four rivets were used to determine the properties of the stiffener away from the crack in a stiffened panel. The specimens with six rivets were used to obtain the properties of a stiffener bridging a crack with rivet holes.
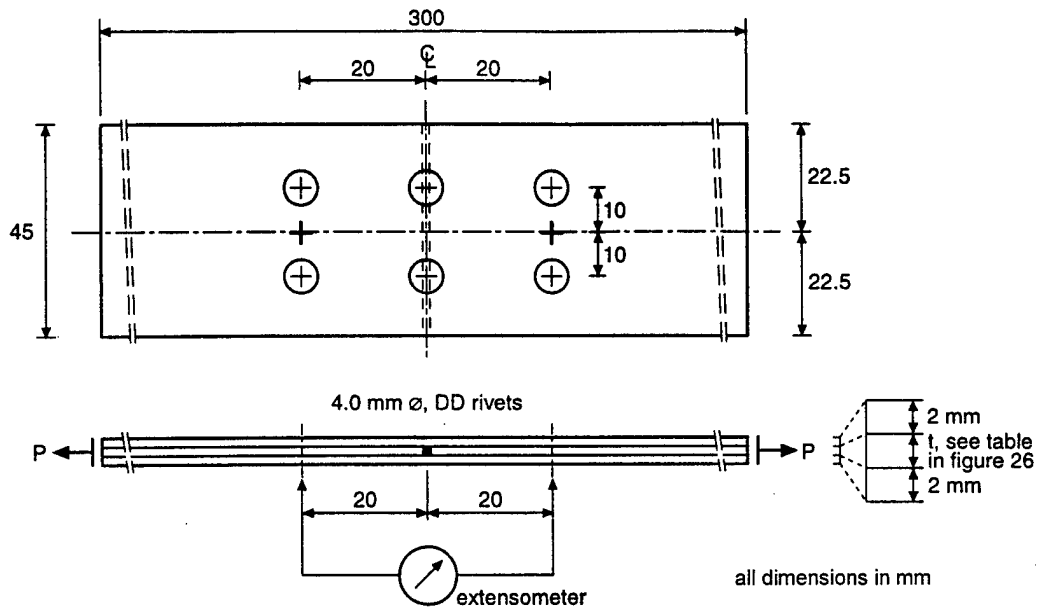

FIGURE 23a. SPECIMEN WITH 6 RIVETS
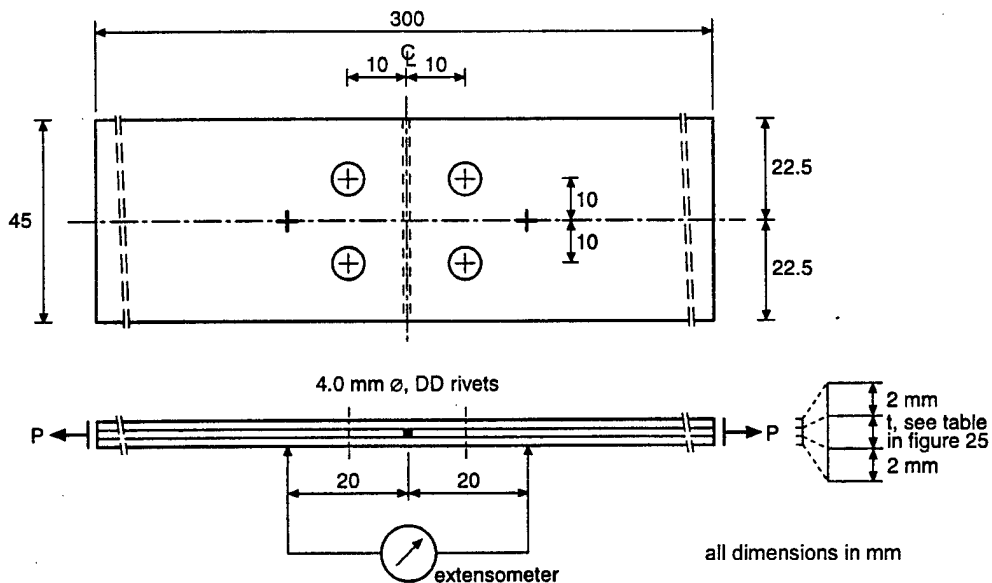
FIGURE 23b. SPECIMEN WITH 4 RIVETS

45

In figure 24, a plot of a specimen end load (P) versus elongation is given for a ratio of rivet load to bypass load of 30 percent. This diagram was determined using a gauge length of 40 mm (corresponding to twice the rivet pitch) and was linearized in a bilinear curve. This linearization results in:

EFL   elastic Young's modulus
EFLYL   plastic Young's modulus
EYIELF   yield strength
EFAILF   failure strength

EFL   = 52866 MPa
EFLYL   =   1312 MPa
EYIELF = 0.62 x 10^-2
EFAILF = 3.17 x 10^-2

FIGURE 24. END LOAD VERSUS ELONGATION DIAGRAM FOR
SPECIMEN NO. 7 (30% RATIO)

46

The bilinear curves of the four and six rivet specimens are presented in figures 25 and 26. The specimens with a continuous strip remain elastic to a higher load lev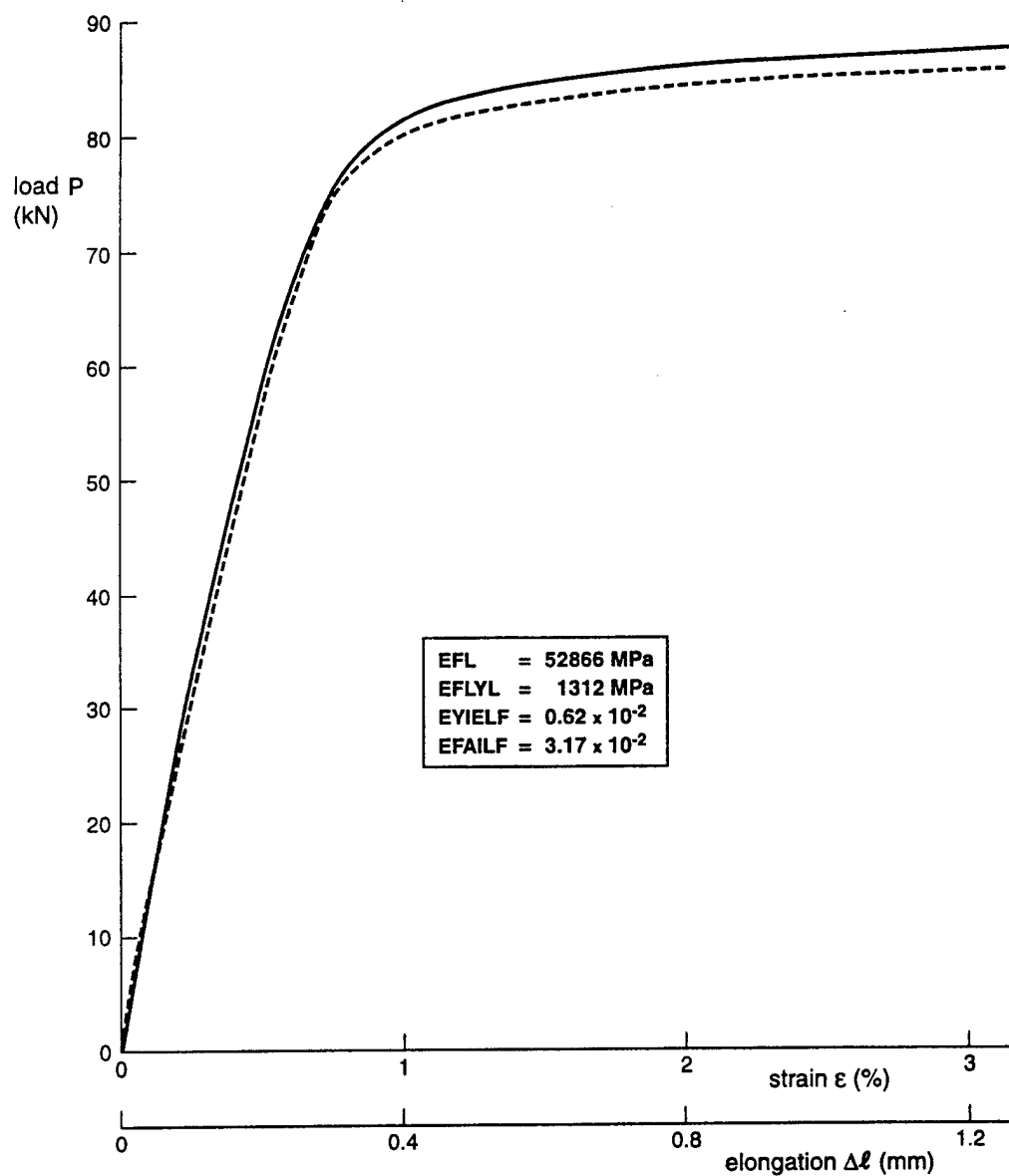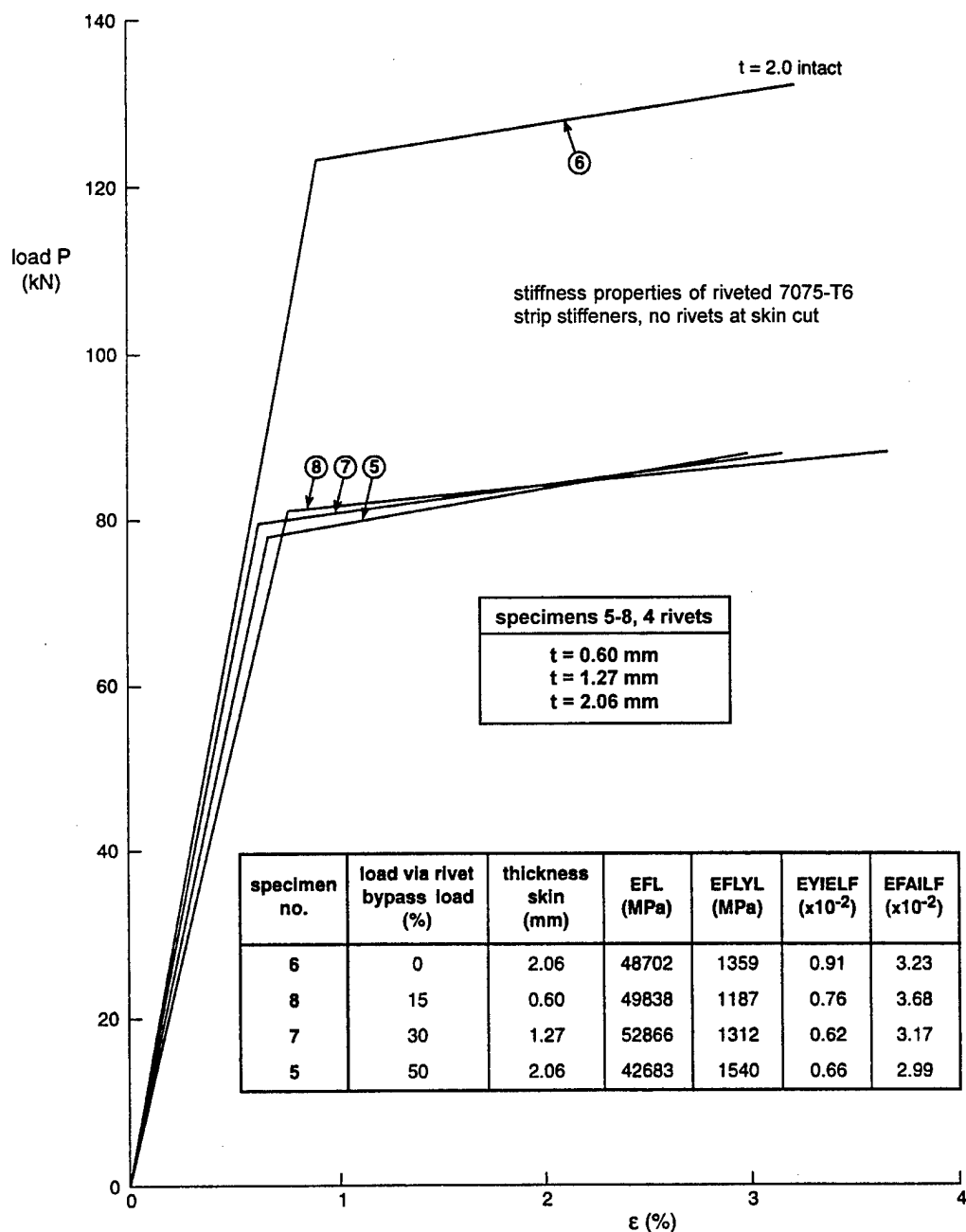el than those with a cut skin strip. The difference in the elastic flexibilities of the different specimens is small. All specimens become plastic at a load level of about 80 kN, and the differences in the plastic flexibilities are also small. The elastic-plastic stiffness properties together with the yield and the failure strains of the riveted skin flange, as found from the linearized diagrams, are compiled in the tables in figures 25 and 26.

stiffness properties of riveted 7075-T6
strip stiffeners, no rivets at skin cut

specimens 5-8, 4 rivets
t = 0.60 mm
t = 1.27 mm
t = 2.06 mm

specimen no.	load via rivet bypass load (%)	thickness skin (mm)	EFL (MPa)	EFLYL (MPa)	EYIELF $(x10^{-2})$	EFAILF $(x10^{-2})$
6	0	2.06	48702	1359	0.91	3.23
8	15	0.60	49838	1187	0.76	3.68
7	30	1.27	52866	1312	0.62	3.17
5	50	2.06	42683	1540	0.66	2.99

FIGURES 25. BILINEAR CURVES OF FOUR-RIVET SPECIMENS WITH RESULTING
STRENGTH AND STIFFNESS PROPERTIES

47
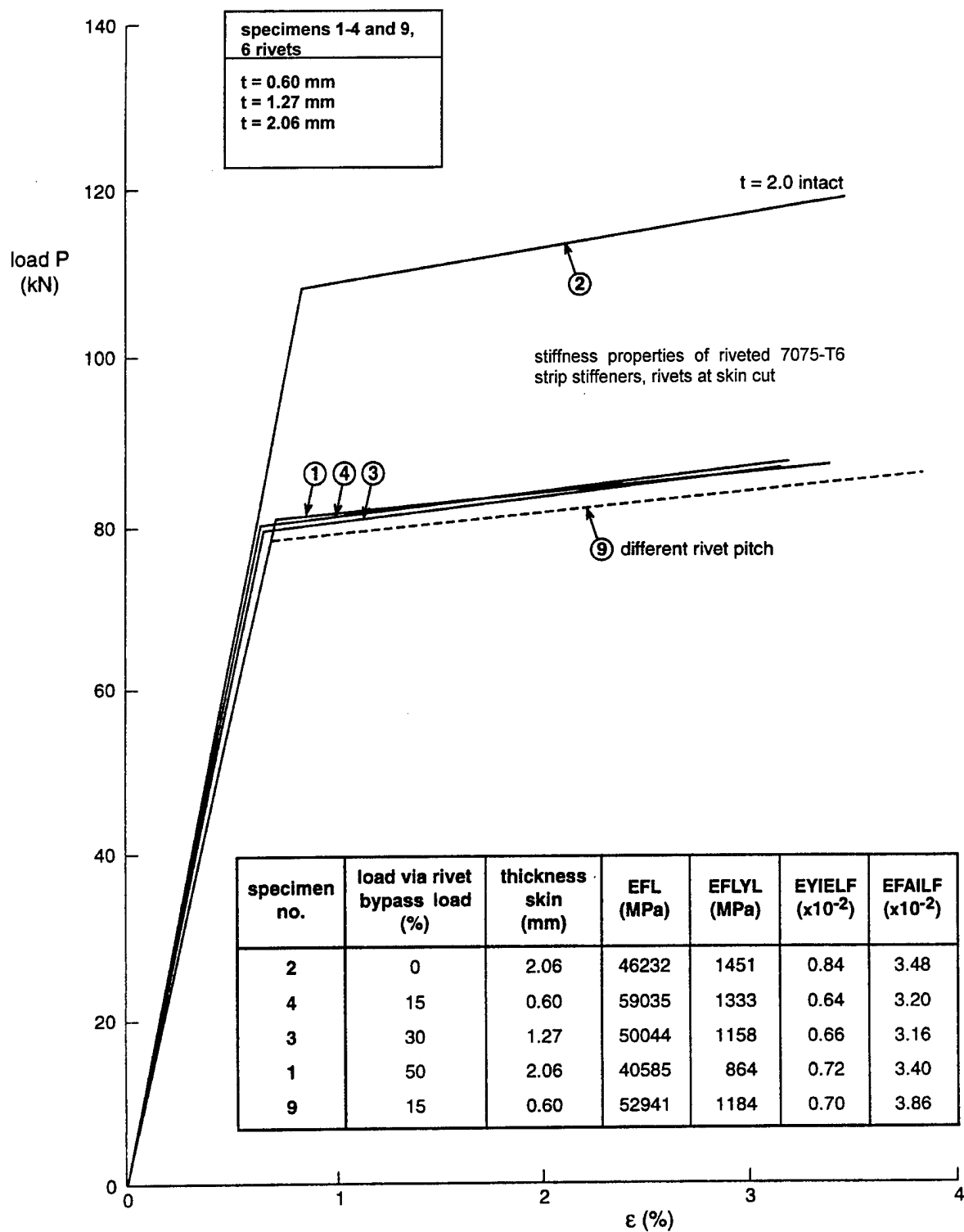
FIGURES 26. BILINEAR CURVES OF SIX-RIVET SPECIMENS WITH RESULTING STRENGTH AND STIFFNESS PROPERTIES

48

4.4 STIFFNESS PROPERTIES OF STIFFENER TO SKIN RIVET CONNECTION.

The stiffness properties of the stiffener to skin connection were determined using tensile specimens as depicted in figure 27. In the skin stiffener specimen, a 1.27-mm-thick Al 2024-T3 skin strip was connected to the 2.06-mm-thick Al 7075-T6 stiffener strips of by means of two rivets (D = 4.0 mm, type DD). The width of the specimen was taken equal to the stiffener flange width of 45 mm.
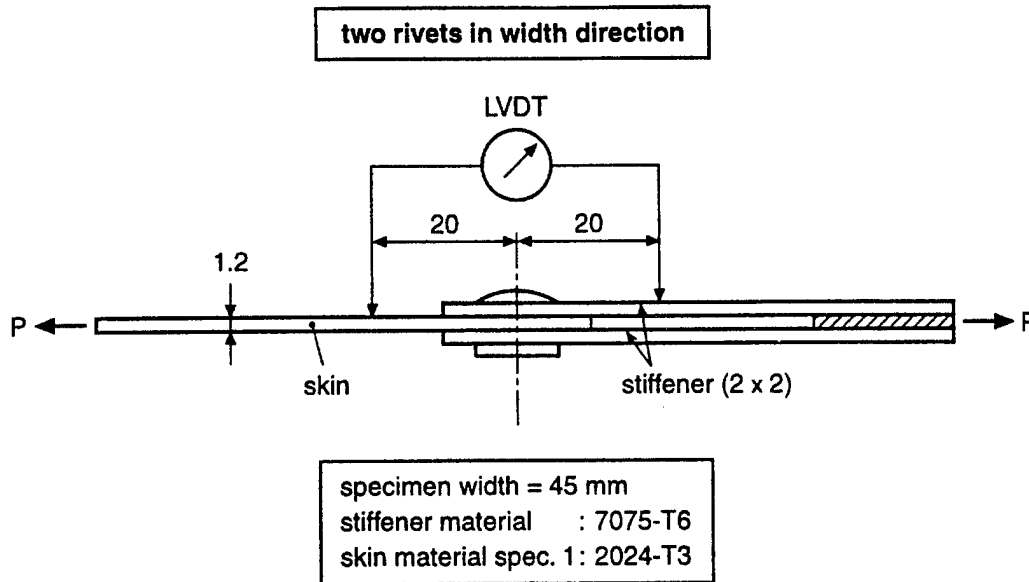
two rivets in width direction

LVDT

20   20

1.2

P ← | skin   stiffener (2 x 2) | → P

specimen width = 45 mm
stiffener material   : 7075-T6
skin material spec. 1 : 2024-T3

FIGURE 27. SPECIMEN TO DETERMINE FLEXIBILITY OF RIVETED
SKIN-STIFFENER CONNECTION

To determine the elastic-plastic load (P) versus elongation diagram of the rivet connection, the specimen was loaded until rivet failure. The measured load-elongation diagrams are presented in figure 28. The average of the measured curves was approximated by two straight lines assuming identical energy contents for the actual and linearized plots.

The elastic and the plastic flexibilities (FLEX1 and FLEX2) of the present rivet connection can be determined from the slopes of the linearized P-Δl diagrams. It should be noted that in this context, the measured displacement includes the elongation of the strips over the gauge length used (40 mm). Consequently, if the flexibility of the rivet connection itself has to be obtained (determined by the shear deformation of the rivet plus rivet hole deformation), the elongation of the strips has to be subtracted from the measured elongation. This procedure is also illustrated in figure 28 (Δl_{strip}).

The values of the flexibility parameters of the skin-stiffener rivet connections as found from the diagram in figure 28 are compiled in the table in this figure. Also, the load at which the rivet connection starts to yield (KYIELD) and the rivet failure load were included in the table.

specimen no.	FLEX 1 (mm/N)	FLEX 2 (mm/N)	KYIELD (N)	failure load (N)
10	0.1013×10^{-4}	0.5531×10^{-3}	6.9×10^3	10.75×10^3

$$1 \triangleq \Delta\ell_{strip} = P \times \left(\frac{\frac{1}{2}\text{ gauge length}}{AE \text{ skin}} + \frac{\frac{1}{2}\text{ gauge length}}{AE \text{ stiffener}} \right)$$

$$2 \triangleq \Delta\ell_{RH}$$

Note: • FLEX $1 = \dfrac{\Delta\ell_{RH}}{P}$

where $\Delta\ell_{RH}$ ts the elongation due to rivet and hole deformation
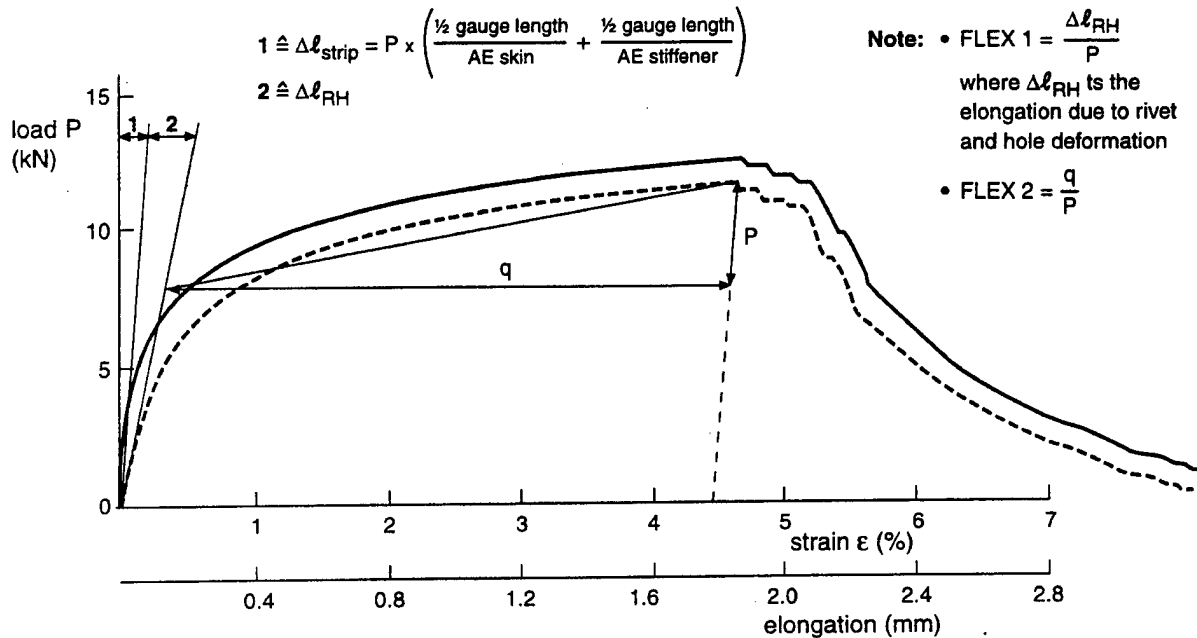
• FLEX $2 = \dfrac{q}{P}$

FIGURE 28. MEASURED END LOAD VERSUS ELONGATION CURVE, LINEARIZED CURVE, AND RESULTING STRENGTH AND STIFFNESS PROPERTIES

5. REFERENCES.

1. Oldersma, A., "Fatigue of Riveted Joints, A Literature Survey and Statistical Analysis of Existing Test Data," NLR CR 92401 L.

2. Vlieger, H., "Results of Uniaxial and Biaxial Tests on Riveted Fuselage Lap Joint Specimens," NLR TP 94250 L.

3. Vlieger, H., "Experimental Results of Uniaxial and Biaxial Fatigue Tests on Riveted Fuselage Lap Joint Specimens," NLR CR 94253 L.

4. Jansen, E.F.M. and Wanhill, R.J.H., "The Role of Corrosion in MSD," NLR CR 94335 C, restricted.

5. Vlieger, H. and Ottens, H.H., "Results of Uniaxial and Biaxial Tests on Riveted Fokker F-28 Fuselage Lap Joint Specimens," CR 94453 C, restricted.

6. Ottens, H.H., "Multiple Crack Initiation and Crack Growth in Riveted Lap Joint," TP 95049 U.

7.   Vlieger, H. and Sanderse, A., "User's Manual of ARREST, a Computer Routine to Predict the Residual Strength of Cracked Panels With Riveted Stiffeners," NLR TR 84134 L.

8.   Müller, R.P.G., "An Experimental and Analytical Investigation on the Fatigue Behavior of Fuselage Riveted Lap Joints," Delft 1995.

9.   Aluminum Standards and Data, 1993 Metric SI, The Aluminum Association.

10. Hart, W.G.J. 't and Schra, L., "Residual Strength of Damage Tolerant Aluminium Lithium Sheet Material," (NLR contribution to BREU 3250, Task 3), NLR TP 92439 L, October 1992.

APPENDIX A—STRESS-COD CURVES

During the residual strength tests, records were made of load versus crack opening displacement (COD). The COD was measured with a clip gauge seated in an 8-mm-diameter hole in the center of the central crack of panels with Configurations I and III. Stress-COD curves were obtained from the load-COD curves by dividing the applied load by the gross section (actual section of skin plus stiffeners) of the panel. The clip gauge could not be mounted in the center of the central crack in panel IIa because the central stiffener of this panel was not cut. For this panel the clip gauge was located at 87.5 mm from the center of the panel, as indicated in figure A-2.

Stress-COD curves for all tested panels are shown in figures A-1 through A-3. The points on the curves correspond with data points in figures 6 through 13 and with stress-crack length data in tables 1 through 6. This enables measured COD values to be related to measured crack lengths (via stresses). The curves for panels Ia1, Ia2, and Ia3 show discontinuities as a result of buckling of the skin, as was discussed in section 3.4.1. No complete stress-COD curves could be obtained for panels IIIa1, IIIb, and IIIc because the measuring range of the clip gauge was limited to 5 mm. For panel IIIa2, deflection due to buckling of the upper and lower side of the skin occurred in different directions. Owing to this, the clip gauge could not be kept fixed in the hole for COD's larger than about 2 mm.
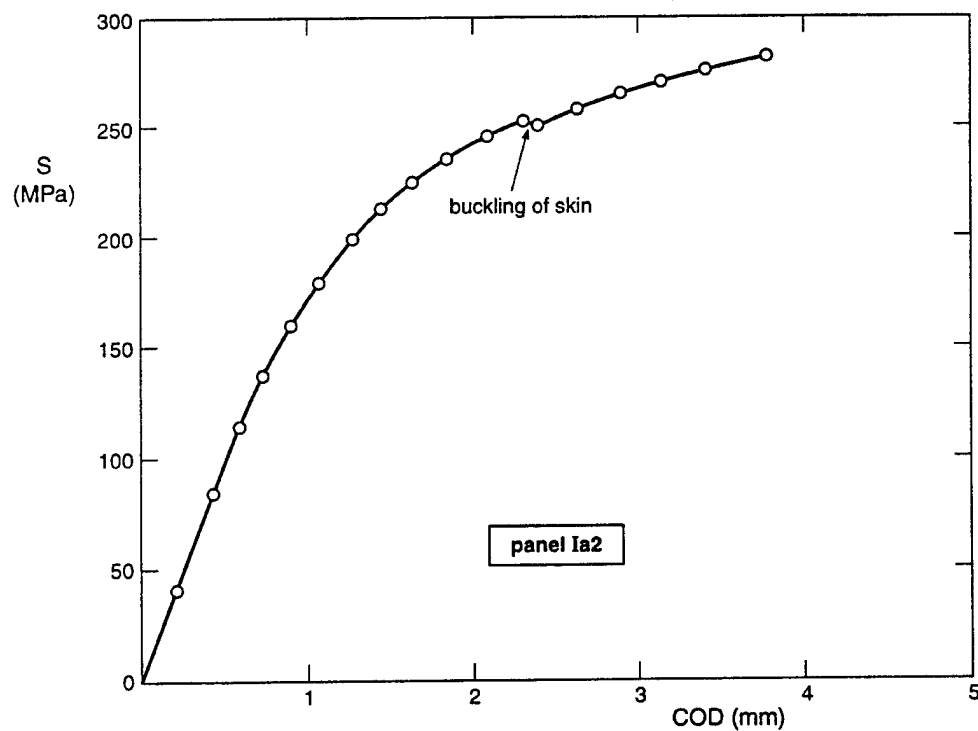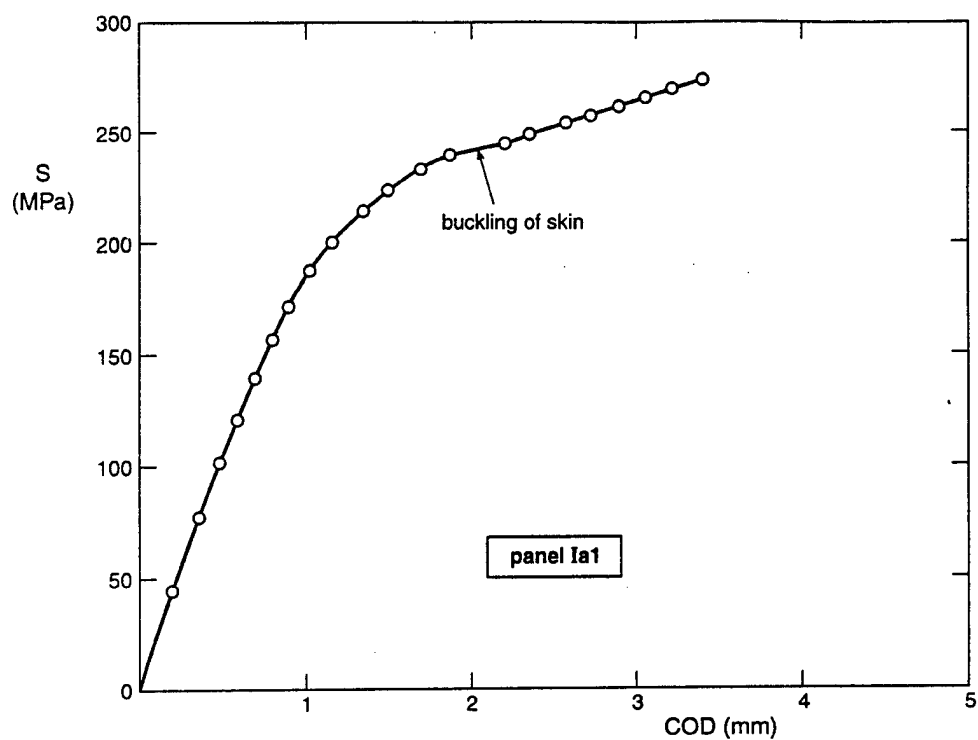
FIGURE A-1. STRESS-COD CURVES FOR CONFIGURATION I PANELS (The points on the curves correspond with data points in figures 6 through 9 and stress-crack length data in tables 1 through 3.)
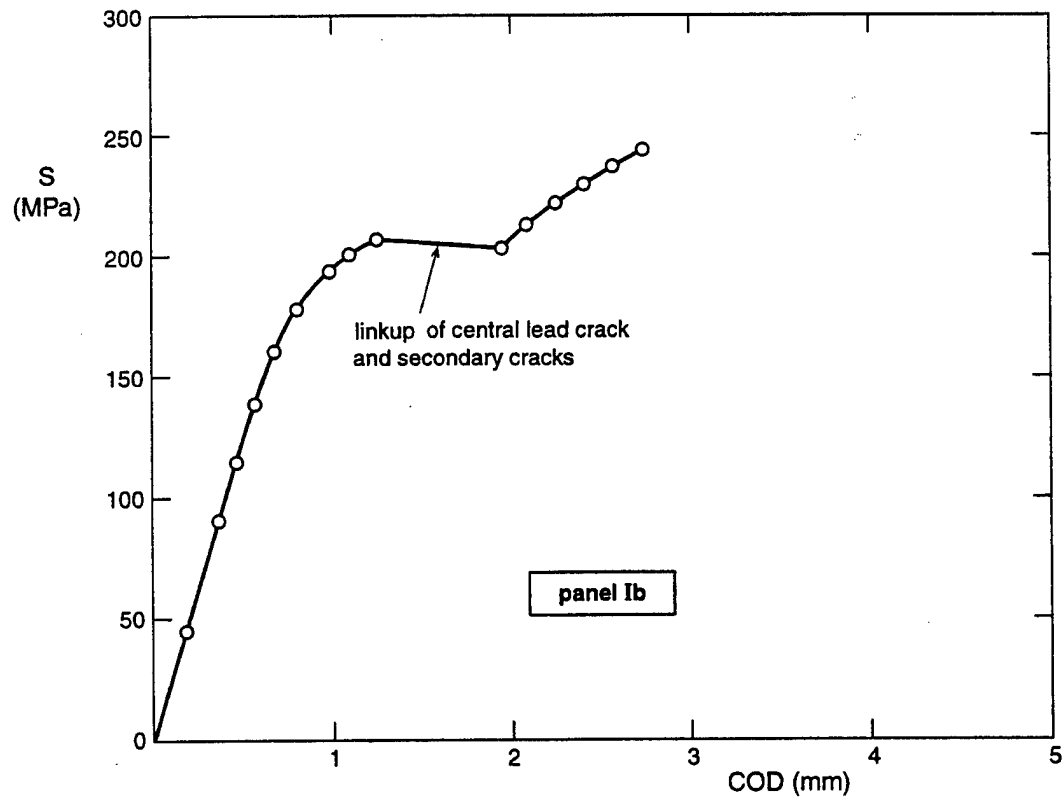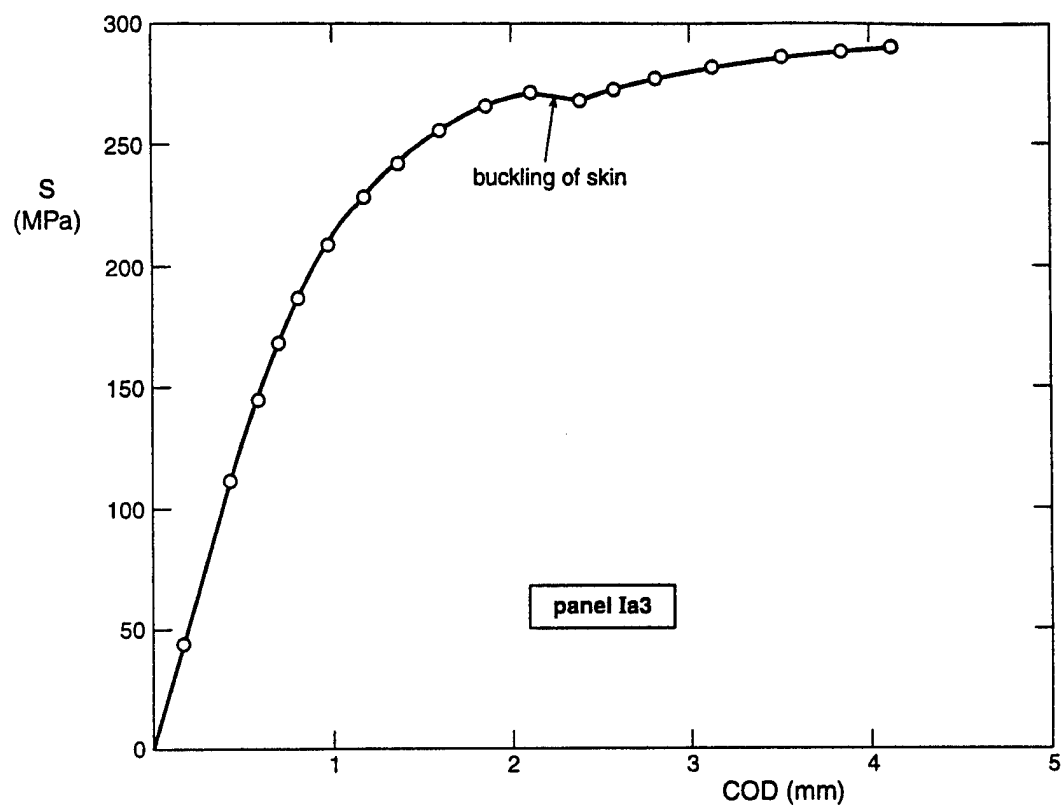
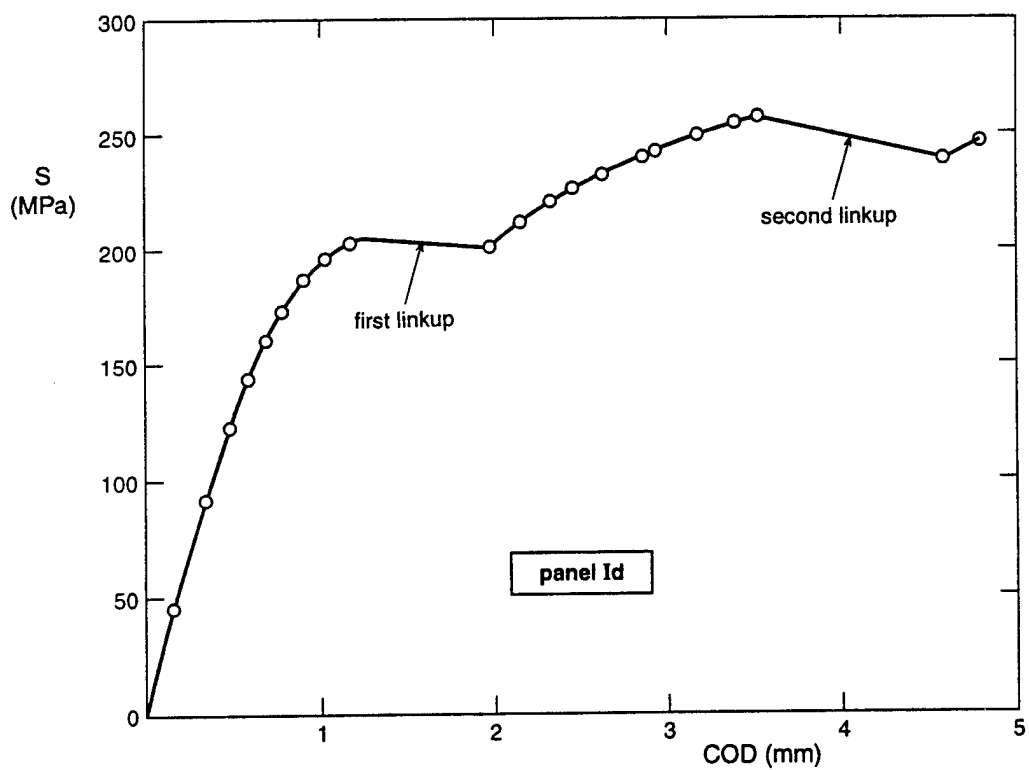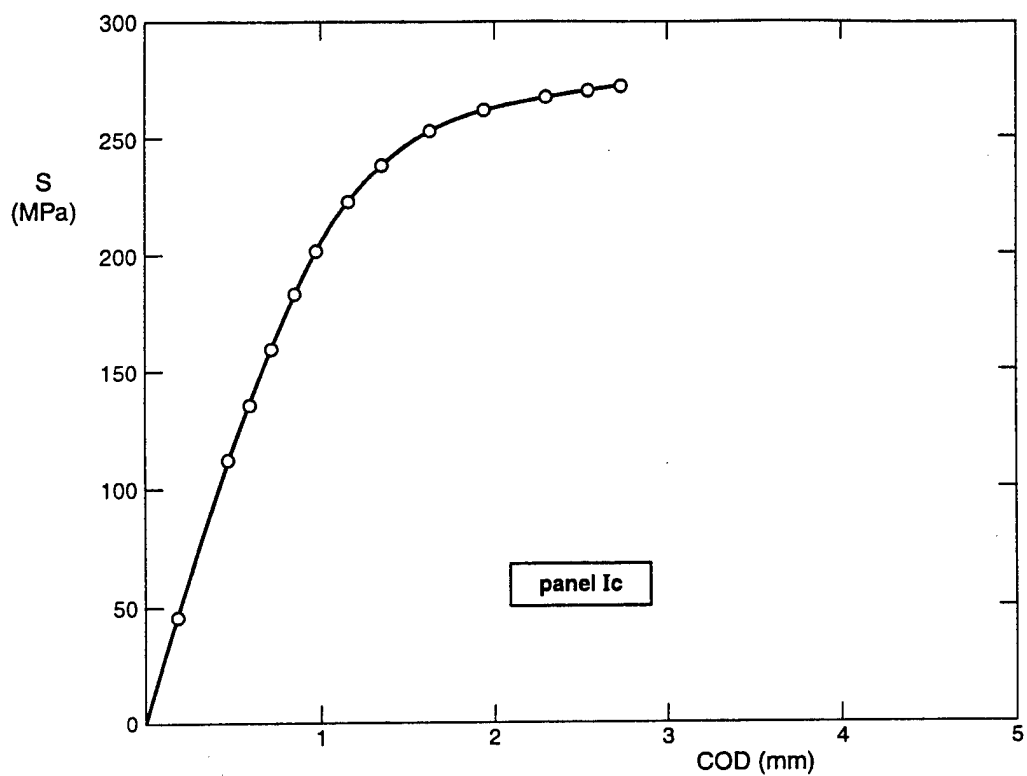FIGURE A-1. STRESS-COD CURVES FOR CONFIGURATION I PANELS (Continued)

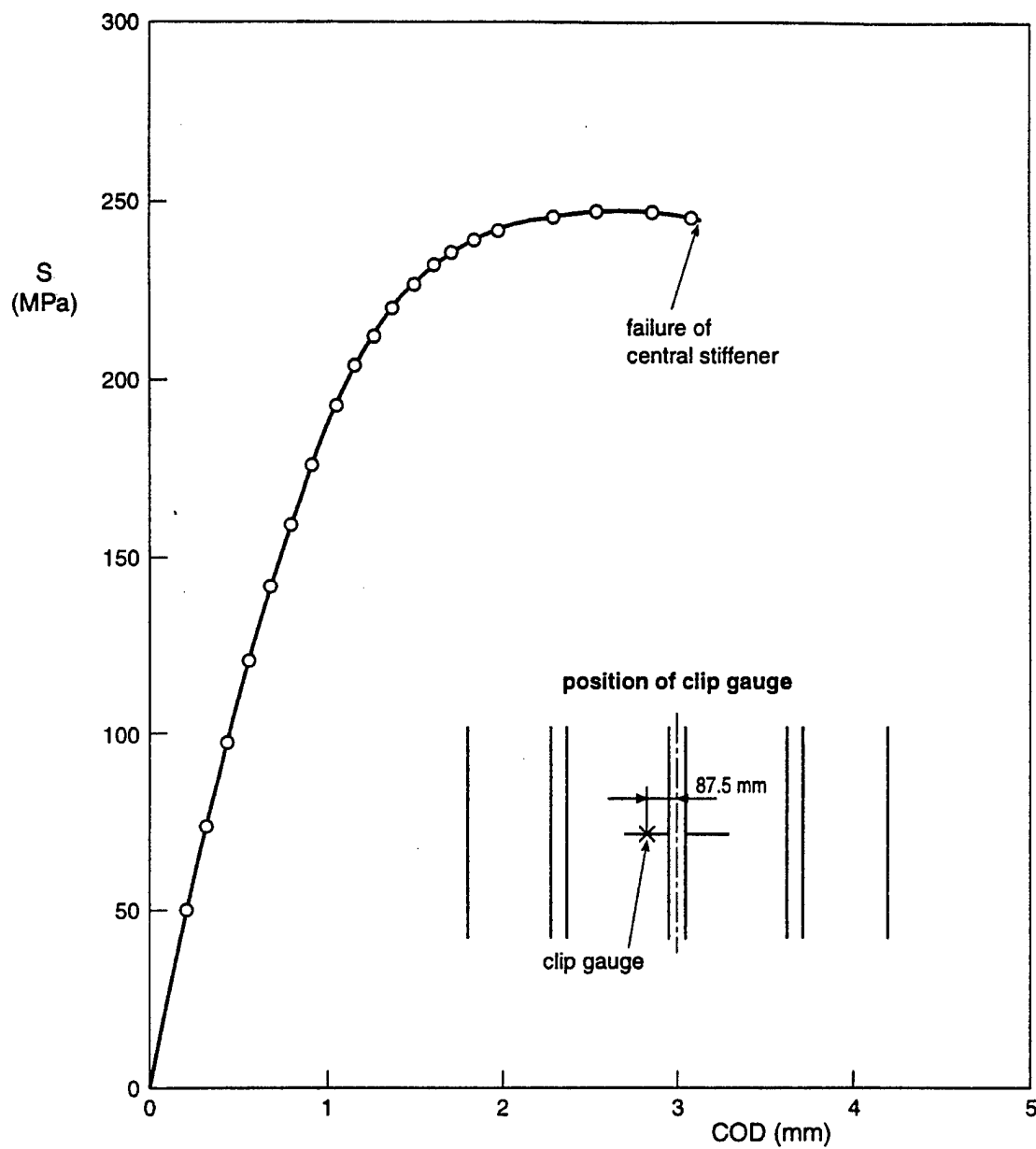FIGURE A-1. STRESS-COD CURVES FOR CONFIGURATION I PANELS (Continued)

FIGURE A-2. STRESS-COD CURVES FOR PANEL IIa (The points on the curves correspond with data points in figure 13 and stress-crack length data in table 4.)
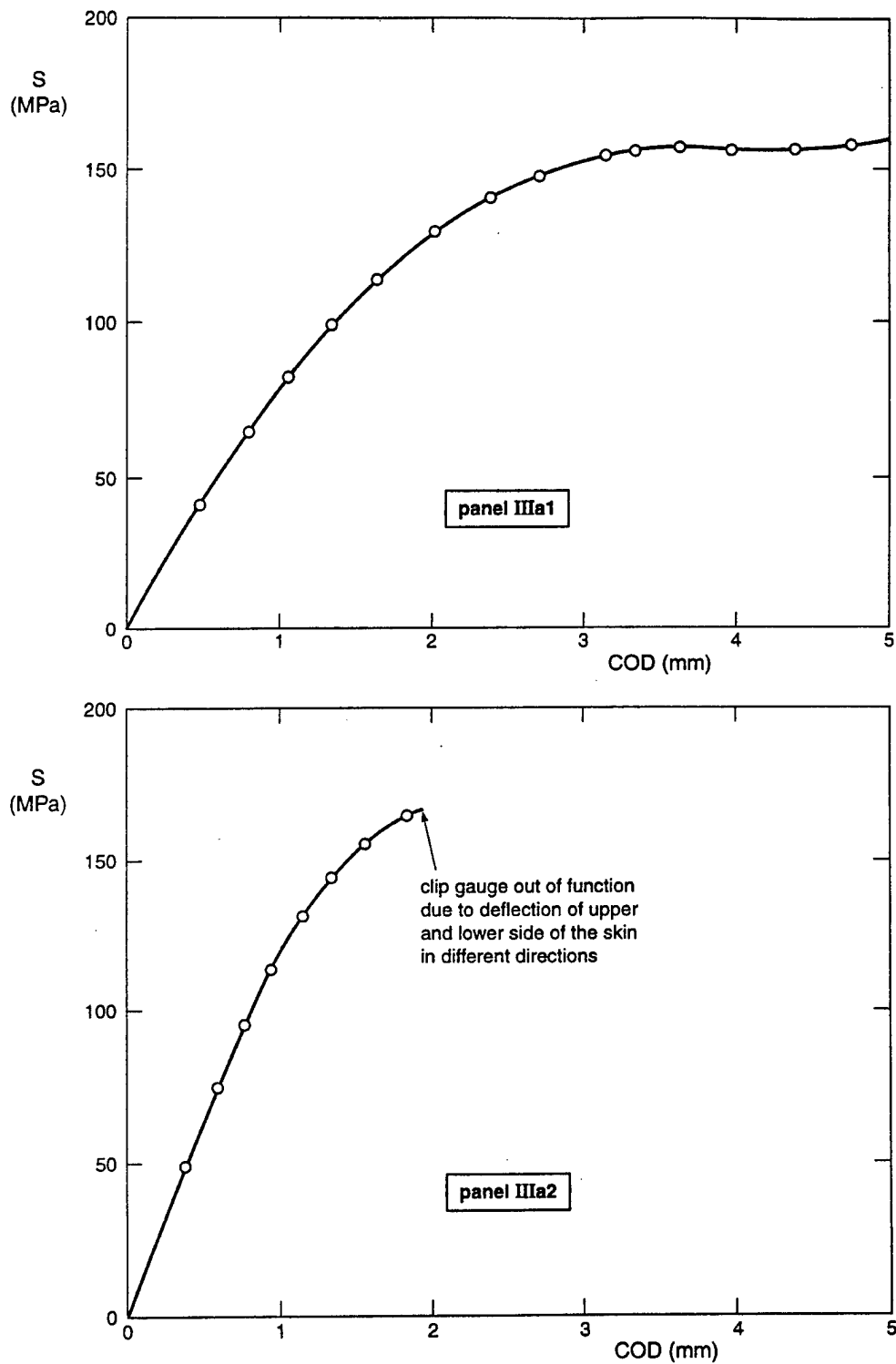
FIGURE A-3. STRESS-COD CURVES FOR CONFIGURATION III PANELS (The points on the curves correspond with data points in figures 10 through 12 and stress-crack length data in tables 4 through 6.)
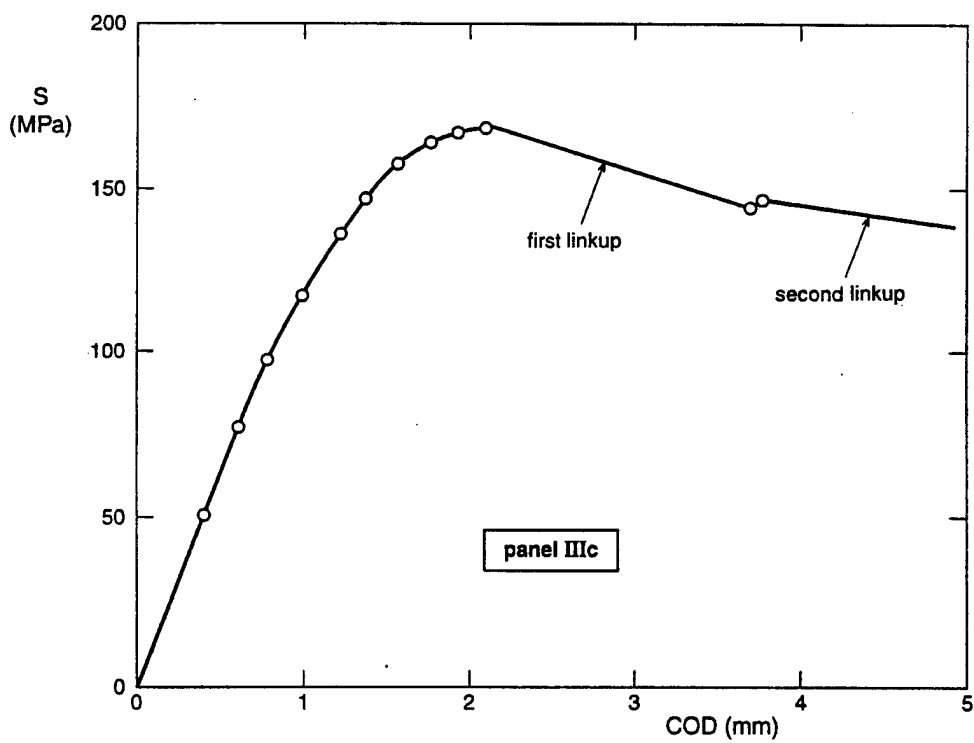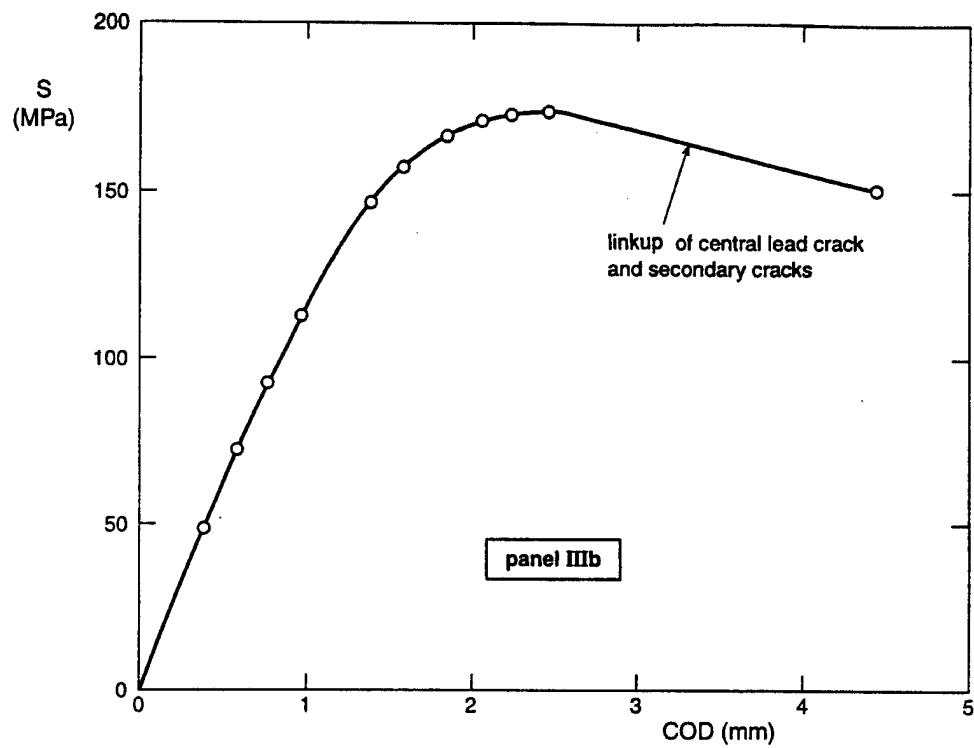
FIGURE A-3. STRESS-COD CURVES FOR CONFIGURATION III PANELS (Continued)

APPENDIX B—BUCKLING OF PANELS

During the residual strength tests of the panels, the displacement controlled loading was stopped at regular intervals for crack length measurement. During some of these test interruptions, the out-of-plane deformations were measured at the upper side of the antibuckling guide at the rear side of most panels (not for panels Ia1 and Ia2), see figure 18. The measurements were done at 11 to 15 positions along the width of the panel using calipers. Trend curves were drawn by hand through the deflection data to visualize the buckling pattern.

The buckling patterns for two or three stress levels in each panel are shown in figures B-1 through B-3. The measured crack lengths corresponding to these stresses can be found in tables 1 through 6 and figures 6 through 13. It must be noted that the deflections indicated by the curves have only limited accuracy owing to the limited number of measurements. It can be seen that all Configuration I panels show the same buckling behavior: a deflection to the rear side in the center of the panel accompanied by deflections to the front side between the center of the panel and the inner stiffeners and then a leveling-off of the out-of-plane deflections. The deflection waves between the stiffeners for panels with a central crack plus secondary cracks (Ib, Ic, and Id) seem to be closer together than those for the panel with only a central crack (Ia3). Crack linkup increased the magnitude of the out-of-plane deflections but did not change the buckling pattern.

Figure B-2 shows the buckling pattern for panel IIa. Although buckling is much more severe after failure of the central stiffener, there is no difference in the buckling pattern before and after failure of this stiffener. Five peaks and four troughs can be observed in both cases.

Figure B-3 shows the buckling patterns for Configuration III panels. There seems to be a difference in the buckling pattern between panels with and without secondary cracks. The panels with only a central crack (IIIa1 and IIIa2) show deflections to the rear side in the center of the panel and have four peaks to the front side. On the other hand, the panels with a central crack plus secondary cracks (IIIb and IIIc) show deflections to the front side in the center of the panel and have three peaks to the front side.

Generally, larger deflections occurred at the front side of the panel than at the rear side. (The reference point for the deflection measurements was the threaded connection of the half-section I-beams of the antibuckling guide.) This is probably related to different stiffnesses of the half-section I-beams of the antibuckling guide at both sides of the panel. The half-section I-beam at the front side of the panel had a smaller stiffness than that at the rear side owing to a cutout in the web for crack length measurement (see figure 3b).

The deformation of the center of the half-section I-beam at the rear side of the panels was measured in addition to the out-of-plane deformations of the panels. The results are given in table B-1 for the same stresses as in figures B-1 to B-3. Deformations of up to about 3 mm were found when the cracks approached the stiffeners. The deformation of the half-section I-beam at the front side of the panel will probably be larger than at the rear side of the panel owing to the smaller stiffness of the half-section I-beam at the front side.
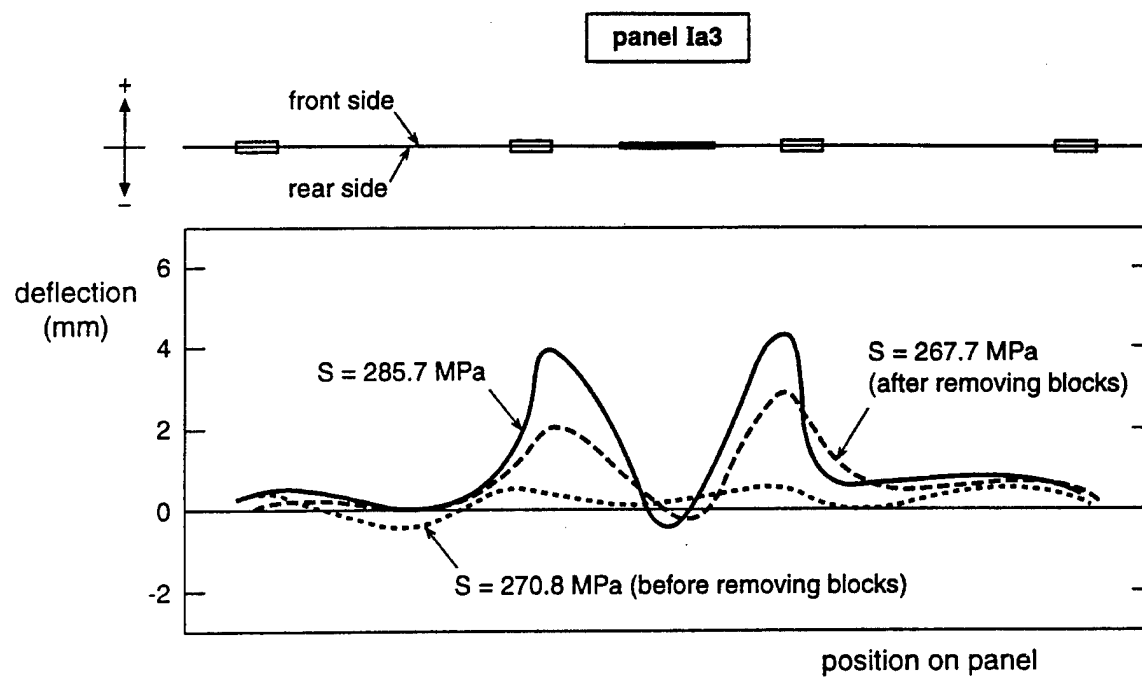
FIGURE B-1. OUT-OF-PLANE DEFORMATIONS DURING RESIDUAL STRENGTH
TESTING OF CONFIGURATION I PANELS

FIGURE B-1. OUT-OF-PLANE DEFORMATIONS DURING RESIDUAL STRENGTH
TESTING OF CONFIGURATION I PANELS (Continued)

FIGURE B-2. OUT-OF-PLANE DEFORMATIONS DURING RESIDUAL STRENGTH
TESTING OF PANEL IIa
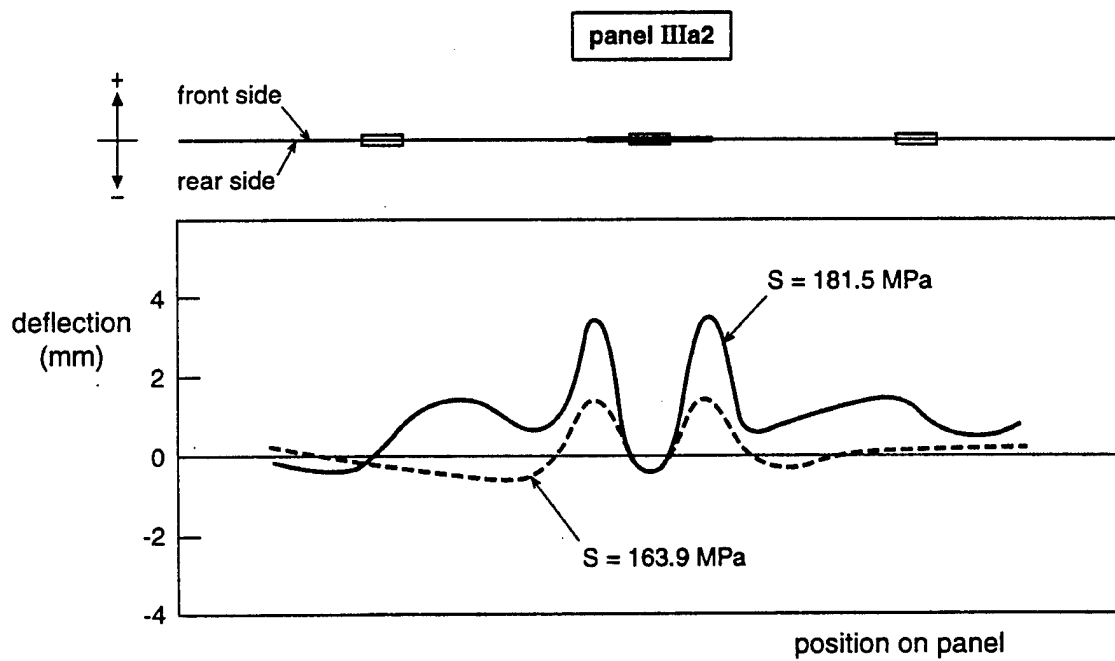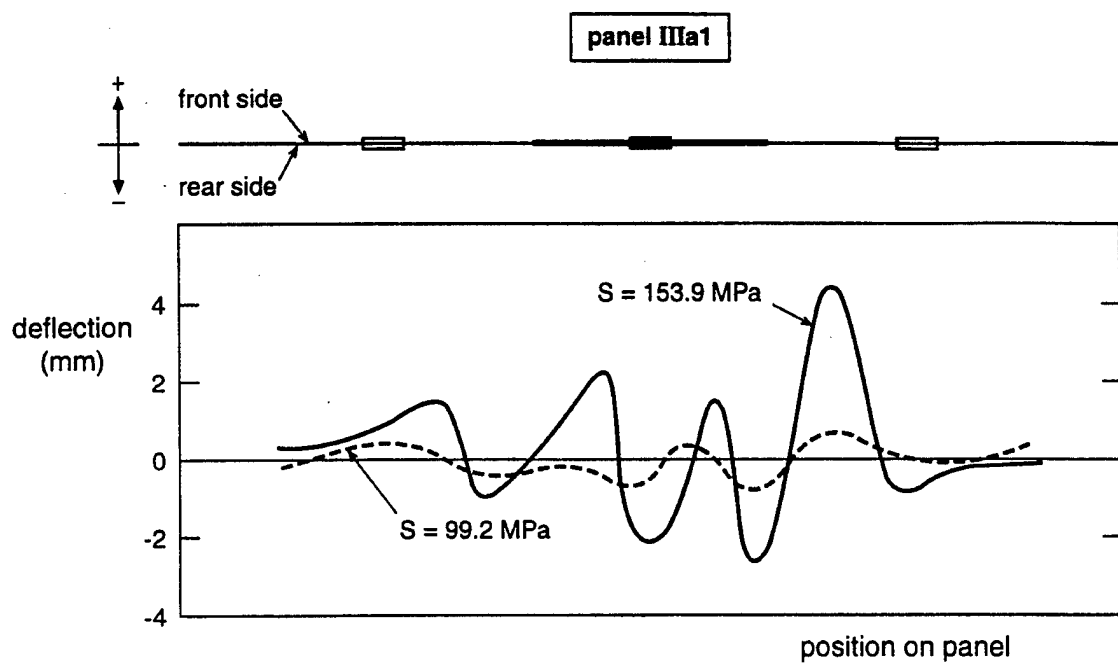
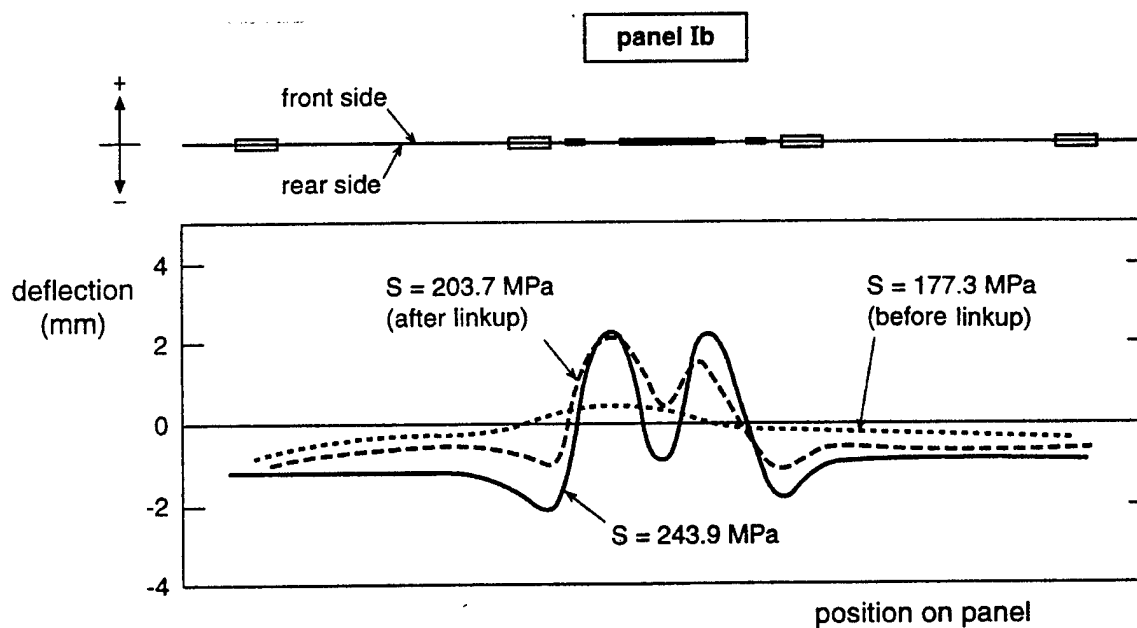**panel IIIa1**

panel IIIa2
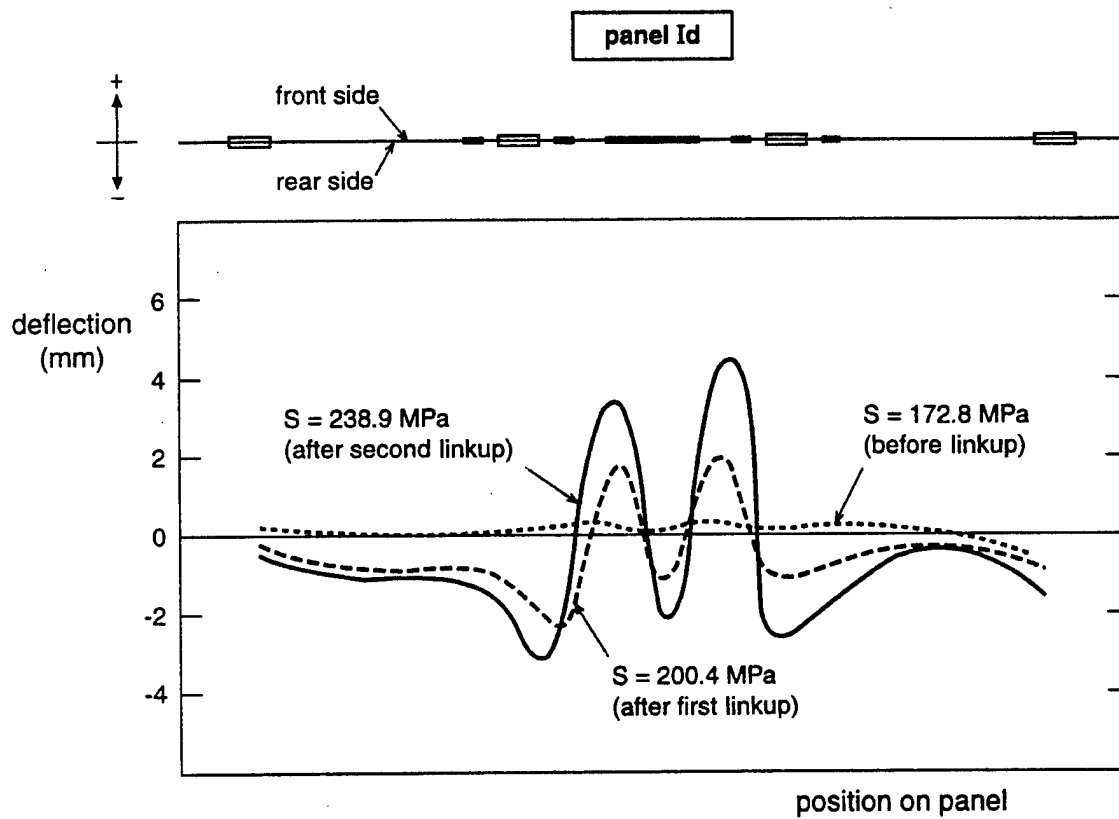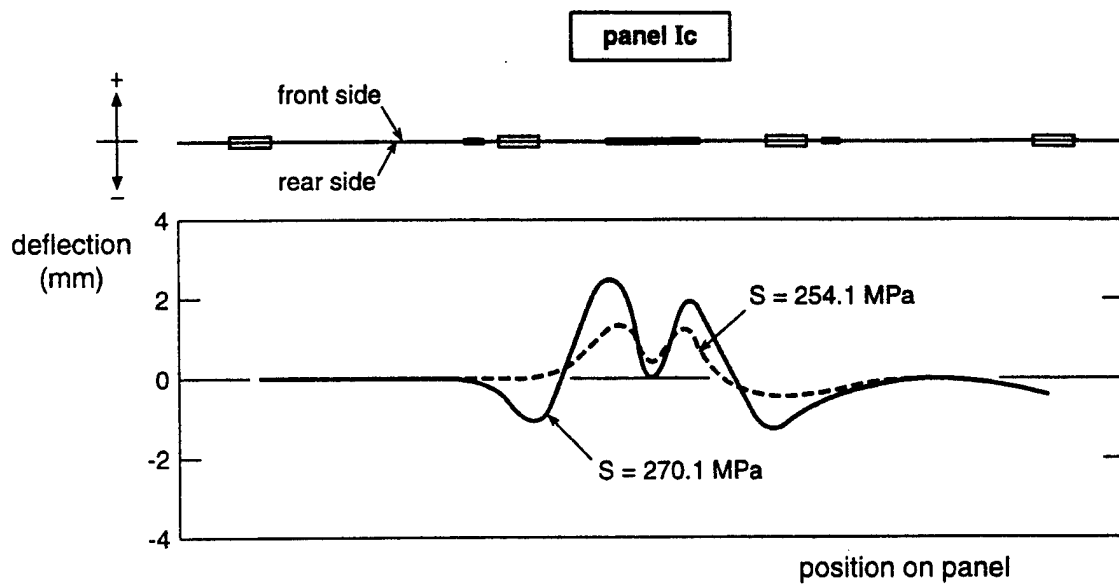
FIGURE B-3. OUT-OF-PLANE DEFORMATIONS DURING RESIDUAL STRENGTH
TESTING OF CONFIGURATION III PANELS

FIGURE B-3. OUT-OF-PLANE DEFORMATIONS DURING RESIDUAL STRENGTH
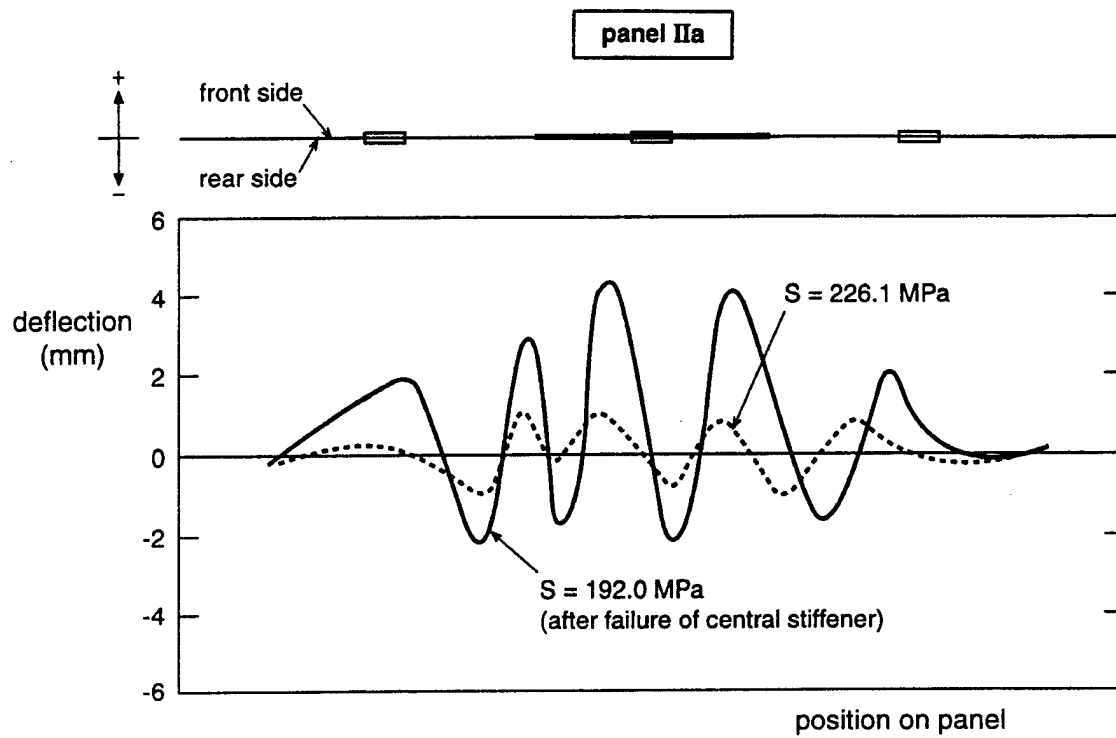TESTING OF CONFIGURATION III PANELS (Continued)

B-6
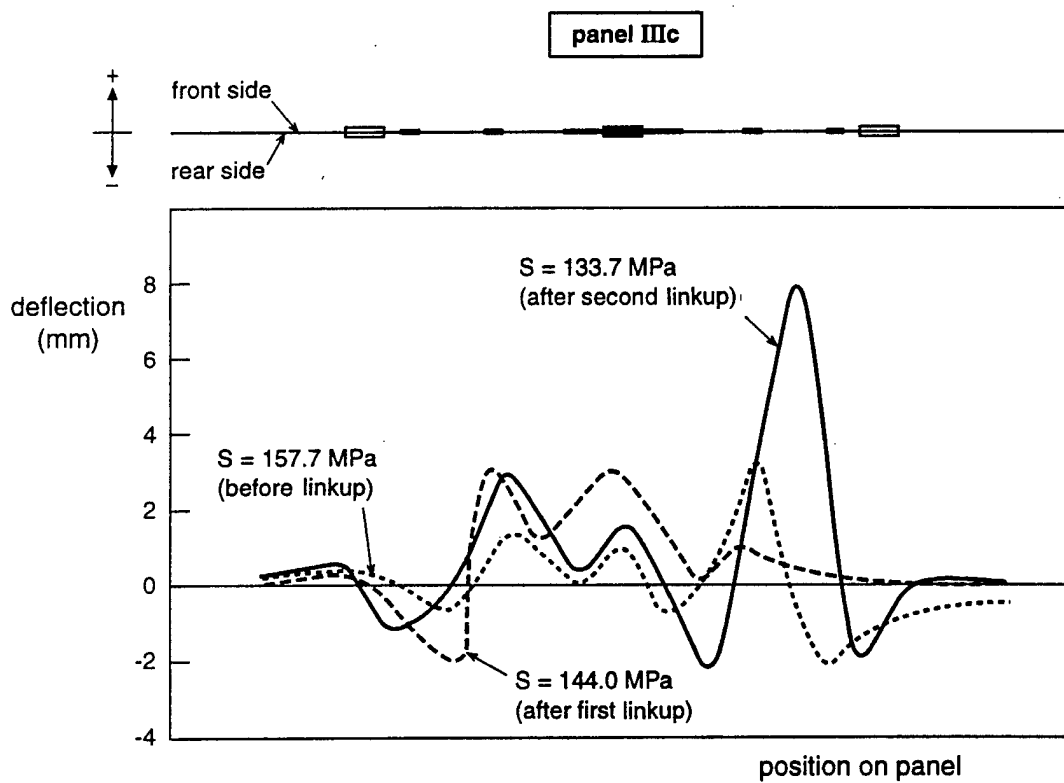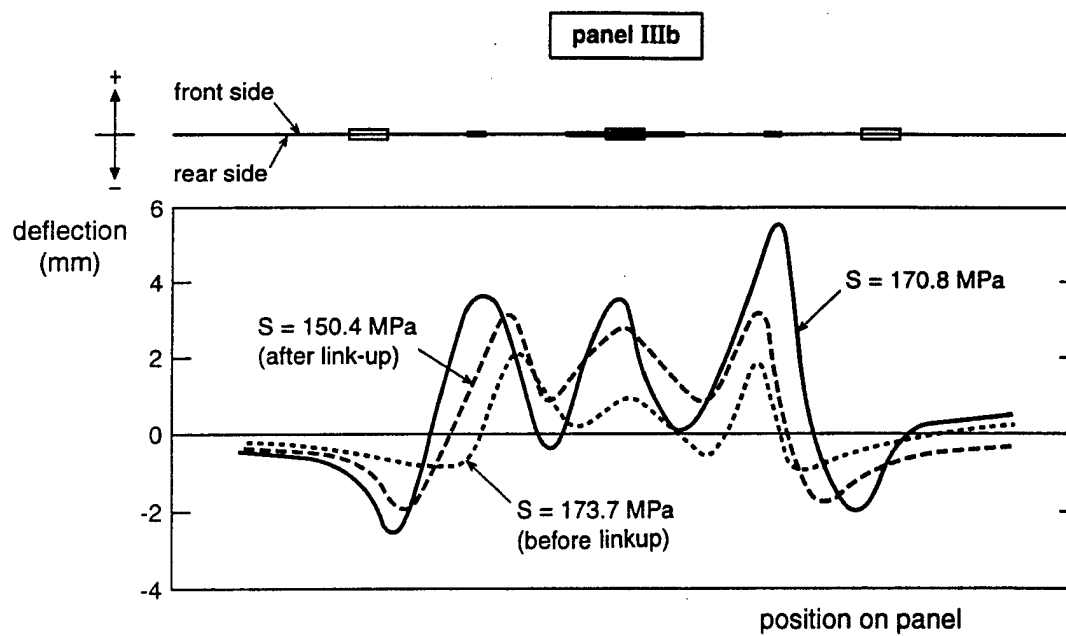
TABLE B-1. DEFORMATION OF THE ANTIBUCKLING GUIDE AT THE REAR SIDE OF THE PANELS

Panel	S (MPa)	f (mm)	Panel	S (MPa)	f (mm)
Ia3	270.8 267.7 285.7	0.4 0.8 0.9	IIIa1	99.2 153.9	0.4 1.8
Ib	177.3 203.7 243.9	0.5 0.8 1.0	IIIa2	163.9 181.5	0.5 2.5
Ic	254.1 270.1	0.5 0.9	IIIb	173.7 150.4 170.8	1.2 2.1 2.5
Id	172.8 200.4 238.9	0.2 1.0 1.8	IIIc	157.7 144.0 133.7	0.7 2.3 1.9
IIa	226.1 192.0	0.6 2.7			

f = deformation of the center of the antibuckling guide at the rear side of the panel

The stresses, S, correspond with the stresses indicated in figures B-1 through B-3.

APPENDIX C— RESIDUAL STRENGTH TESTS ON SKIN MATERIAL OF STIFFENED PANELS

Two residual strength tests were carried out on the 1.28-mm-thick sheet material used for the skin of the stiffened panels. The tests were done for the L-T orientation of 500-mm-wide panels with initial crack lengths of $2a_o = 100$ mm and 156 mm. Testing and data evaluation were done according to ASTM specification E561-86 for R-curve determination.

The tests were carried out in a 900 kN capacity Wolpert-Amsler servo-hydraulic testing machine. The specimens were fatigue precracked at R = 0.1 and maximum fatigue stresses of 47 MPa and 34 MPa respectively to obtain 2-mm fatigue crack growth at each crack tip until initial crack lengths of 100 and 156 mm for the residual strength tests were reached. A clip gauge for displacement measurements was seated in an 8-mm-diameter central hole. Buckling was restrained by two half-section I-beams, one of which had a cutout for installing the clip gauge and reading the crack length. Aluminum inserts were used in the cutout to obtain maximum support of the panel. Both the half-section I-beams and inserts were provided with a low friction plastic foil to prevent load transfer to the antibuckling guide.

Fatigue precracking was done under load control, but the residual strength tests were done under displacement control. Load-crack opening displacement (COD) records were made to derive effective crack lengths. The displacement increase was periodically interrupted for visual crack length measurements. Fracture toughness values, as well as R-curves, were derived from the load-COD records.

A survey of critical crack lengths and fracture toughness properties is given in table C-1. Different fracture toughness values based on three different crack lengths were derived for each specimen. The fracture toughnesses were slightly smaller than found in an earlier investigation for 1.6-mm-thick bare 2024-T3 sheet [10] using the same specimen type.

Numerical results of the R-curve determination are given in table C-2, while the crack growth resistance, K_R, is plotted as a function of the increase of the effective crack length, Δa_e, in figure C-1.

$$\Delta a_e \text{ is defined as } a_e - a_o$$

where: a_o = initial half crack length
a_e = effective half crack length, including plasticity at the crack tip.

a_e was derived from the load-COD records using an analytically developed expression for the compliance according to ASTM E561-86. This expression is

$$\frac{Ev}{\sigma W} = 2\left(\frac{\pi a/W}{\sin \pi a/W}\right)^{\frac{1}{2}}\left\{\frac{2W}{\pi Y}\cosh^{-1}\left(\frac{\cosh \pi Y/W}{\cos \pi a/W}\right) - 1 + \mu\left[1 + \left(\frac{\sin \pi a/W}{\sinh Y/W}\right)^2\right]^{\frac{1}{2}} + \mu\right\}Y/W$$

where: E = Young's modulus
  v = crack opening displacement (COD)
  σ = gross stress
  W = panel width
  a = a_e = effective half crack length
  Y = half span of gauge (4 mm in present investigation)
  μ = Poisson's ratio

The analytical compliance Ev/σW was calculated for the initial crack length. Ev/σW was also derived from the lower linear part of the load-COD record using E = 73000 MPa. This ought to result in equal compliances. However, the experimentally determined compliance appeared to be about 12 percent larger than the analytically determined compliance. A similar difference was found in reference 10 for 1.6-mm-thick 2091-T84, 8090-T81, and 2024-T3 sheet. A correction factor based on the ratio of experimentally and analytically determined compliances for the initial crack length was applied as recommended in ASTM E561-86. This correction factor is indicated in table C-2. All experimentally determined compliances were multiplied by this correction factor before a_e/W, and subsequently a_e, was determined from the previous expression.

The crack growth resistance, K_R, was calculated from:

where: P = applied load or force
  t = sheet thickness
  W = panel width
  a = a_e = effective half crack length.

Figure C-1 shows a good agreement between the data points for the two initial crack lengths. A trend line was drawn by hand through the data points. On the curve, points are indicated where $\sigma_{net} = \sigma_{0.2}$ for the two tested specimens; the R-curve can be considered valid up to these points. The R-curve is slightly lower than the R-curve given in reference 10 for 1.6-mm-thick bare 2024-T3 sheet.

TABLE C-1. FRACTURE TOUGHNESS PROPERTIES OF THE SKIN MATERIAL OF THE STIFFENDED PANEL

Initial crack length a_o, mm	Maximum load			Fracture toughness		
	S_{max} MPa	a_{cp} mm	a_{ce} mm	K_{co} MPa√m	K_{cp} MPa√m	K_{ce} MPa√m
49.8	256.4	68.3	98.8	103.9	124.5	158.4
78.0	211.4	96.5	120.7	111.4	128.4	152.8
			Mean	108	126	156

Material: 2024-T3
Orientation: L-T
Thickness: 1.28 mm, Width: 500 mm

a_o = initial half crack length
a_{cp} = physical half crack length at maximum load
a_{ce} = effective half crack length at maximum load, including crack tip plasticity

$$K_{co} = S_{max} \left[\frac{\pi a_o}{\cos \dfrac{\pi a_o}{W}} \right]^{1/2} \qquad K_{ce} = S_{max} \left[\frac{\pi a_{ce}}{\cos \dfrac{\pi a_{ce}}{W}} \right]^{1/2}$$

$$K_{cp} = S_{max} \left[\frac{\pi a_{pc}}{\cos \dfrac{\pi a_{cp}}{W}} \right]^{1/2}$$
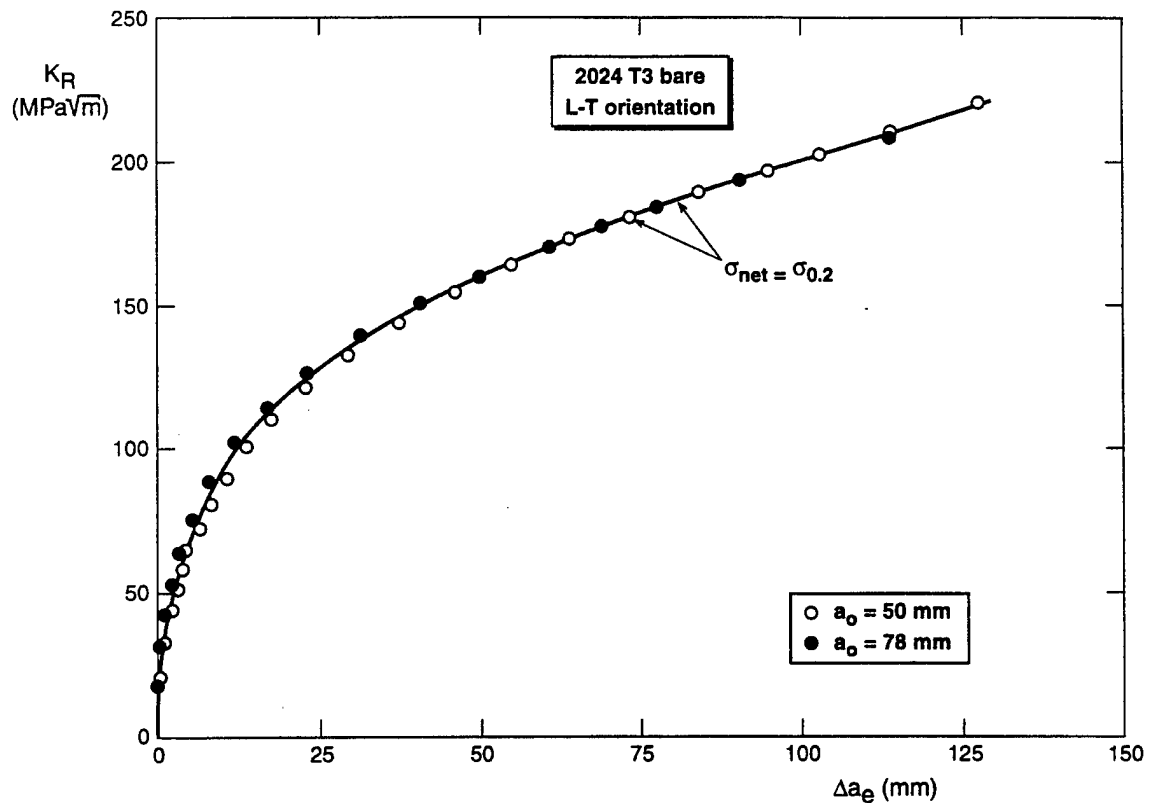

FIGURE C-1. R-CURVE FOR THE SKIN MATERIAL OF THE STIFFENED PANELS

TABLE C-2. NUMERICAL RESULTS OF THE RESIDUAL STRENGTH TESTS ON THE SKIN MATERIAL OF THE STIFFENED PANELS (Material: 2024-T3 Bare, L-T Orientation)

E = 73000 MPa, $\sigma_{0.2}$ = 366 MPa, W = 500 mm, t = 1.28 mm, η = 0.33, Y = 4.0 mm

Specimen H100, a_n = 49.8 mm

Correction on exper. determined Ev/SW: 0.8795

a_p mm	S MPa	S_{net} MPa	a_e mm	Δa_e mm	K_R MPa√m
49.78	0.0	0.0	49.78	0.00	0.0
49.78	48.8	61.0	50.25	0.47	19.9
49.78	78.1	97.5	51.00	1.22	32.1
49.87	105.1	131.3	52.15	2.37	43.7
50.00	121.1	151.4	53.05	3.27	50.9
50.21	136.9	171.3	53.90	4.12	58.0
50.53	152.3	190.9	54.25	4.47	64.8
50.96	166.4	209.0	56.40	6.62	72.3
51.59	181.8	229.1	58.20	8.42	80.5
52.25	197.3	249.4	60.70	10.92	89.4
53.48	216.4	275.3	63.60	13.82	100.8
54.98	229.1	293.7	67.35	17.57	110.4
56.83	240.6	311.4	72.70	22.92	121.4
59.51	249.4	327.3	79.30	29.52	132.8
62.95	254.1	339.6	87.30	37.52	144.1
67.00	256.3	350.1	96.15	46.37	155.2
71.30	255.5	357.4	105.10	55.32	165.2
75.70	252.0	351.4	114.15	64.37	173.8
80.71	246.1	363.4	123.70	73.92	181.7
87.87	238.3	367.4	134.70	84.92	190.4
94.66	229.1	368.7	145.35	95.57	198.0
100.47	221.5	370.3	153.50	103.72	203.7
108.13	210.9	371.7	164.45	114.67	211.9
118.31	196.3	372.6	178.00	128.22	222.0

Specimen H156, a_n = 78.0 mm

Correction on exper. determined Ev/SW: 0.8870

a_p mm	S MPa	S_{net} MPa	a_e mm	Δa_e mm	K_R MPa√m
77.98	0.0	0.0	77.98	0.00	0.0
77.98	33.2	48.3	78.10	0.12	17.5
77.98	58.6	85.2	78.50	0.52	31.0
77.98	79.1	115.0	79.30	1.32	42.1
78.19	98.2	143.0	80.50	2.52	52.8
78.71	117.4	171.3	81.50	3.52	63.6
79.41	136.7	200.4	83.60	5.62	75.3
80.56	156.6	231.1	86.20	8.22	88.1
82.10	175.8	261.7	90.15	12.17	101.8
84.31	189.5	285.9	95.10	17.12	113.9
86.95	200.6	307.6	101.25	23.27	126.1
90.84	209.0	328.3	109.70	31.72	139.7
95.67	211.1	342.0	119.05	41.07	150.8
100.13	210.7	351.5	128.30	50.32	160.8
106.00	207.4	360.1	139.30	61.32	171.4
110.90	203.1	365.1	147.55	69.57	178.5
116.27	196.3	367.0	156.30	78.32	184.6
124.54	185.5	369.7	169.30	91.32	194.2
141.45	160.4	369.3	192.45	114.47	209.6